Durham University

Durham E-Theses

Electro-luminescence and associated two carrier effects in cadmium sulphide

Rushby, A. N.

How to cite:

Rushby, A. N. (1966) *Electro-luminescence and associated two carrier effects in cadmium sulphide*, Durham theses, Durham University. Available at Durham E-Theses Online: http://etheses.dur.ac.uk/8572/

Use policy

The full-text may be used and/or reproduced, and given to third parties in any format or medium, without prior permission or charge, for personal research or study, educational, or not-for-profit purposes provided that:

- a full bibliographic reference is made to the original source
- a link is made to the metadata record in Durham E-Theses
- the full-text is not changed in any way

The full-text must not be sold in any format or medium without the formal permission of the copyright holders.

Please consult the full Durham E-Theses policy for further details.

Academic Support Office, The Palatine Centre, Durham University, Stockton Road, Durham, DH1 3LE
e-mail: e-theses.admin@durham.ac.uk Tel: +44 0191 334 6107
http://etheses.dur.ac.uk

Electro-Luminescence and associated two carrier effects in cadmium sulphide

by

A. N. Rushby, M. A.

Presented in candidature for the degree of Doctor of Philosophy in the University of Durham.

November, 1966

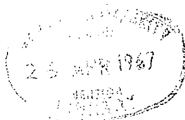

P 250.

ACKNOWLEDGEMENTS

The author wishes to thank C.V.D. Admiralty for financial support during the course of this work, and Professor D.A.Wright for permitting the use of his laboratory facilities. He is deeply indebted to Dr. J.Woods for his supervision and for guidance throughout the work and preparation of this thesis. He would like to thank the other members of the CdS group for many useful discussions and in particular Dr. L.Clark who enabled the thesis to be submitted in the authors absence. The efforts of the departmental workshop staff headed by Frank Spence are acknowledged with gratitude.

DURHAM UNIVERSITY
26 AUG 1967
LIBRARY

ABSTRACT

The properties of cadmium sulphide are such that the material has some potential for use in the semiconductor industry. The potential has so far not been realised because of the difficulty of preparing crystals with controlled properties. In order to improve the material available, much work has been carried out to identify and measure the parameters of the defects in the material. The study of double injection phenomena is one tool which enables defects to be investigated. During the work which forms the basis of this thesis, a large number of double injection devices have been fabricated from crystals grown by sublimation of CdS powder in a stream of argon. The devices have been studied at temperatures in the range 90 to 300 ^{o}K, and at temperatures below about 150 ^{o}K visible green light is emitted when currents above about 5 mA flow. The light is due to recombination in the bulk and on the surface of the crystals. A comparison of the photo-, electro-, and cathodo-luminescent spectra has been made. The electrical measurements reveal that the current flow is governed by a class II centre located 0.98 eV above the valence band. The presence of this centre leads to a switching effect which is such that the device can be turned on when a voltage pulse or a pulse of light is applied to the device when biased below threshold. When pulsed voltages are applied, the current pulse has a step in it due to a fraction of the class II

centres capturing electrons while the pulse is off. The maximum frequency of sine wave modulation of the light has been found to be less than 1 megacycle so that the CdS device is unlikely to compete with injection lasers in other materials as a source of light for optical telecommunication systems.

INTRODUCTION

1. The choice of CdS as a material to study.

Since the invention of the transistor in 1948, the semiconductor device industry has grown enormously. In order to improve the performance, and extend the range of applications of semiconductor devices it is necessary to examine not only the materials that are already widely employed in device manufacture, but also to search for materials with better properties. Cadmium sulphide is one material the properties of which make it highly suitable for use in devices such as photo-cells, gamma ray detectors, and thin film transistors. Unfortunately its technology has not yet been developed to the stage where this potential can be realised.

2. Double injection as an experimental tool.

The injection of holes and electrons into a semiconductor, simultaneously, leads to a variety of phenomena. The current flow depends not only on the free and bound space charge, but also on the recombination mechanisms that are active. These considerations lead to a variety of power law dependences of the current-voltage characteristics. Further, in a direct gap material, the double injection process can lead to the emission of light at low temperatures. In particular, the electro-luminescence from CdS is visible green light. Thus a study of double injection effects in CdS should give information about the defect levels in the forbidden energy gap which govern the performance of devices, and this in turn should

enable improvement of device performance to be achieved.

3. Unexplained double injection effects in CdS.

Prior to the present work, some preliminary double injection experiments had been performed in this laboratory by Guy Marlor[1]. Marlor's work revealed two effects of interest:

1. There was a delay between the application of a current pulse and the emission of light from the crystal. This effect showed up most clearly at short pulse lengths of the order of one microsecond where most of the light was emitted after the end of the voltage pulse. If it could be shown that the delay was associated with the transit of holes between the electrodes then this would be evidence for the Lambe-Klick[2] model for luminescence in CdS.

2. Under certain conditions the current pulse consisted of a low plateau followed by a plateau at higher current. The duration of the lower plateau was found to depend on the pulse duration and the repitition rate. Marlor suggested tentatively that the step was due to the freeing of trapped carriers by impact ionisation which would cause the current to rise.

4. The aims of this work.

The aims of this work at the outset were:

1. To investigate the two effects observed by Marlor.

2. To improve the CdS electro-luminescent devices so that sufficiently intense light could be emitted for the spectral distribution of the light to be measured.

3. To see if, and under what conditions, a CdS injection laser could

be fabricated.

4. To provide a unified explanation of the double injection effects in CdS.

During the course of the work, emphasis was placed on aims 1, 2, and 4 since the double injection structures employed in the course of the work were found unsuitable for the production of stimulated emission.

CONTENTS

Title page	
Acknowledgements	i
Abstract	ii
Introduction	iv
Contents	vii
Chapter 1: Electrical conduction in semiconductors	1
Chapter 2: Double injection in insulators	21
Chapter 3: Recombination radiation	34
Chapter 4: Summary of the properties of cadmium sulphide and experiments related to this work	48
Chapter 5: Growth of CdS single crystals	61
Chapter 6: Measurements of the spectral distribution of the luminescence from cadmium sulphide	74
Chapter 7: Electrical and optical double injection effects	81
Chapter 8: Discussion of the spectral distribution measurements	97
Chapter 9: Discussion of the electrical measurements	111
Chapter 10: Conclusions	124
Appendix 1: Details of crystal growing runs	127
Appendix 2: Programme for calculating the position of the peaks	130

Appendix 3: Programme for scaling the emission spectra 131

Appendix 4: Construction of the electro-luminescent devices 132

Appendix 5: Double injection effects and electro-luminescence in CdS 135

References 136

CHAPTER 1

Electrical conduction in semiconductors

1.1. Energy band theory.

The movement of an electron with energy E in a potential V is described by Schrodinger's equation

$$\frac{\hbar^2}{2m}\nabla^2\psi + (E-V)\psi = 0 \qquad 1.1.$$

where $\hbar = h/2\pi$, h = Planck's constant,

ψ = electron wave function,

m = electron mass.

For a free electron in zero potential, equation 1.1 can be solved to give the result

$$E = \frac{\hbar^2 k^2}{2m} \qquad 1.2.$$

where k is the wave vector.

When an electron in a periodic lattice is considered, an exact solution is impossible because the potential that the electron experiences cannot be defined exactly. However, by averaging the interactions due to all the other electrons, and by assuming a square well potential due to the nuclei of the atoms, a one electron model can be solved to give results that are in qualitative agreement with practice. Kronig and Penney[1] considered the simplest one dimensional case of no electronic interactions and a delta function potential. Their model gives the following results:

1. The forbidden energy gap.

The E versus k continuum is divided into regions of allowed and forbidden energy giving rise to allowed energy bands separated by

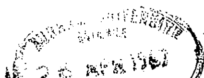

Energies allowed to electrons.

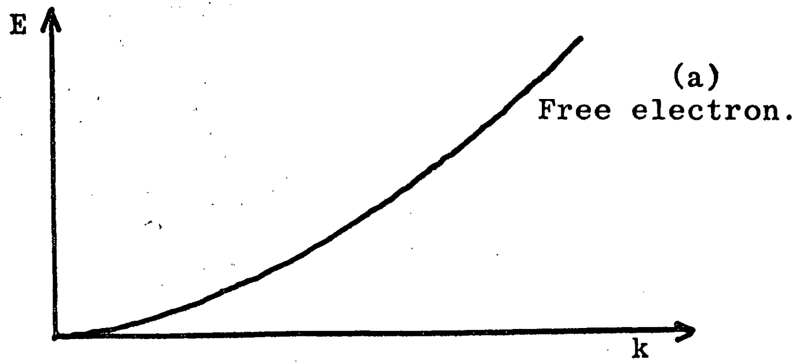

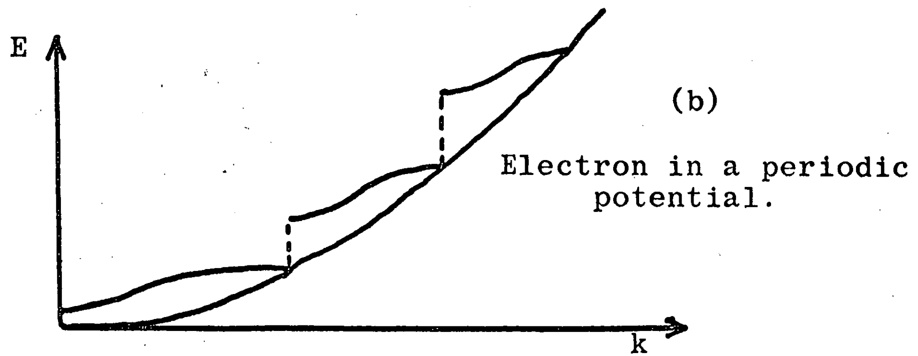

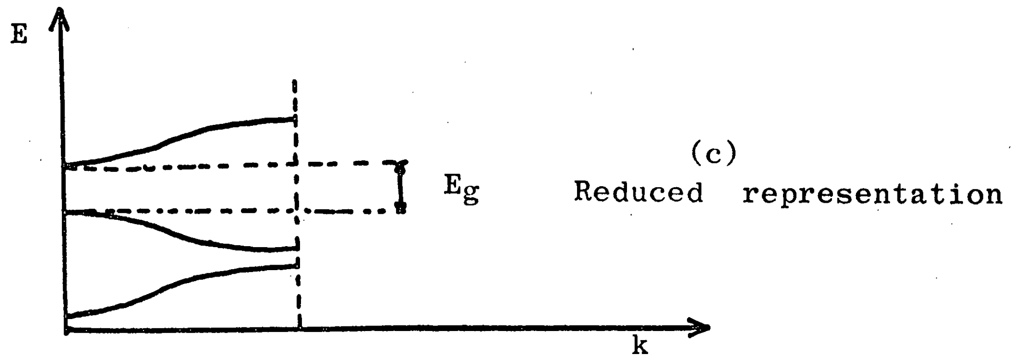

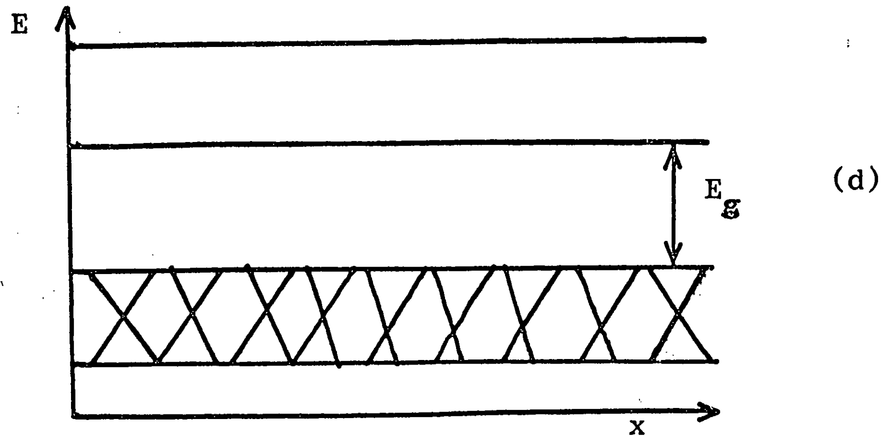

Figure 1.1.

forbidden energy gaps. The highest full band and the lowest empty band at absolute zero are the two most important bands for the majority of semiconductor effects and are called the valence and conduction bands respectively. Figure 1.1 compares the E-$\underline{k}$ relationship for a free electron with that for an electron in a periodic potential (1.1a and 1.1b).

Consider an electron in a crystal at $\underline{k}=0$. Application of an electric field will accelerate the electron until at $\underline{k}=\pi/a$ it suffers Bragg reflection and reverses direction and appears at the left hand side of the curve at $\underline{k}=-\pi/a$. If the band is full there can be no net current flow since for every electron with positive $\underline{k}$ value there is one with a corresponding negative $\underline{k}$ value. The region in 3-dimensional $\underline{k}$ space through which the electron moves between successive Bragg reflections is called a Brillouin zone[2]. Bloch[3] has shown that the wave functions for electrons in a perfect 3-dimensional lattice are of the form

$$\psi = u_k(r).\exp(i\underline{k}.\underline{r}) \qquad 1.3.$$

where u_k is some function with theperiodicity of the lattice and $\underline{r}$ is the distance vector. Because the wave functions have the periodicity of the lattice the E versus $\underline{k}$ plot can be drawn in reduced representation within the first Brillouin zone i.e. between the $\underline{k}$ values $-\pi/a < k < \pi/a$. The reduced representation of the Kronig-Penney model is shown in figure 1.1c. Figure 1.1d shows the forbidden energy gap without regard to momentum but with energy plotted against a spatial coordinate. The forbidden energy gap E_g is indicated in figures 1.1c and 1.1d. The magnitude of the forbidden energy gap determines the nature of the material. The distinction between a semiconductor and an insulator is somewhat

arbitrary and the criterion adopted in this thesis will be that a material with a forbidden energy gap between zero and 2 eV will be called a semiconductor, and one with energy gap greater than 2 eV will be termed an insulator. For many cases the distinction is trivial and for such cases the term semiconductor will be taken to include insulators.

2. The effective mass.

As well as imposing restrictions on the allowed energies of an electron, the lattice also modifies the dynamic properties of an electron. In this case it is convenient to replace the free electron mass, m, with an effective mass, m^* which takes account of the effect of the lattice on the electron. In this way the classical relations such as $E = p^2/2m$ still hold but with m replaced by m^*. It can be shown by analogy with a free electron that the effective mass is given by

$$\frac{1}{m^*} = \frac{1}{\hbar^2} \cdot \frac{d^2E}{dk^2} \qquad 1.4.$$

Figure 1.2 shows the first and second derivatives of the energy with respect to momentum for one band. At the bottom of the band the effective mass is positive rising toward the centre of the zone where it changes discontinuously from a large positive value to a large negative value. The magnitude of the effective mass then decreases towards the zone edge. The concept of negative effective mass means that the electrons are accelerated in the opposite direction to the applied electric field. This is conveniently replaced by considering the current at the top of a band to be carried by a particle with positive charge called the hole. The hole is the result of the collective movementof the electrons and

$E, \frac{dE}{dk}, \left(\frac{d^2E}{dk^2}\right)^{-1}$ versus k.

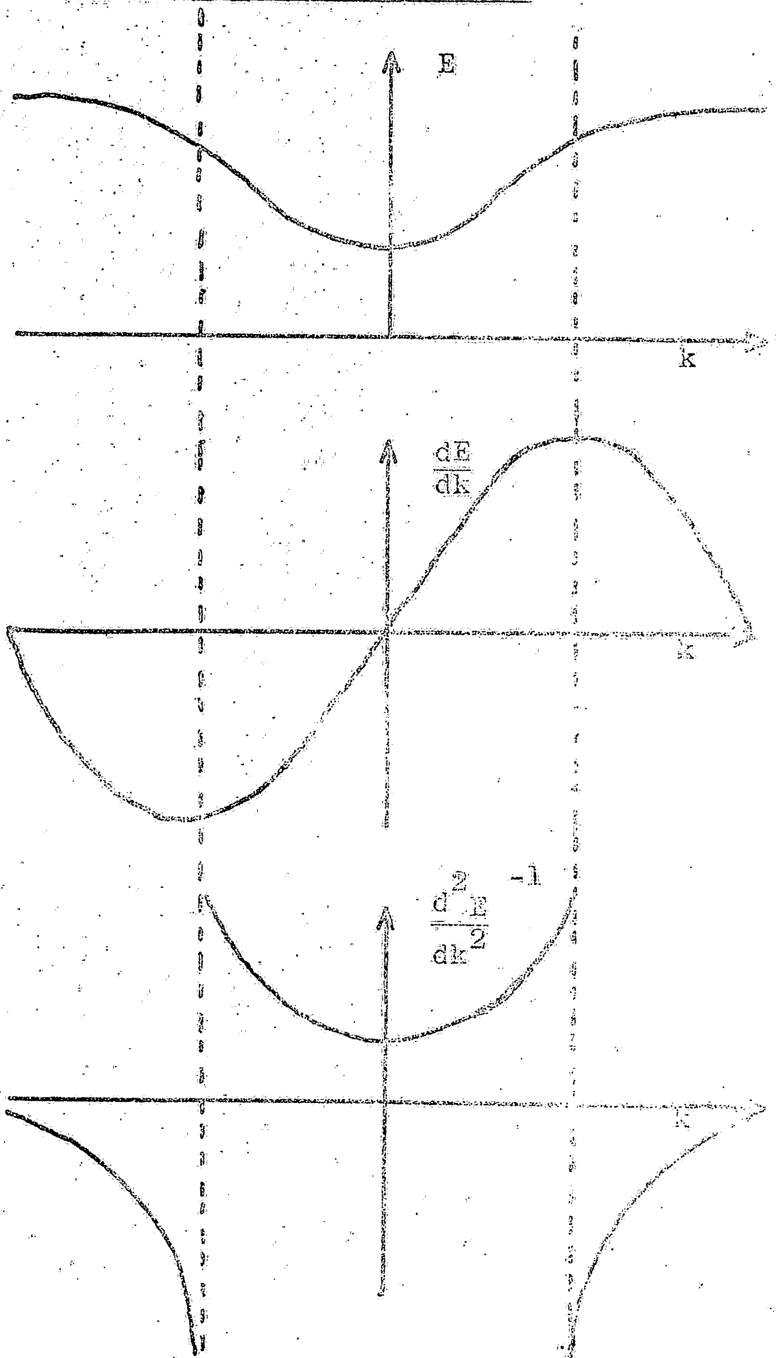

Figure 1.2.

has analogous properties to the electron.

1.2. Electron Scattering.

Another essential difference between a free electron and an electron in a periodic lattice is with regard to their drift velocities in an electric field. A free electron in an electric field gains a drift velocity dependent on the change in potential energy of the electron. In a crystal however, the electron is scattered by lattice vibrations and by defects in the lattice, and moves with a constant drift velocity superimposed on its random thermal motion. The drift velocity ,v, in an electric field $\underline{E}$ is given by

$$v = \mu \underline{E} \qquad 1.5.$$

where μ is the electron mobility. At high fields this relation breaks down and the mobility becomes dependent on the field. The effective mass and the mobility can be related by considering the relaxation of a disturbance to the velocity distribution of the electrons. In the absence of an applied electric field the drift velocity, v, satisfies the relation

$$\frac{dv}{dt} + \frac{1}{\tau_r} . v = 0$$

Thus $v(t) = v(0).\exp(-t/\tau_r)$, and therefore the time τ_r is the characteristic decay time for the disturbance. With an applied electric field, the expression for the drift velocity is

$$m^*(\frac{dv}{dt} + \frac{1}{\tau_r} .v) = e\underline{E}$$

This equation has the solution

$$v = \frac{e\tau_r\underline{E}}{m^*} \qquad 1.6.$$

Thus comparing 1.5 with 1.6, we have

$$\mu = \frac{e\tau_r}{m^*} \qquad 1.7.$$

If there is more than one scattering process active i.e. a unique relaxation time cannot be defined, the relaxation time is given by

$$\frac{1}{\tau_r} = \sum_n \frac{1}{\tau_n}$$

The relationship is reciprocal because $1/\tau_n$ is the number of collisions of type n that the electron suffers per second. From equation 1.5 it can be seen that the conductivity σ is given by

$$\sigma = ne\mu \qquad 1.8.$$

for electronic conduction. If the hole contribution to the current is also included then

$$\sigma = e(n\mu_n + p\mu_p) \qquad 1.9.$$

where μ_n and μ_p are the electron and hole mobilities and n and p are their densities.

The important scattering mechanisms in semiconductors are:

1. Lattice scattering.

The periodic potential that the electron moving through the lattice experiences is modified by the mechanical vibrations of the atoms about their equilibrium positions. This gives rise to a perturbation of the bottom of the conduction band which scatters the electrons moving in it. Both acoustic and optical modes of the lattice vibrations contribute to the scattering which can occur either through longitudinal or transverse vibrations. Clearly the higher the temperature the stronger the thermal vibrations of the atoms will be, andthus

Dependence of mobility on effective mass and temperature.

Mechanism	$\mu \quad (m^*)^x . T^y$	
	x	y
Acoustic	-5/2	-3/2
Polar	-3/2	exp
Ionised Impurity	-1/2	3/2
Neutral Impurity	1	ind
Electron-Hole	-1/2	3/2
Piezo-electric	-3/2	-1/2

Figure 1.3.

when lattice scattering is dominant a reduction in the mobility is expected as the temperature is raised. The temperature variation of mobility due to the various scattering mechanisms is shown in figure 1.3 following Hilsum and Rose-Innes.[4] For acoustic mode scattering the mobility varies as $T^{-3/2}$ whereas for optical mode scattering the dependence is more complex, being approximately proportional to $T^{1/2}.(e^{\theta/T}-1)$ where θ is the optical phonon temperature.

2. Impurity scattering.

When impurities are incorporated into the lattice a further contribution to the scattering of the carriers can occur. The case when the impurity atoms are ionised is formally similar to the Rutherford scattering of α particles. Conwell and Weisskopf[5] have shown that the mobility varies as $T^{3/2}$ with a weakly varying logarithmic term involving T^2. Even if the impurity is not ionised scattering can occur but this type of scattering is is independent of the temperature. When two or more scattering mechanisms occur simultaneously, the mobility is obtained by adding the limit mobilities for the mechanisms reciprocally. This is for the same reason that the lifetimes add reciprocally.

3. Inter-carrier scattering.

Electron-electron and hole-hole scattering are only important at very high carrier densities. The most important inter-carrier scattering is the scattering of an electron by a heavy hole. The problem is formally similar to ionised impurity scattering and the same temperature dependence results, namely the mobility varying as $T^{3/2}$.

4. Piezo-electric scattering.

In a piezo-electric material the acoustic vibrations give rise to a longitudinal electric field which contributes to the scattering. Hutson[6] has calculated the magnitude of this effect and found that the mobility is proportional to $T^{-1/2}$.

5. Other scattering mechanisms.

Apart from the sources of scattering already mentioned, carriers are scattered by lattice defects such as inclusions, grain boundaries, voids, and dislocations. With materials suitable for use in device construction the densities of such defects are so low that they can be neglected with respect to the dominant mechanisms. One other mechanism for scattering which is important in some semiconductors is inter-valley scattering. The phenomenon arises if the band structure of the material has more than one potential minimum in k-space. With the assistance of an energetic phonon the electron may be scattered from one valley to the next. The large change in k value needed in most materials means that the process is unlikely at low temperatures.

1.3. Diffusion of carriers.

In the absence of an applied electric field and in thermal equilibrium, the carrier densities in a homogeneous semiconductor are uniform. If a disturbance is made to the carrier density at some point in the material, then the carriers will diffuse in an attempt to establish a a uniform distribution. Since the carriers are charged, their diffusive flow gives a contribution to the electric current. This diffusion contribution is of magnitude De.grad n for electrons and may add to

or subtract from the drift current. The diffusion coefficient D, and the mobility μ are related by the Einstein relation

$$\frac{De}{kT} = \mu \qquad 1.10.$$

1.4. Lifetime.

A carrier moving through a crystal under the influence of an applied electric field may become localised at some defect or may be annihilated by recombination with a carrier of opposite species. The average free time that a carrier spends in its appropriate band is called the lifetime τ. The average distance that a carrier diffuses in one lifetime is called the diffusion length L_D. The diffusion length and the lifetime are related by the expression

$$L_D = (D\tau)^{1/2} \qquad 1.11.$$

Because of the equilibrium between electrons in the conduction band and those localised in trapping levels, the value obtained for the mobility of the electrons depends upon the way in which it is measured. In particular it is necessary to distinguish between the conductivity mobility μ_c and the drift mobility μ_d. The conductivity mobility is defined by equation 1.8. ~~and is the velocity per unit field with which a conduction band electron moves between collisions.~~ The drift mobility is the velocity of ~~the~~ injected electrons per unit field. ~~averaged over a time interval containing a large number of collisions.~~ In the trap free situation the drift and conductivity mobilities are equal. When trapping effects are included the ratio of the two mobilities is given by

$$\frac{\mu_d}{\mu_c} = \frac{N_c}{N_t} \exp(-E_t/kT) \qquad 1.12.$$

where N_C is defined in section 1.6, and N_t is the density of traps at an energy E_t below the conduction band. The Hall mobility is defined as the product of the Hall coefficient $R = r/ne$ and the conductivity. Thus this value differs from the conductivity mobility by the factor r. r depends on the nature of the equal energy surfaces in k-space, on the scattering processes, and whether the semiconductor is degenerate or not. For the case of spherical equal energy surfaces, non-degenerate statistics, and isotropic scattering by longitudinal acoustic phonons the value of r is $3\pi/8$. When other scattering processes dominate, r is of the order of unity.

1.5. Capture cross section.

Impurities in the lattice may capture a carrier if the activation energy involved is large enough compared to kT. If the centre is ionised then the coulombic attraction for the appropriate carrier is important, although it is possible for neutral defects to capture carriers. Having captured a carrier a level may act either as a trap, in which case the carrier will probably be thermally released into the band, or as a recombination centre when the trapped carrier will probably be anihilated by a carrier of the opposite sign. If there are n empty donors per cm^3 i.e. an electron density in the conduction band n per cm^3, then the rate of capture of electrons by such centres is Svn^2 where v is the thermal velocity of the electrons and S is called the capture cross section. An attempt to escape frequency ν can be defined such that the rate of thermal excitation of electrons from the level is $\nu \exp(-E_d/kT)$ where E_d is the donor activation energy.

The attempt to escape frequency and the capture cross section are related by the expression[8]

$$\frac{\nu}{S} = 8m^{*}(\pi/h)^{3/2}(kT)^{2} \qquad 1.13.$$

1.6. The Fermi level.

In perfect crystals at a finite temperature there are equal numbers of electrons and holes in their respective bands due to the thermal excitation of electrons from the valence to the conduction band. The concentration of electrons, $n(E)$, in the states within the energy interval between E and E+dE is given by

$$n(E) = g(E).f(E).dE$$

where $g(E)$ is the density of states function, and $f(E)$ is the probability that a given state at an energy E will be occupied.

By treating the electrons as independent particles subject to the Pauli exclusion principle, the Fermi function, $f(E)$, can be evaluated as

$$f(E) = \frac{1}{1+\exp\left(\frac{E-E_f}{kT}\right)} \qquad 1.14.$$

where E_f is the Fermi level and is the energy at which the probability of a state being occupied is 1/2. When dopants are added to to a material, the Fermi function is still applicable and gives the occupancy probability, but the value of E_f is different from the intrinsic case. If $E_f \gg 3kT$ from the conduction band, the exponential in the denominator of the Fermi function is much greater than 1 for electrons in the conduction band , and the function approximates to the Maxwell-Boltzmann distribution and the semiconductor is said to be non-

degenerate. When $E_f \ll 3kT$ from the conduction band the semiconductor is degenerate. A corresponding definition applies for p-type material.

Near the bottom of the conduction band, the density of states function, $g(E)$, is given by

$$g(E) = \frac{1}{2\pi^2}(2m^*/\hbar^2)^{3/2}\,(E-E_c)^{1/2} \qquad 1.15.$$

It is convenient to define an effective density of states, N_c, such that

$$N_c = 2\left(\frac{2\pi m^* kT}{h^2}\right)^{3/2} \qquad 1.16.$$

and a similar effective density N_v for holes in the valence band. The effective densities of states are the numbers of states within kT of the band edges. N_c and N_v are of the order of 10^{19} cm^{-3} at 300 °K. The density of states for an impurity level in the forbidden energy gap is equal to the density of unoccupied levels i.e. $(1-f(E)).N_t$, where N_t is the concentration of levels.

For a non-degenerate semiconductor, the concentration of electrons in the conduction band is given by

$$n = N_c.\exp-\frac{(E_c-E_f)}{kT} \qquad 1.17.$$

and for holes in the valence band

$$p = N_v.\exp-\frac{(E_f-E_v)}{kT} \qquad 1.18.$$

Thus

$$np = N_c.N_v.\exp(-E_g/kT) \qquad 1.19.$$

and this is constant at a fixed temperature.

Equation 1.19 implies that there will in general be many more carriers

of one sign than of the other in extrinsic material. The more numerous carrier is called the majority carrier, and the lesser the minority carrier. This nomenclature arises becaues the majority carrier carries most of the current except in materials such as InSb where b, the ratio of the electron to the hole mobility is large so that the current in lightly doped p-type material is carried mostly by electrons.

1.7. Non-equilibrium carrier concentrations.

When the equilibrium carrier concentration is disturbed for example by irradiating the semiconductor with light which generates free electrons and holes, the concept of a single Fermi level is no longer valid. However if a steady state is achieved it is convenient to introduce a quasi-Fermi level for each carrier so that the concentrations of the carriers in their respective bands are given by equations similar to 1.17 and 1.18. Thus

$$n = N_c . \exp - \frac{(E_c - E_{fn})}{kT} \qquad 1.20.$$

$$p = N_v . \exp - \frac{(E_{fp} - E_v)}{kT} \qquad 1.21.$$

where E_{fn} and E_{fp} are the electron and hole quasi-Fermi levels.

1.8. Injection of excess carriers.

Consider a semiconductor with electrodes applied to opposite parallel faces separated by a distance L. Assume that the thickness of the crystal is small compared to the lateral dimensions so that a one dimensional analysis may be applied. For a trap free n-type semiconductor a current carried by the thermal equilibrium electron concentration, n, will flow when a potential difference between the electrodes is applied, and Ohm's law will be obeyed. However,

departures from Ohm's law may be observed at relatively low voltages due to injection of electrons into the crystal from the cathode. The effect is most easily observed if the thermal equilibrium electron concentration is small. This condition is fulfilled by semiconductors at low temperatures or by insulators. Under conditions of excess electron injection the current is limited by the space charge of the electrons themselves, in an analogous way to the current flow in an unsaturated thermionic diode. The Analysis of two carrier space charge limited (SCL) current flow will be discussed in chapter 2. The one carrier SCL current flow can be solved analytically subject to certain assumptions. The equations governing the current flow are:

1. Poisson's equation

$$\frac{dE}{dx} = \frac{ne}{\epsilon} \qquad 1.22.$$

2. The total current flow

$$J = ne\mu E + De.\frac{dn}{dx} \qquad 1.23.$$

It is assumed that the hole contribution to the current flow is negligible and that the semiconductor is trap free. The situation in which the diffusion term in the total current flow is significant is difficult to analyse theoretically so the solution will be derived for the case where the diffusion term can be neglected.

1.9. The theory of Mott and Gurney[9].

The solution of equations 1.22 and 1.23 depends upon the choice of boundary conditions for the electron density, n, and the electric field, E. Mott and Gurney took the value of the electron concentration

at the surface of the semiconductor, $n(0)$, to be given by

$$n(0) = N_c . \exp -\left(\frac{\phi_m - \chi_s}{kT}\right) \qquad 1.24.$$

where ϕ_m is the metal work function, and χ_s is the semiconductor electron affinity. As the boundary condition for $\underline{E}$ they took $\underline{E} = 0$ at $x = -x_0$. The result of this model was that the current density, J, was given by

$$J = \frac{9}{8}\epsilon\mu\frac{V^2}{L^3} \qquad \text{for } x_0 < L \qquad 1.25.$$

and

$$J = e\mu n(0) . \frac{V}{L} \qquad \text{for } x_0 > L \qquad 1.26.$$

1.10. <u>The thermionic analogy.</u>

The objection to the analysis of Mott and Gurney is that there is no physical reason for the choice of the $\underline{E}$ boundary condition that puts the x origin at a distance x_0 beyond the potential minimum in the conduction band. A more logical choice is to consider the situation as analogous to the thermionic diode and to consider the potential minimum to be a virtual cathode and to put the origin there. The boundary condition is now $\underline{E} = 0$ at $x = 0$, and equations 1.22 and 1.23 can be solved immediately to give the result

$$J = \frac{9}{8}\epsilon\mu\frac{V^2}{L^3} \qquad 1.27.$$

which is in agreement with Mott and Gurney but which has a sounder physical basis. This result can be compared with the result for the space charge limited current flow in a thermionic diode where the well known Child's law

$$J = \frac{4}{9}\epsilon_0(2e/m)^{1/2} . \frac{V^{3/2}}{L^2} \qquad 1.28$$

is obeyed. The difference between the power law dependences of V

and L in a solid and in a vacuum arises from the difference in the transport mechanisms of the electrons already mentioned in section 1.2.

1.11. Lampert's analysis of an insulator with traps.

The current densities measured in real crystals are many orders of magnitude less than those predicted by equation 1.27. In order to explain this discrepancy Lampert[10] analysed the case of an insulator with a single discrete set of trapping levels in the forbidden energy gap. He showed that the current-voltage characteristic was divided into regimes. These regimes are:

1. The ohmic regime.

At low voltages there is no significant injection and the current is carried by the low density of electrons in thermal equilibrium in the conduction band. Thus the current density is given by Ohm's law.

Thus $$J = \sigma E = n_0 e \mu \frac{V}{L} \qquad 1.29.$$

where n_0 is the thermal equilibrium density of electrons.

2. The trap limited regime.

At some higher voltage the number of injected electrons becomes sufficient to make a significant contribution to the current flow. This takes place when $n \simeq 2n_0$, where n is the total electron density in the conduction band. Mott and Gurney's analysis does not hold in this regime because some of the injected charge is trapped where it contributes to the space charge but not to the current flow. Lampert showed that the Mott and Gurney equation must be modified by a factor θ, the ratio of free to trapped charge.

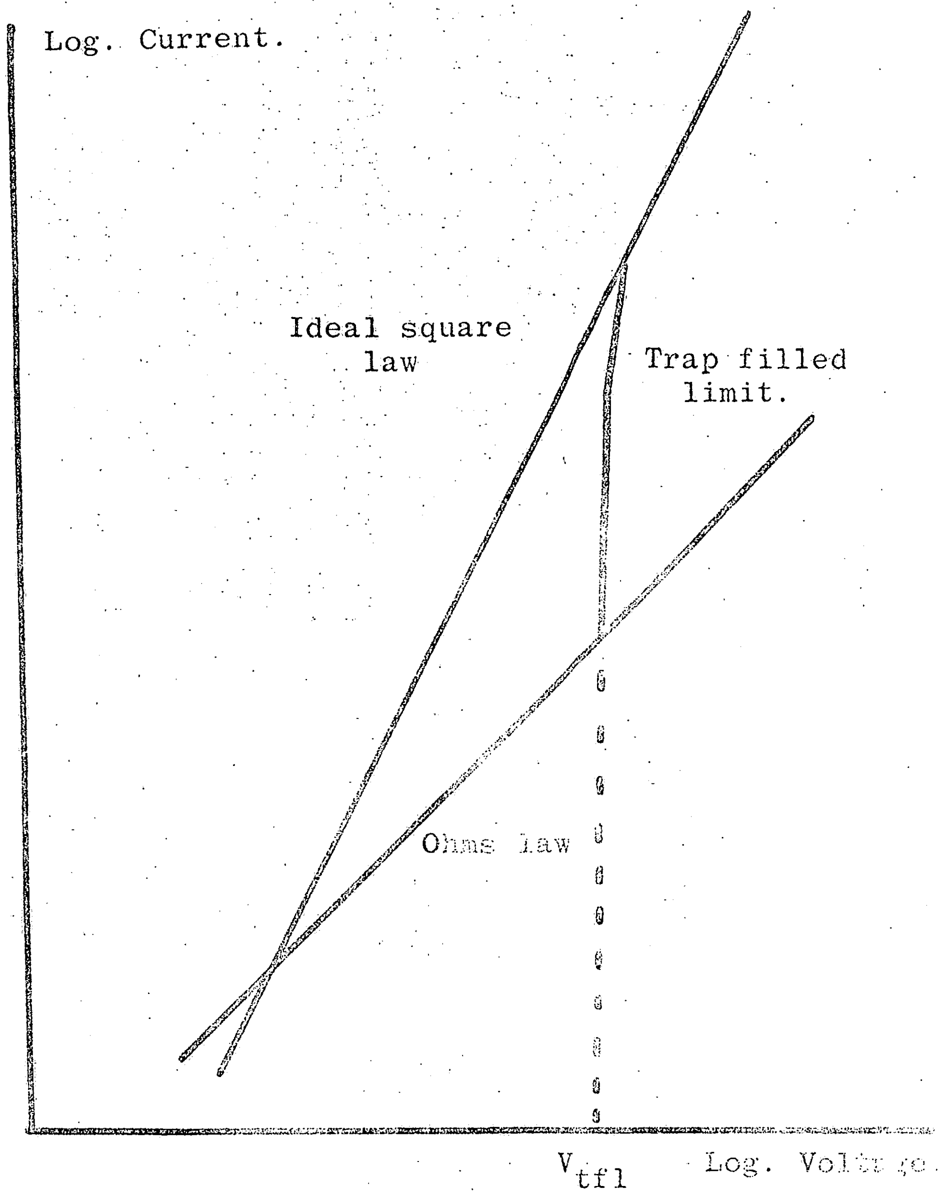

Limiting current-voltage characteristic.

(after Lampert)

Figure 1.4.

Thus $$J = \frac{9}{8}\epsilon\mu\theta\frac{V^2}{L^3} \qquad 1.30.$$

where $$\theta = \frac{n}{n_t} = \frac{N_c}{N_t}\exp(-E_t/kT) \qquad 1.31.$$

3. Trap filled limit.

As the injection level increases the electron quasi-Fermi level moves upwards towards the conduction band and at some voltage V_{tfl} moves through the trapping level. At this voltage the traps are completely filled and all further injected carriers remain free. This leads to a steep rise in the current through several orders of magnitude after which Mott and Gurney's expression holds. The regimes are shown in figure 1.4. Lampert's theory gives the trap filled limit voltage

$$V_{tfl} = \frac{eL^2}{2\epsilon} N_t \qquad 1.32.$$

Hence in principle the measurement of V_{tfl} provides a method for estimating the trap concentration N_t.

4. Saturation regime.

At still higher voltages departures from the square law dependence are possible. These can arise either because of contact saturation or the electron mobility becomes field dependent and scattering by optical phonons becomes appreciable.

1.12. The theory of Marlor and Woods.

Marlor and Woods[11] have shown that Lampert's theory must be applied with caution as a means of estimating trap densities, since the steep rise in the current may not be due to the traps filled limit but could be associated with trap emptying. Lampert's value for the

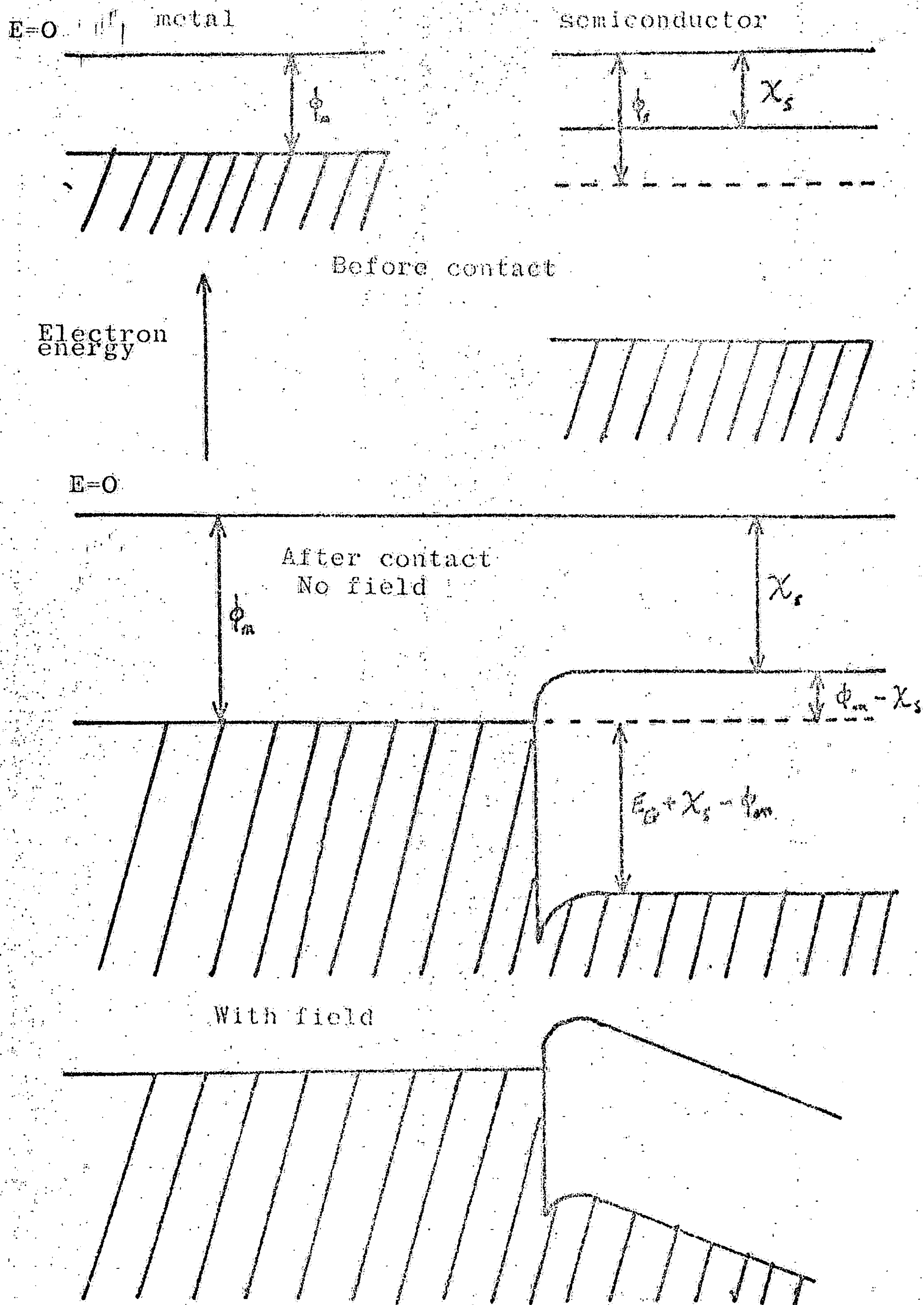

Figure 1.5.

voltage at which the transition from the Ohmic to square law regime occurs must be modified by the trapping ratio θ, thus

$$V_1 = \frac{eL^2}{2\epsilon} \cdot \frac{1}{\theta} \cdot n_o \qquad 1.33.$$

The trap emptying can occur either by impact ionisation or by field ionisation. These authors concluded that a model with a shallow donor level compensated by a deep trap was necessary to explain their results and that equation 1.32 was inapplicable.

1.13. The metal-semiconductor contact.

All the work described in this thesis is concerned with metal contacts on n-type material and consequently this discussion will be limited to contacts on n-type semiconductors. All the arguments can easily be adapted for the p-type case. The two kinds of contact under discussion are the electron injecting and the hole injecting contacts.

1.13.1. The electron injecting contact.

A good electron injecting contact on n-type material is known as an Ohmic contact. An Ohmic contact is defined as one that is electrically invisible. This criterion means that the metal must be able to supply electrons which can pass into the semiconductor unhindered by potential barriers. Figure 1.5 shows the energy band scheme for an Ohmic contact on an n-type semiconductor. The metal has a lower work function than the semiconductor and the step that electrons in the metal with the Fermi energy have to surmount is $\phi_m - \chi_s$. The electrons in the Fermi tail have energies greater than this at temperatures above absolute zero. In equilibrium with no applied electric

Metal-semiconductor contact.

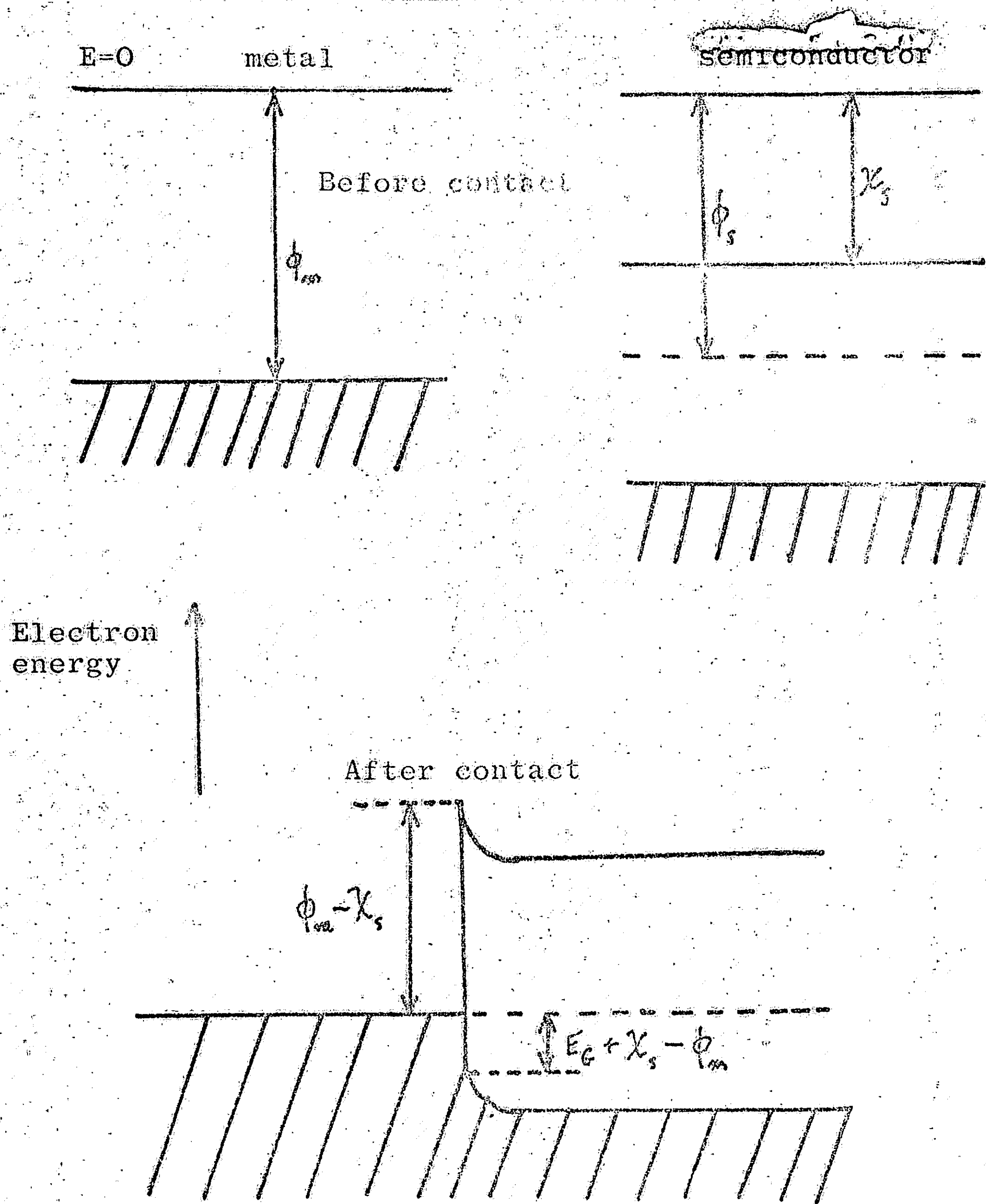

Figure 1.6.

field the diffusion of electrons into the conduction band is balanced by the reverse flow due to the bending of the conduction band, and no net current flows. When a field is applied any electrons reaching the potential minimum are swept into the semiconductor by this field and injection results. The existence of a potential barrier does not prohibit a contact from being Ohmic provided that the barrier is thin enough for the electrons to tunnel through. This is one proposed model for Ohmic contacts on CdS.

1.13.2. The hole injecting contact.

If a reverse bias is applied to an Ohmic contact, hole injection does not take place as can be seen in figure 1.5. In order for hole injection to occur, the electrons near the top of the valence band must gain enough energy to reach the empty states near the Fermi level of the metal. The energy required is $E_g+\chi_s-\phi_m$ which is very large for wide gap materials. In order to achieve hole injection the step must be reduced. For a given material E_g and χ_s are fixed but ϕ_m depends upon the choice of the metal. Thus high work function metals are favourable for hole injection. The energy level scheme for the hole injecting contact is shown in figure 1.6.

There are two other ways of injecting the holes. The first is to form a p-n junction. With forward bias the p-type region injects holes into the n-type region if suitable doping levels are chosen. In a material like CdS which cannot be prepared p-type this necessitates the formation of a hetero-junction. The second method is to tunnel

the holes through a thin layer of an insulator. Both these methods will be discussed in later chapters.

1.14. Contact saturation.[12]

As stated in 1.11 the departure from the ideal square law of the current-voltage characteristic may be due to contact saturation. This arises because only a certain number of electrons can be emitted from the metal into the semiconductor. The maximum current that can be drawn from the metal is thus the thermionic emission over the potential step $\phi_m - \chi_s$, as in the case of a thermionic cathode. Thus the saturation current density is given by a modified Richardson's equation

$$J_s = \frac{4\pi m^* e k^2}{h^3} T^2 . \exp -\frac{(\phi_m - \chi_s)}{kT} \qquad 1.34.$$

The saturation field is obtained by equating 1.34 with the Ohmic value for the current density since the first effect of contact saturation is a return to Ohm's law. In practice the value of the saturation current density may be lower than that given by equation 1.34 because of space charge in front of the cathode. This result has been derived assuming that Schottky emission and field emission do not occur.

1.15. Surface states.

The presence of surface states may have a deleterious effect on the metal-semiconductor contact. The existence of states on a perfect surface was first considered by Tamm[13] who dealt with an asymmetrical termination of the lattice, and later by Shockley[14] for the symmetrical case. The surface levels or Tamm levels as they are called are due to the disruption of the lattice which leaves dangling bonds at the surface.

Surface states on semiconductors.

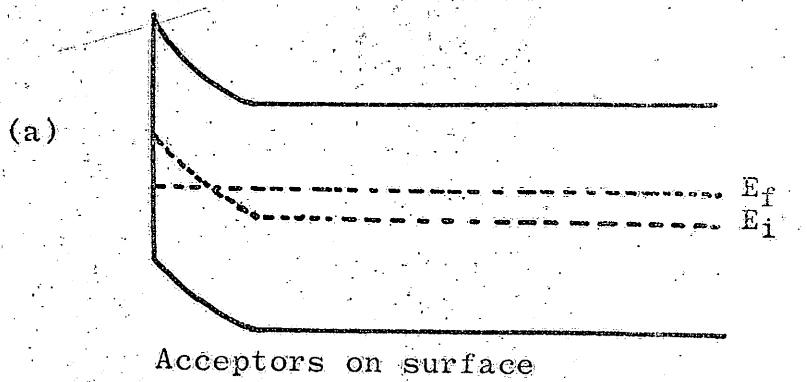

Acceptors on surface

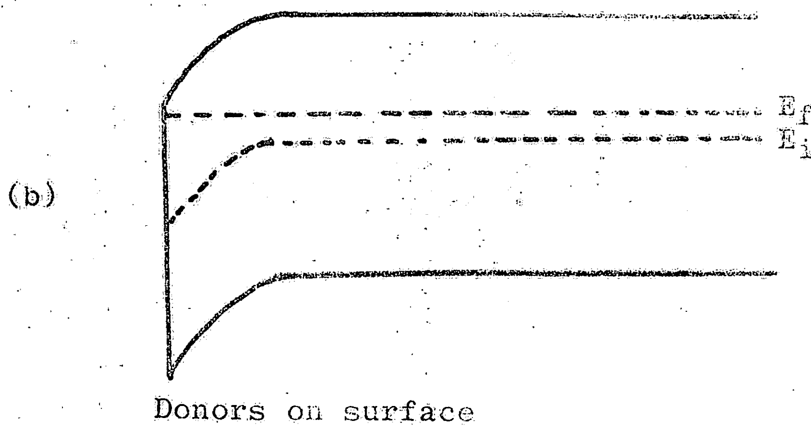

Donors on surface

Figure 1.7.

These are thought to produce acceptor like levels. More important states occur on real surfaces because of shallowly diffused impurities or impurities adsorbed onto the surface. The effect of these impurities is to bend the bands at the surface. This arises in the following way. Consider acceptor impurities on an n-type semiconductor surface. Any free negative charge that tries to pass through the surface will be trapped at these levels and the surface will aquire a net negative charge. Consequently the surface repels free electrons and attracts free holes which recombine with the electrons. Charge neutrality requires that the surface negative charge is balanced by a positive charge in the bulk and a depletion layer results. The energy level system for such a depletion layer is shown in figure 1.7a. To make a good Ohmic contact in the presence of acceptor surface states it is necessary to alloy donors to a shallow depth to compensate them. An excess of donors on the surface bends the bands in the opposite direction so as to facilitate electron injection. This is shown in figure 1.7b. Therefore, it is desirable to choose an n-type dopant for the electron injecting contact as well as one with a low work function as already discussed. Analogous considerations apply to hole injecting contacts on p-type material.

CHAPTER 2

Double injection in insulators

2.1. Introduction.

The analysis of two carrier SCL currents in insulators in much more difficult than the single carrier case because the former involves many more complicated processes and large differences can arise depending on the choice of model. Since the aim of this thesis is to explain two carrier effects in real crystals, only brief mention will be made of the trap free models. The problem is to draw up the simplest model which will explain the observed phenomena and also correspond to the known properties of the material.

2.2. The trap free model of Parmenter and Ruppel[1].

These authors neglected diffusion and solved the problem for a perfect insulator. The two carrier current density was found to be several orders of magnitude higher than the one carrier SCL current under the same conditions, but to have the same voltage (V^2) and thickness ($1/L^3$) dependences, provided that the contacts were ohmic for their respective carriers. They contrasted the enhancement in current with that for a gaseous plasma containing non-recombining positive ions and electrons, where the enhancement is only 4-fold for the best possible case. The reason for the difference between the gas discharge and the insulator is that in the former, space charge neutralisation is much less efficient since the velocity of the charge carriers increases with the distance that they have traversed, and does not depend on the local field as in an insulator.

2.3. <u>The injected plasma.</u>

Lampert and Rose[2] considered the injected plasma where the injected electrons and holes remained free. The contacts were assumed to impose no restraint on the current flow and the diffusion current was taken to be zero. If the common average lifetime of the injected carriers τ is independent of the injection level, the current-voltage characteristic for an n-type semiconductor having thermal equilibrium densities of electrons n_T and holes p_T, is given by

$$J = e\tau\mu_n\mu_p(n_T - p_T).\frac{V^2}{L^3} \qquad 2.1.$$

when the mode of relaxation of the injected charge is ohmic. The dependence of the current density on $n_T - p_T$ is interpreted as meaning that the effective density of electrons available to relax the charge disturbance due to excess holes is $n_T - p_T$. If there are few carriers present in the material in thermal equilibrium so that any injected charge is relaxed by the carriers making a transit through the material or if the transit time is much less than the ohmic relaxation time so that the thermal carriers play no part in the relaxation process, then the current density in this insulator regime is given by

$$J = e\tau\mu_n\mu_p.\frac{V^3}{L^5} \qquad 2.2.$$

Larabee[3] has measured current-voltage characteristics of long germanium p-i-n structures at different temperatures and his results confirm that the current density depends on $n_T - p_T$ in the square law region of the characteristic. As would be expected in germanium at the temperatures that he used, the cube law dependence of the insulator

regime was not observed.

2.4. Double injection into a perfectly compensated insulator.

2.4.1. Introduction.

Lampert[4] has analysed the current-voltage characteristic for an insulator with a single discrete set of recombination centres filled with electrons from an equal number of donor levels. The density of the recombination centres at an energy E_R below the conduction band is N_R cm^{-3}. The analysis incorporates the following assumptions:

1. Charge neutrality is maintained throughout the insulator.
2. The current is volume controlled (i.e. the contacts do not impose any restraint on the current.).
3. Diffusion current is negligible.
4. Mobilities are independent of the field.
5. Thermal re-emission of the carriers from the recombination centres is negligible.
6. Thermally generated carriers are neglected.
7. The recombination centres have unequal capture cross sections for electrons and holes, and in particular

$$s_p^- \gg s_n^o$$

where s_p^- is the capture cross section of a centre occupied by an electron for a hole, and s_n^o is the capture cross section of an empty centre for an electron. This model is to be expected in practice since a charged centre attracts a carrier more strongly than an uncharged one. This model gives a current-voltage characteristic conveniently divided into regimes.

2.4.2. The voltage threshold.

At some voltage the onset of 2 carrier conduction takes place and the current rises vertically at constant voltage. This occurs at V_{th} where

$$V_{th} = \frac{L^2}{2\,\mu_p . \tau_{p,low}} \qquad 2.3.$$

At this voltage the hole transit time $t_{p,tr}$ is given by

$$t_{p,tr} = \frac{L^2}{\mu_p V_{th}} \qquad 2.4.$$

Therefore the threshold for double injection occurs when

$$t_{p,tr} \simeq 2\tau_{p,low} \qquad 2.5.$$

2.4.3. Negative resistance.

Because of assumption 7, as the hole injection rate increases the recombination centres become increasingly populated with holes. This increases the hole lifetime and the holes can make the transit between the electrodes at progressively lower voltages, and negative resistance results, the current rising as the voltage falls. The limit of the process occurs when all the recombination centres are occupied by holes, and the hole lifetime has reached the value $\tau_{p,high}$. The minimum value of the voltage is given by

$$V_M = \frac{s_n}{s_p} . V_{th} \qquad 2.6.$$

with corresponding value of

$$\tau_{high} = \frac{s_p}{s_n} . \tau_{p,low} \qquad 2.7.$$

2.4.4. The semiconductor regime.

The region of the current-voltage characteristic after the

Double injection in insulators (Lampert).

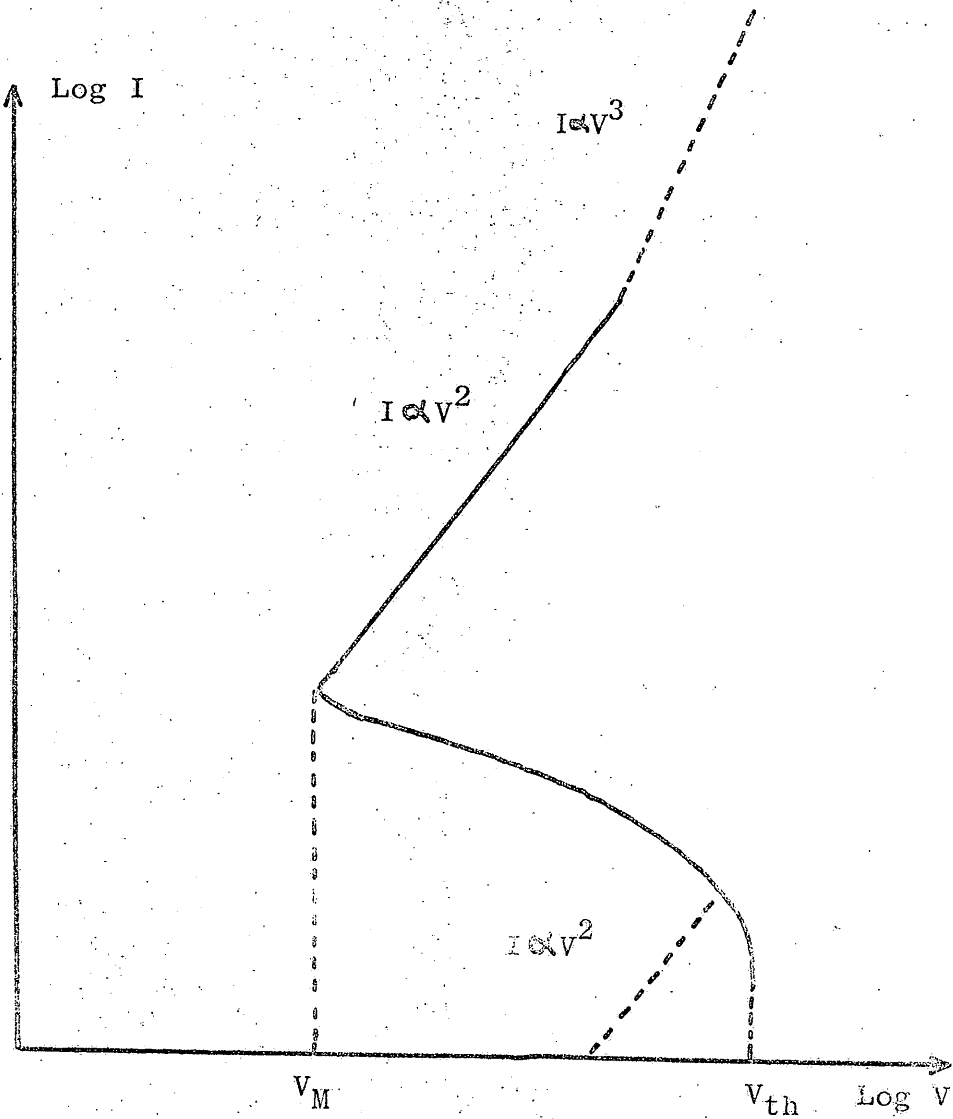

Figure 2.1.

negative resistance regime is called the semiconductor regime. This nomenclature arises because the process of populating the recombination centres with holes involves releasing electrons from the centres to the conduction band. When the centres are full of holes they thus appear to behave as shallow donors having released N_R electrons into the conduction band, and the analysis is formally similar to that of an n-type semiconductor. Lampert's expression for the current density in this regime is given by

$$J = \frac{9}{8} \cdot e \tau_{high} \mu_n \mu_p N_R \cdot \frac{V^2}{L^3} \qquad 2.8.$$

where τ_{high} is the common high injection lifetime.
This result is the same as that of the injected plasma discussed in 2.3 but with $n_T - p_T$ replaced by N_R.

At still higher injection levels assumption 1 is no longer valid and the current becomes limited by the space charge of the carriers, and the current density is given by

$$J = \frac{125}{18} \cdot e \tau_{high} \mu_n \mu_p \cdot \frac{V^3}{L^5} \qquad 2.9.$$

The complete current-voltage characteristic is shown in figure 2.1. Lampert points out that in the region where the assumption of charge neutrality obtains, the current is in no way limited by the space charge but by the recombination process. Both at very low voltages and at high voltages this is not so. In the former case the current is one carrier electron SCL current for a trap free insulator, and varies as the square of the voltage, and in the latter is 2 carrier SCL current. These two regimes which lie outside the assumptions

of the model are shown dotted in figure 2.1.

2.5. Double injection into a semi-insulator with arbitrary recombination centre occupancy.

2.5.1. The model.

Ashley and Milnes (AM)[5] extended Lampert's model of the insulator with a fully occupied recombination centre and considered the situation where there was arbitrary occupation of the recombination centre. They used this model to represent p-type germanium with an excess of acceptor levels. The device was assumed to be several diffusion lengths long and the other assumptions were the same as Lampert's assumptions numbers 2,3,4, and 7 as discussed in section 2.4. The model is split into regimes as previously.

2.5.2. The ohmic regime.

The thermal density of holes is much greater than the density of injected carriers at low voltages, so Ohm's law is obeyed. The current density is given by

$$J = e\mu_p p_T . \frac{V}{L} \qquad 2.10.$$

2.5.3. The square law region.

At any voltage both kinds of carrier can recombine owing to the presence of full and empty centres. This would lead to a space charge barrier to current flow due to electrons being trapped on the recombination centres near the cathode and to holes being trapped in front of the anode. However AM assume a finite value for p_T

and these thermal holes can relax the space charge barrier to electron flow, and prevent any significant shift in the recombination centre occupancy near the cathode. Thus the density of free electrons, n, can exceed the free hole density, p, since $p \simeq p_T$ due to the recombination barrier to hole injection in front of the anode.
AM showed that under these conditions the resulting current density was given by

$$J = \frac{9}{8} \cdot \left(\frac{\tau_n}{\tau_{rel}}\right) \cdot \epsilon \mu_n \cdot \frac{V^2}{L^3} \qquad 2.11.$$

Which is different from the trapfree insulator value by the factor τ_n/τ_{rel}. Thus the transition from the ohmic to square law region occurs at a voltage V_o, where

$$V_o = \frac{8}{9} \cdot \frac{L^2}{\mu_n \tau_n} \qquad 2.12.$$

since

$$\tau_{rel} = \frac{\epsilon}{e \mu_p p_T} \qquad 2.13.$$

2.5.4. The breakdown region.

At the breakdown voltage, the density of injected holes is large compared with p_T and thus the breakdown voltage is independent of p_T. The value of the breakdown voltage V_B was shown by AM to be

$$V_{B(AM)} = \frac{L^2 \cdot n_{RO}}{2\sqrt{\pi}} \cdot \left(\frac{e \cdot s_p \cdot N_{tp} \cdot p_{RO}}{\epsilon \cdot \mu_p \cdot N_R}\right)^{\frac{1}{2}} \qquad 2.14.$$

which can be compared with Lampert's value

$$V_{B(L)} = L^2 \cdot n_{RO} \cdot \left(\frac{s_p \cdot v_{tp}}{\mu_p}\right) \qquad 2.15.$$

Double injection into semiconductors (Ashley and Milnes).

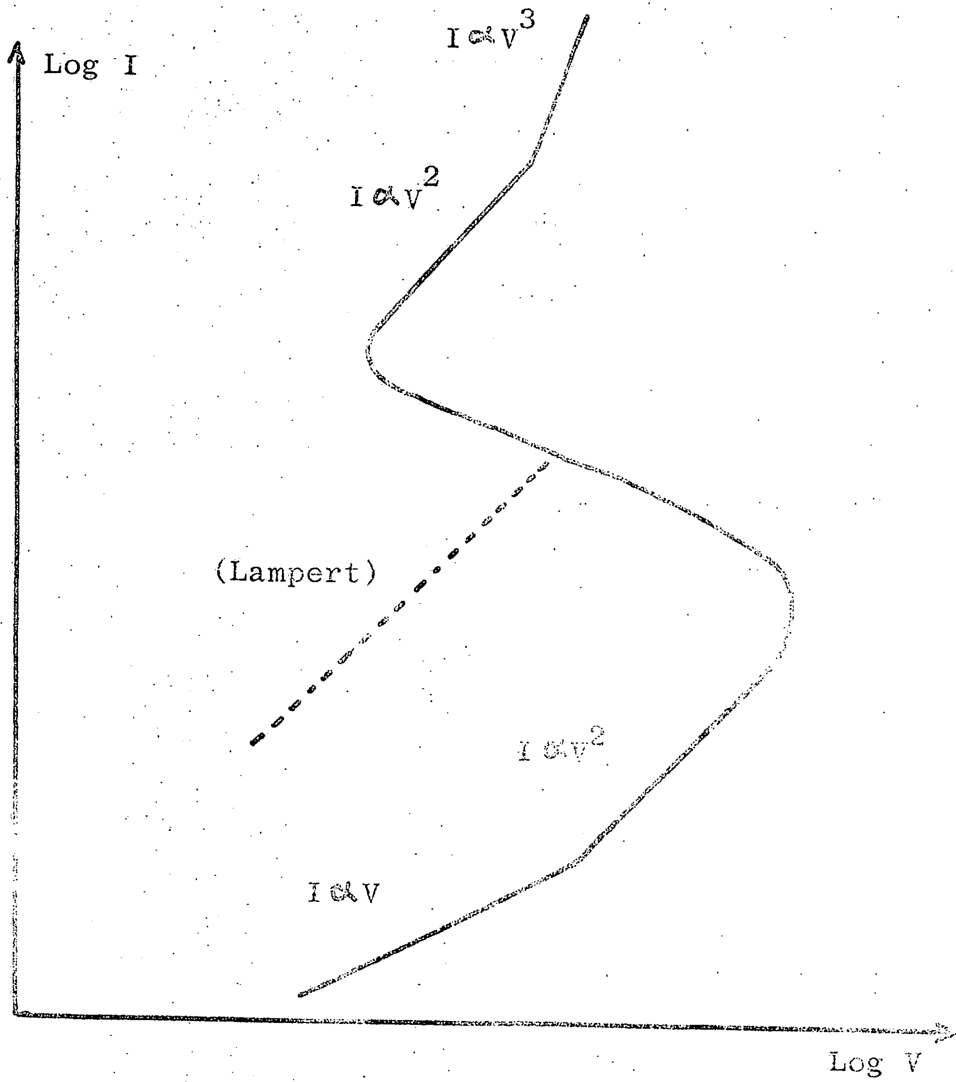

Figure 2.2.

Thus following AM we see

$$\frac{V_{B(AM)}}{V_{B(L)}} = f(Q) = Q' \qquad 2.16.$$

where

$$Q = \frac{e \mu_p p_{RO}}{\epsilon N_R \cdot s_p \cdot v_{tp}} \qquad 2.17.$$

AM took typical values for gold doped germanium on which they performed their experiments and showed that

for $Q = 10^3$, $Q' \simeq 10$

and $Q = 10^4$, $Q' \simeq 20$.

Thus it can be seen that the space charge barrier increases the breakdown voltage by about an order of magnitude.

2.5.5. The post breakdown region.

Once the holes can make a transit between the electrodes the AM model becomes similar to that of Lampert's and negative resistance followed by square then cube law dependence of the current on voltage is predicted. The conclusions of AM and Lampert are compared in figure 2.2.

2.6. A plasma injected into a semiconductor of finite cross section.

The case of an injected plasma in a semiconductor has been investigated by Hirota, Tosima, and Lampert[6] by extending the model of Lampert and Rose[2] from one dimension to two dimensions. The transverse current flow was assumed to be purely diffusive, and the

solution was obtained for cylindrical and infinite slab cross sections. They showed that provided $L_t \ll L$ where L_t is the transverse dimension and L is the electrode separation, and also $L \gg L_D$ where L_D is the diffusion length, that the equation obtained by Lampert and Rose for an n-type semiconductor, namely,

$$J = \frac{9}{8} \cdot e \tau \mu_n \mu_p (n_T - p_T) \cdot \frac{V^2}{L^3} \qquad 2.18.$$

was still valid provided that τ was replaced by τ_{eff}. τ_{eff} is an effective lifetime which takes account of the effect of surface recombination, and depends upon the geometry and on the surface recombination velocity S.

2.7. Double injection due to avalanche breakdown at a point contact.

Steele, Ando, and Lampert (SAL)[7] have explained negative resistance phenomena in germanium point contact diodes in terms of double injection in the bulk of the material after the initiation of avalanche breakdown at the point contact. The negative resistance arises because of injection of a large number of minority carriers when avalanche breakdown occurs, and the bulk current is then a 2 carrier SCL current which is maintained at a lower voltage than would be the case if the current was ohmic or a one carrier SCL current. These authors showed that for n-type material where the length of the bulk of the sample was much greater than D_1, the diameter of the majority carrier injecting contact, negative resistance would be observed when

$$E_A \cdot \left(\frac{D_2}{D_1}\right)^2 \cdot \frac{\mu_p \tau}{L} > 1 \qquad 2.19.$$

E_A is the field at which avalanche breakdown occurs in the bulk, D_1 and D_2 are the contact diameters, and L is the electrode separation. SAL also observed relaxation oscillations associated with the negative resistance and found that the maximum frequency of oscillation was consistent with minority carrier transit through the bulk being necessary for the negative resistance to occur.

2.8. Negative resistance due to internal re-absorption of light.

Dumke[8] has explained the negative resistance in GaAs p^+-p^o-n diodes as being due to the internal re-absorption of the recombination radiation associated with the double injection. The light removes electrons from the Mn levels which lie 0.1 to 0.12 eV above the valence band giving a free electron in the conduction band and a hole bound to the Mn centre. This is an analogous process to that of Lampert's[4] already discussed in section 2.4 where the recombination centres become depopulated when holes become trapped. Dumke showed that the condition for electrical breakdown was

$$\phi\gamma.\frac{\tau_n}{t_t} \simeq 1 \qquad 2.20.$$

where γ is the quantum efficiency, ϕ is the fraction of photons re-absorbed, and t_t is the electron transit time across the p region. This condition implies that during the lifetime of an optically produced bound hole τ_n/t_t electrons traverse the p^o region, one of which on average produces a photon which is re-absorbed to give a free electron-bound hole pair. Since

$$\phi\gamma.\frac{\tau_n}{t_t} = \frac{\phi\gamma\tau_n\,\mu_n}{L^2}.V \qquad 2.21$$

where V is the voltage across the p^o region, if γ is an increasing function of the current, then the breakdown condition can be maintained at progressively lower voltages and negative resistance results. Support for this theory comes from the observation that the radiated light intensity is virtually constant over a change in the current by a factor 10 in the negative resistance regime. The change in the current-voltage when external illumination is applied, and the observed steep rise in the current at constant voltage after the negative resistance region can also be explained with this model.

2.9. Current control by modulation of diffusion length.

Stafeev[9] has shown that in diodes whose thickness L is greater than the effective diffusion length $L_D = l_D \cdot \left(\frac{2b}{b+1}\right)^{1/2}$, where l_D is the hole diffusion length and b is the mobility ratio, the current is very strongly dependent on L_D and that under these circumstances the current through the diode could be controlled by modulating L_D. In fact if $\exp(L/L_D) \gg 1$ then the current I is given by

$$I = \frac{kT \cdot ch(L/L_D)}{2q\,\rho_o\,L_D(b+1)} \cdot \left\{\exp\left(\frac{qV}{ckT}\right) - 1\right\} \qquad 2.22.$$

where $$c \simeq \frac{\exp(L/L_D)}{b+1}$$

and ρ_o is the resistivity of the starting material. Because I is an exponential of an exponential of L_D, and L_D is given by

$$L_D = \sqrt{\frac{2b}{b+1}} \cdot \sqrt{\frac{kT\,\mu_p\,\tau}{q}}$$

then changes in the mobility μ_p or the lifetime τ should bring changes

in L_D, and hence large changes in I. For example if $L/L_D = 6$, a change of 20% in L_D can lead to a change in I by more than a factor 50. Stafeev predicted the following ways of modulating L_D, and hence the current through the diode.

1. Application of a magnetic field.

A magnetic field deflects the carriers and in general reduces the mobilities and in turn reduces L_D (Neglecting the change in b). For high resistivity germanium application of a field of 20,000 oersted should change the current by a factor 10.

2. Variation of lifetime with injection level.

If the carrier lifetime changes with injection level, due to a change in the occupancy of the recombination centres, then L_D also changes. In particular if the lifetime increases with injection level, then the diode should have a negative resistance region in the current-voltage characteristic.

3. Variation of lifetime with external illumination.

Application of external illumination not only produces electron-hole pairs but also changes the lifetime by altering the occupancy of the recombination centres, and thus changes L_D and hence I.

The effects 2 and 3 have relevance to the present work and the experimental evidence for their existence in CdS will be discussed later in chapter 7.

2.10. Other double injection models.

Rose[10] has compared the different models of double injection structures. The field driven models applicable to this thesis have

already been summarised. For the case where diffusion is important Rose has shown that a long extrinsic semiconductor will always begin at low voltage with field driven current flow, and will change to diffusion dominated current flow at a voltage V_{diff} given by

$$V_{diff} \simeq 2(kT/e).\ \exp(L/2L_D) \qquad 2.23.$$

where L_D is the diffusion length for free pairs. At this voltage the current starts to rise with steep exponential dependence of the form

$$J \propto \exp(e.\Delta V/kT) \qquad 2.24.$$

where $\Delta V = 0.5(V-V_{diff})$

The double injection model for CdS from the measurements performed in the course of this work will be described later in section 10.1.

CHAPTER 3

Recombination Radiation

3.1. Introduction.

If an electron makes a transition from a higher to a lower energy state, the energy lost must either be dissipated as heat in the crystal lattice by the emission of phonons, or emitted in the form of a photon of energy E where E is given by Planck's law

$$E = h\nu \qquad 3.1.$$

where ν is the photon frequency. Both processes can occur simultaneously, and the conservations of energy and momentum give the results that

$$E_i = E_f + \hbar\omega + h\nu \qquad 3.2.$$

$$\underline{k}_i = \underline{k}_f + \underline{k} + \underline{k}_L \qquad 3.3.$$

where i and f are the subscripts describing the initial and final electron states, ω is the phonon angular frequency, $\underline{k}$ is the phonon wave vector, and $\underline{k}_L$ is the photon wave vector.

3.1.1. Direct energy gap.

When the semiconductor has an E-$\underline{k}$ relationship of the form of figure 3.1.a, an electron in the conduction band makes a transition to the valence band without the co-operation of phonons and the conservation of momentum gives the condition that

$$\underline{k}_i = \underline{k}_f + \underline{k}_L$$

However, the magnitude of $\underline{k}_L$ is so small that to a good approximation

$$\underline{k}_i = \underline{k}_f$$

Direct and indirect gap semiconductors.

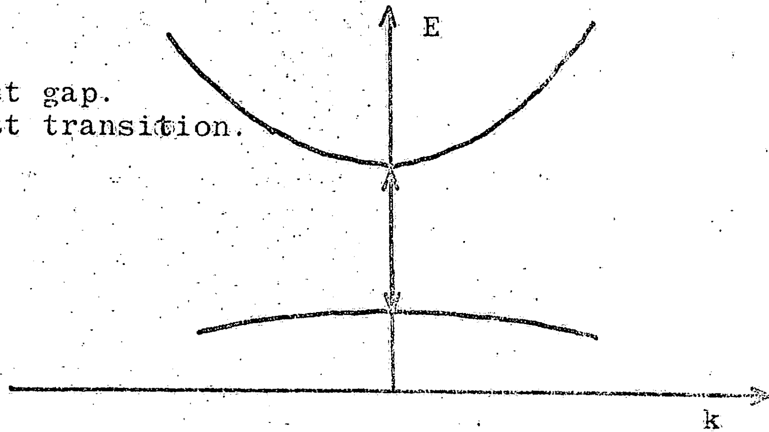

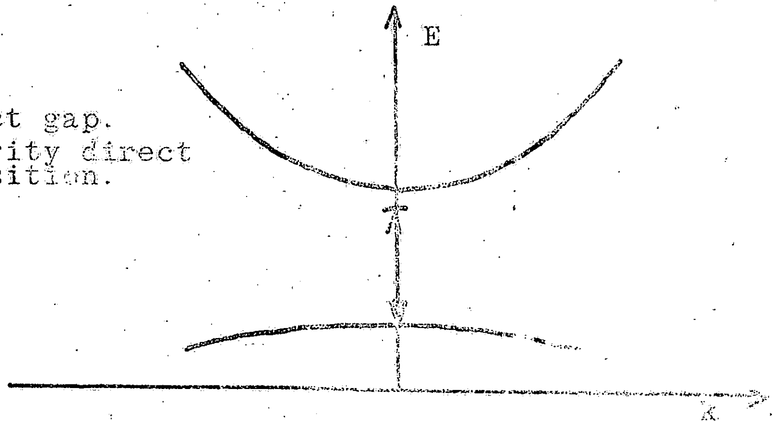

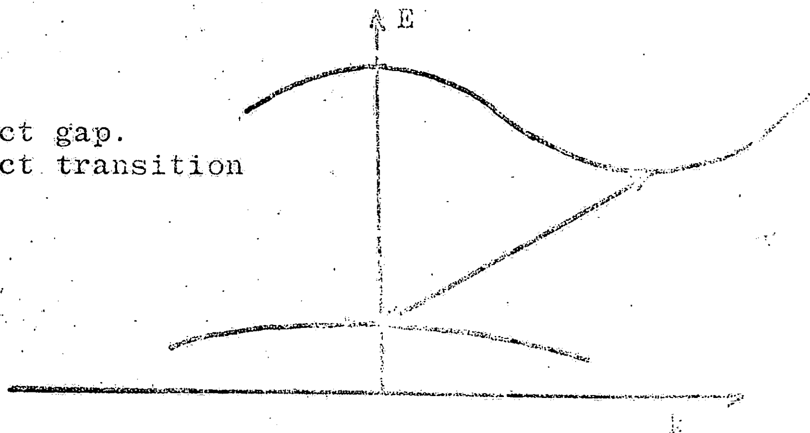

Figure 3.1.

and the transition is vertical in k-space, and this type of semiconductor is said to have a direct energy gap. The probability of an electron in the conduction band making a direct transition to an empty state in the valence band is low, and efficient direct transitions usually take place via defects which produce levels in the forbidden energy gap. This is indicated in figure 3.1.b.

3.1.2. Indirect energy gap.

When the energy gap is of the form of that in figure 3.1.c, the most probable transition is from the valley in the conduction band to the top of the valence band, and in order for the conservation of momentum to obtain, the co-operation of phonons is necessary. This is then termed an indirect transition. Direct transitions in indirect gap materials are possible but in general they have a low probability. However, light output due to direct impurity transitions has been detected from both germanium and silicon despite both these materials being indirect gap semiconductors. In practice both direct and indirect gap materials are employed in device fabrication. GaAs, CdS, and ZnS are three direct gap materials and Ge, Si, and GaP are three indirect gap materials often encountered in semiconductor technology.

3.2. Luminescence[1].

Luminescence is the term given to the emission of light following the recombination of an electron and a hole when some form of excitation is applied to the material, as distinct to the radiation that is emitted when the material is heated, which is called incandescence.

It is necessary to distinguish two types of luminescent process:

1. Fluorescence.

Fluorescence is the emission of light due to one or more spontaneous transitions from excited to ground states. A spontaneous transition is one which takes place directly without involving any intermediate state. Such transitions take place within a very short time of the application of the excitation. The fluorescent lifetime can be as short as 10^{-8} sec.

2. Phosphorescence.

Phosphorescence is that luminescent process which takes place when the emission proceeds via the release of a carrier from a metastable state to an excited state, followed by fluorescent emission. The phosphorescent lifetime can be as long as several seconds, and in general is always longer than the fluorescent lifetime. However, it is difficult to distinguish between long fluorescence due to forbidden transitions and short phosphorescence via shallow traps.

Luminescence may be initiated by a variety of excitation processes. In this thesis the three main types of luminescence to be considered are:

1. Photo-luminescence
2. Electro-luminescence
3. Cathodo-luminescence

Photo-luminescence occurs when a crystal is irradiated with light having photon energy greater than that of the forbidden energy gap.

Under such illumination, the densities of electrons and holes are greater than their thermal equilibrium values, and an enhancement of the recombination rate results. The increased recombination can lead to luminescence and when this occurs the process is termed photo-luminescence. In real crystals enhanced recombination and photo-luminescennce can result from the emptying of traps with light of photon energy less than that of the forbidden energy gap but sufficient to raise the carrier from a trap into the band. The radiative recombination is usually due to, from, or within luminescent centres having energy levels in the forbidden energy gap. These centres will be discussed in the next section.

Electro-luminescence occurs when an electric field is applied to a solid in such a way as to produce excess electrons and holes in their respective bands. Avalanche effects at high fields, in Schottky barriers for example, can create excess carriers , or alternatively the carriers may be injected into the material from opposite sides if suitable electrical contacts are used. Injection electro-luminescence is the only process of this kind to be discussed in this thesis.

When a crystal is bombarded with high energy particles, electrons may be raised from the valence to the conduction band, creating excess carrier densities in the bands. An electron gun is a convenient way of producing such excitation and with the production of excess carrier densities, radiative recombination can result as was the case with

Luminescent and non-luminescent materials.

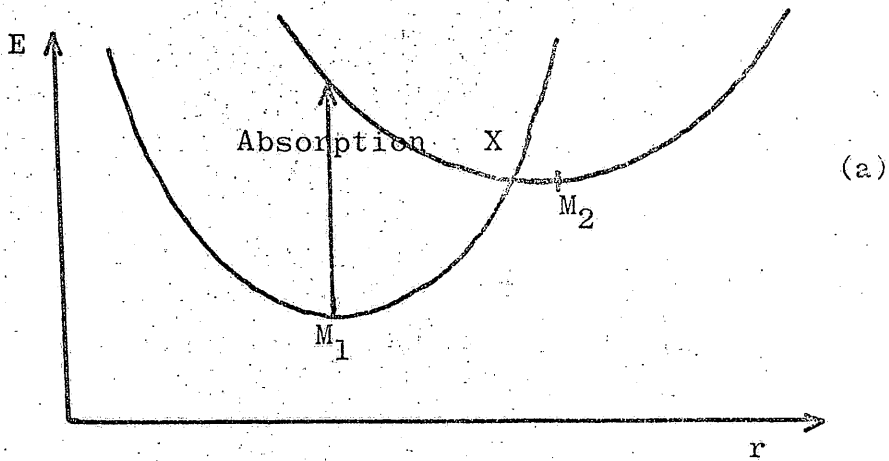

Non- Luminescent material

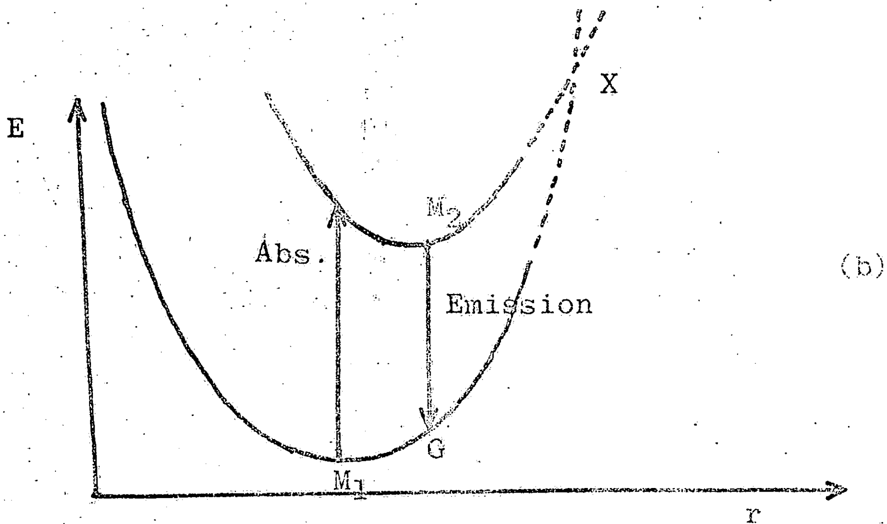

Luminescent material

Figure 3.2.

photo-excitation. Cathodo-luminescence is the term used to describe this luminescence under electron beam excitation.

3.3. Luminescent centres.

Defects and impurities in a crystal introduce discrete levels in the forbidden energy gap. Such levels can give rise to luminescent transitions. The difference between a luminescent and a non-luminescent solid may be seen by considering the configurational co-ordinate diagram shown in figure 3.2. Figure 3.2.a shows the diagram for a non-luminescent solid. An electron excited from the ground state to the excited state settles into states close to the potential minimum M_2. De-excitation of the electron can now occur by thermal activation from M_2 to X, followed by a return to the ground state potential minimum M_1 by phonon emission. In the case of a luminescent solid illustrated in figure 3.2.b, an electron in the excited state can lose energy either by thermal activation followed by phonon emission as in figure 3.2.a or by a radiative transition M_2G. The greater the energy difference between M_2 and X, the less likely the thermal activation process is and the more efficient the radiative transition becomes.

The efficiency of the luminescent process decreases as the temperature is raised. One explanation of the efficiency-temperature relationship is provided by the Schon-Klasens model. Consider a luminescent centre at an energy level E_R above the valence band. As the temperature, T, is raised the number of the centres occupied by electrons increases because the probability that an electron in the valence band can be thermally excited into the level increases.

Since free electrons in the conduction band cannot make transitions into electron occupied levels, the efficiency of the luminescence falls. This decrease in efficiency is given by

$$\eta = \frac{1}{1+A.\exp(-E_R/kT)} \qquad 3.4.$$

where η is the efficiency and A is a constant.

3.4. Recombination kinetics[2].

3.4.1. Intrinsic semiconductor.

In an intrinsic semiconductor in the absence of a disturbance there exists a dynamic equilibrium between thermally excited electrons making transitions from the valence to the conduction band, and the recombination of free electrons and holes. The rate R_{cv} at which electrons make transitions from the conduction to the valence band is given by

$$R_{cv} = rnp$$

where r is a constant. The average time that a carrier spends in the band is thus $n/R_{cv} = 1/rp$ for electrons and $p/R_{cv} = 1/rn$ for holes. If an external disturbance is applied to the semiconductor, the rate of generation of electrons from the valence to the conduction band is increased from the thermal generation rate R_{vc}, to $R_{vc} + g$, and this in turn increases the recombination rate to R'_{cv} to preserve equilibrium. Thus

$$g = R'_{cv} - R_{vc}$$

If the increases in the carrier concentrations due to the disturbance are Δn and Δp, then

$$g = r(n+p).\Delta n + r(\Delta n)^2 \qquad 3.5.$$

since $\Delta n = \Delta p$.

There are two special cases of interest:

1. Low generation rate, $\Delta n \ll n+p$

In this situation,

$$g = r(n+p)\Delta n \qquad \text{from equation 3.5.}$$

and therefore
$$\Delta n = g/r(n+p) = g\tau \qquad 3.6.$$

where τ is the lifetime of the excess carriers.

2. High generation rate, $\Delta n \gg n+p$

Equation 3.5. now simplifies to give

$$g = r(\Delta n)^2$$

and thus
$$\Delta n = (g/r)^{1/2} \qquad 3.7.$$

i.e. the excess carrier densities are proportional to the square root of the generation rate. Under these conditions no constant lifetime exists.

3.4.2. Extrinsic semiconductor—The Shockley-Read model.

The recombination of a free electron and a free hole is a relatively unlikely process and in real crystals recombination radiation is mainly associated with transitions involving a free carrier and a carrier of opposite sign trapped at a recombination centre. The analysis of such recombination is very complicated and only the simplest case will be treated. This is the Shockley-Read model[3] which consists of a semiconductor with a single set of recombination centres of density N_t at an energy level E_t. The possible transitions and

Transition rates for Shockley-Read Model.

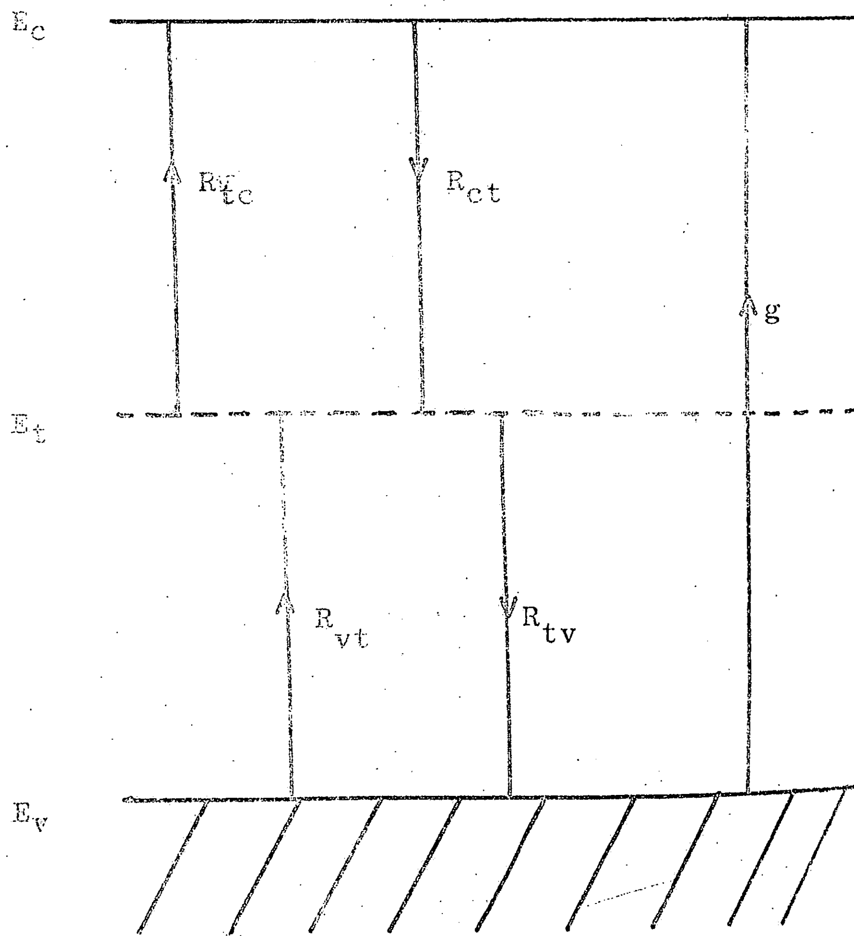

Figure 3.3.

their rates are shown in figure 3.3. The model is analysed for the case when the occupancy of the recombination centres is unchanged in the presence of excess carrier densities. Following the analysis of 3.4.1. the two cases of interest are:

1. Low injection.

The excess carrier densities are given by

$$\Delta n = \Delta p = g\tau_s \qquad 3.8.$$

where

$$\tau_s = \tau_{po}\cdot\frac{n_o + n1}{n_o + p_o} + \tau_{no}\cdot\frac{p_o + p_1}{n_o + p_o}$$

and

$$\tau_{po} = \frac{1}{r_v N_t}, \quad \tau_{no} = \frac{1}{r_c N_c}$$

r_c and r_v are the probability coefficients for the transitions, thus

$$R_{ct} = r_c \cdot n_o \cdot p_{to}$$

and

$$R_{tv} = r_v \cdot p_o \cdot n_{to}$$

n_1 and p_1 are the densities of electrons and holes which would be present in their respective bands if the Fermi level was located at the energy level E_t, i.e.

$$n_1 = N_c \cdot \exp -(E_c - E_t)/kT$$

$$p_1 = N_v \cdot \exp -(E_t - E_v)/kT$$

τ_{no} and τ_{po} are the steady state lifetimes of the minority carriers in intrinsic p- and n-type materials respectively.

2. High injection..

The excess carrier densities are now given by

$$\Delta n = \Delta p \quad (\tau_{no} + \tau_{po})g \qquad 3.9.$$

where the quantities are as already defined.

Thus the excess carrier densities are linear with the generation rate for both low and high injection, but with different steady state lifetimes in the two cases.

3.5. Excitons.

When radiation with photon energy greater than the forbidden energy gap is incident on a semiconductor, free electron-hole pairs may be created. Under certain conditions however the electron-hole pairs may be bound together in such a way that the electron executes an orbit around the hole. Such an electron-hole pair is called an exciton. An exciton has a set of allowed energy levels below the conduction band. Their depth E_n may be calculated using a simple Bohr model. Thus

$$E_n = \frac{1}{2} \cdot \frac{m' e^4}{h^2 \epsilon^2 n^2} \qquad 3.10.$$

where m' is the reduced mass of the electron-hole pair i.e. $1/m' = 1/m_e + 1/m_h$, ϵ is the dielectric constant, and n is an integer. A detailed treatment of the exciton leads to a series of energy bands rather than discrete levels, and these give rise to bands in the absorption and emission spectra of many semiconductors.

3.6. Injection electro-luminescence.

Electro-luminescence was first discovered in 1923 by Lossew[4] but the subject has advanced rapidly in the last 5 years as a result of such inventions as the injection laser which will be discussed in

section 3.7. The development of a very intense source of light which can be modulated at high frequencies is necessary for the establishment of optical telecommunication systems with large information carrying capacity, and injection electro-luminescence is one means by which this can conceivably be achieved. Electro-luminescence is usually obtained either by applying a high field to the material so that avalanche processes generate free carriers which recombine radiatively, or by injecting carriers into the bands. The former process is normally in-efficient, and the latter mechanism is the one which has the greatest potential for producing an intense efficient light source. As well as for the production of light, electro-luminescence has another use in that a study of the emission process provides information about the crystals themselves. There are three electro-luminescent structures which are of relevance to the present work.

3.6.2. Metal-semiconductor-metal.

As was shown in section 1.13 by choosing metals with suitable work functions, either kind of carrier can be injected into the semiconductor from the electrical contacts. The simplest possible structure for double injection studies consists of a semiconductor with one electron injecting and one hole injecting contact. The condition that the electrode separation should be small so that reasonably large currents can be obtained without high power dissipation in the crystal means that the metal-semiconductor-metal

structure is most conveniently fabricated by applying the electrodes to opposite faces of thin plate-like crystals.

In n-type material the choice of a low work function metal for the electron injecting contact is not difficult and indium is found to give good ohmic contact to most n-type semiconductors. However, to achieve hole injection into n-type material it is necessary to have not only a high work function metal but also the potential step that the holes have to surmount must be as small as possible. This condition means that the Fermi level should be as close to the middle of the forbidden energy gap as possible, which in turn means that the material should be as close to intrinsic as possible or should be compensated to produce as high resistivity as possible. Because gold has a fairly high work function, and can readily be applied by vacuum deposition it is a suitable hole injecting metal for n-type material. With indium and gold as electrodes on opposite faces of a CdS platelet, injection electro-luminescence has been observed at liquid nitrogen temperature. Although the efficiency decreases considerably as the temperature is raised, the light output can still be detected at room temperature.

3.6.3. The p-n junction.

This structure is used in materials which are amphoteric semiconductors, and variations of the doping levels on either side of the junction enable the ratio of the excess carrier concentrations to be varied. Efficient electro-luminescence has been observed from p-n

junctions of many of the III-V compounds. The efficiency is found to depend on the doping level of the starting material, and external efficiencies as high as 40% have been reported under conditions where the device lases. The p-n structure cannot be easily fabricated in CdS because of the high activation energy of the acceptors in the material. However, suitable hetero-junctions can be prepared. Keating[5] obtained electro-luminescence from CdS by evaporating a film of p-type Cu_2S onto high resistivity n-type CdS. Contact to the film of Cu_2S was made with an evaporated gold electrode. The emitted light was red at room temperature but too feeble for spectroscopic measurements to be made.

3.6.4. Tunnel injection.

Hole injection from a metal contact on CdS is only efficient if the Fermi level is close to the centre of the forbidden energy gap. An alternative way of injecting holes even into highly n-type material has been proposed by Fischer and Moss[6] who suggested that the semiconductor should be coated with a very thin (500 Å) film of a very wide band gap insulator e.g. Al_2O_3. The electron injecting contact may be a simmilar thin film or the usual indium contact. When a voltage is applied to the device and the resistance of the CdS reduced by irradiation with light, most of the applied voltage is developed across the insulating film. This leads to electrons tunnelling out of the valence band of the CdS into the metal through the insulator which means that holes are injected into the valence band of the CdS.

Tunnel injection.

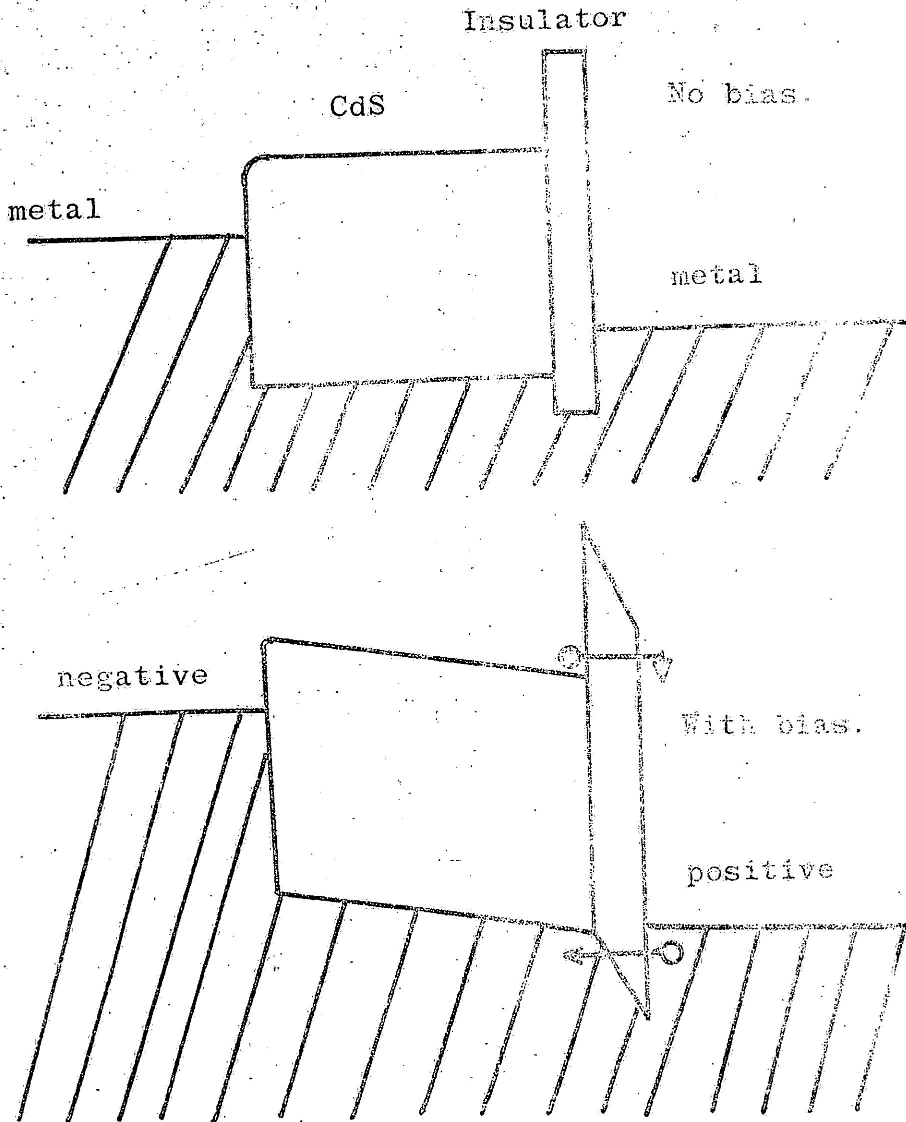

Figure 3.4.

Once the holes are injected into the bulk of the CdS the electro-luminescence proceeds as in the structure of 3.6.2. The energy band scheme for tunnel injection is shown in figure 3.4. The efficiency of the electro-luminescence can be improved by preventing the tunnel extraction of the electrons. This is achieved by using a p-type semi-conductor to make contact to the insulator so there are no states for the electrons in the conduction band to tunnel into. This structure shows promise for producing a CdS injection laser.

3.7. <u>Injection lasers</u>.

In solids where the allowed energies of the electrons form a set of discrete levels, population inversion consists in having more electrons in states of higher energy than in states of lower energy, and is equivalent to a negative temperature in the Boltzmann distribution. In semiconductors, the criterion for population inversion was found theoretically by Bernard and Duraffourg[7] who predicted the possibility of obtaining stimulated emission from semiconductors and showed that the necessary condition was

$$E_{fn}-E_{fp}=\Delta E>h\nu \qquad 3.11.$$

where ν is the frequency of the emitted photons and E_{fn} and E_{fp} are the quasi Fermi levels for electrons in the conduction band and holes in the valence band respectively. Lasing action due to injection of carriers into semiconductors has now been observed in many of the III-V compounds, and lasing action in semiconductors excited by high energy beams of electrons has also been observed. The III-V injection lasers consist of a p-n junction degenerately doped on both sides of the

junction with two parallel Fabry-Perot reflectors perpendicular to the plane of the junction. Since the III-V compounds have good cleavage properties, the reflectors may be formed by cleaving an accurately oriented slice or alternatively by polishing the crystal. At the lasing threshold the light output increases by more than two orders of magnitude, and the spectrum of the light changes from a broad band to a series of narrow lines less than 1 Å wide corresponding to the Fabry-Perot modes of the system.

CHAPTER 4

Summary of the properties of cadmium sulphide and experiments related to this work

4.1. Introduction.

Cadmium sulphide is a yellow solid at room temperature with a density of 4.82 gm cm^{-3}. It can exist in two crystallographic forms namely the α and β phases. The α phase has the hexagonal wurzite structure, and is the stable phase with lattice parameters $a = 4.14$ Å and $c = 6.72$ Å, and nearest interatomic spacing 2.52 Å. The β phase has the cubic zincblende structure and although it is unstable, thin films of this form have been reported[1].

4.2. Crystal growth.

The growth of CdS single crystals is described in Chapter 5. CdS melts at 1500 °C under a pressure of 100 atmospheres, and this high melting point coupled with the high pressure needed makes growth from the melt difficult. However, CdS sublimes readily at temperatures above 950 °C and growth of small crystals from the vapour phase can easily be achieved. The vapour phase crystals grow either as hexagonal rods typically 1 cm long and 1 mm across, or as plates with dimensions 5 mm by 5 mm by 100 microns.

4.3. Band structure.

The band structure of the II-VI compounds has been investigated theoretically by Birman[2], and by Balkanski and Des Cloiseaux[3]. The conduction band arises from the 5s cadmuim levels and the three

Band structure for CdS at k=0.

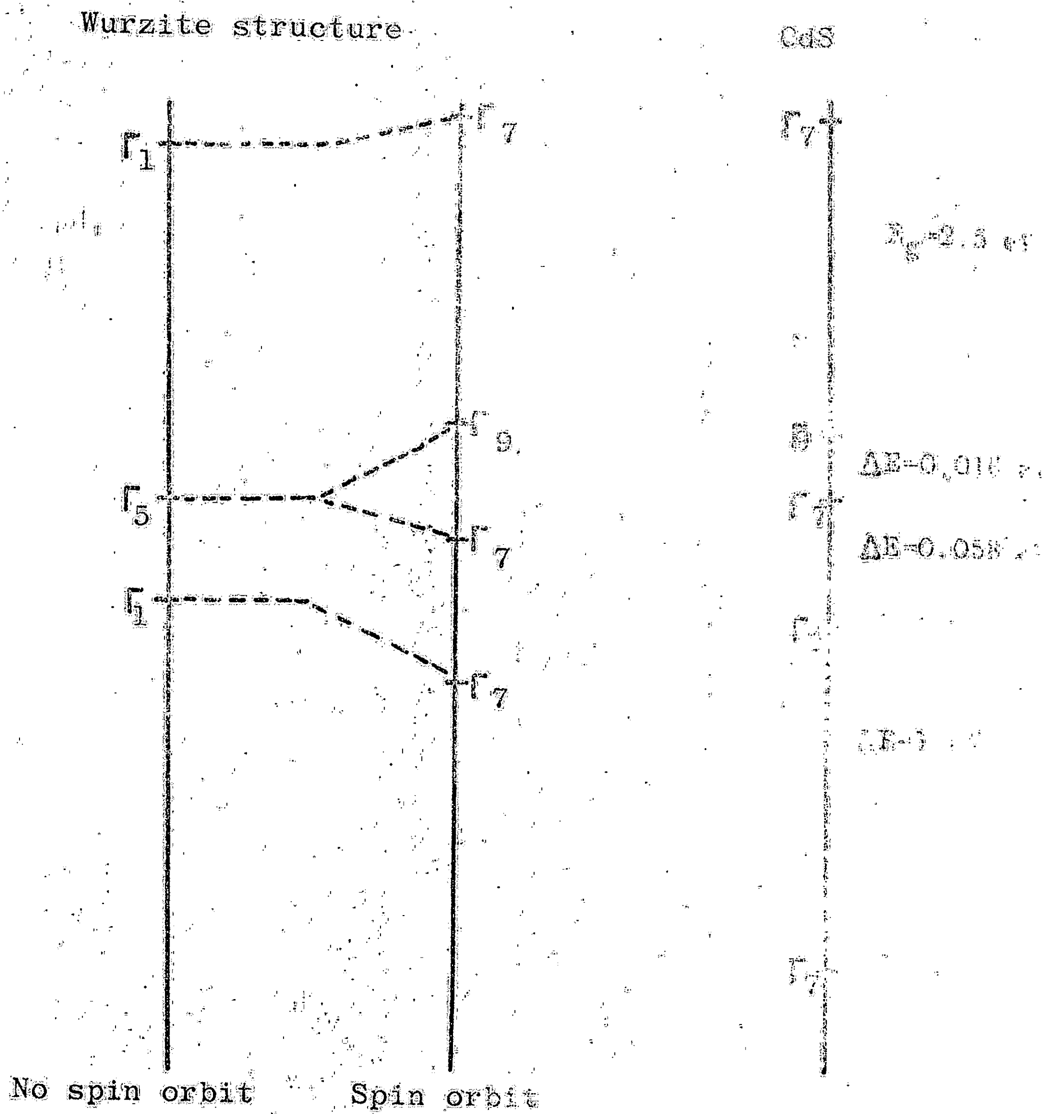

Figure 4.1.

valence bands arise from the 3p sulphur levels. Without spin-orbit coupling the top valence band is twofold degenerate and arises from the p_x and p_y states. The p_z state gives rise to the lowest valence band which is split off from the other level by the action of the crystal field. The spin-orbit coupling lifts the degeneracy of the higher level and gives rise to two levels with different symmetry. The selection rules for transitions between the valence and conduction bands are:

$\Gamma_9 \rightarrow \Gamma_7$ allowed $E \perp z$ only.

$\Gamma_7 \rightarrow \Gamma_7$ allowed $E \perp z$ and $E \parallel z$.

Balkanski and Waldron[4] determined the valence band separations by measuring the infra-red absorption with polarised light and found that the spacings were 0.016 and 0.058 eV as indicated in figure 4.1. The value of the forbidden energy gap depends upon the way in which it is measured. Sommers, Berry and Sochard[5] measured the variation of the photo-electromagnetic (PEM) effect with wavelength and found a threshold corresponding to a minimum energy gap of 2.48 eV at room temperature. Curie[6] defines the energy gap as that corresponding to the energy of radiation for which the absorbtion coefficient is 100 mm^{-1}. The values for CdS based on this definition are 2.43, 2.52, 2.55 eV at 291, 77, and 4 °K respectively. These values will be used in this thesis. They correspond to a shift of the band gap with temperature of -4.2×10^{-4} eV/°K. The actually measured shift of the band gap with temperature is 5.2×10^{-4} eV/°K in the range 77 to 291 °K[7].

The band gap is also dependent upon the applied pressure and the shift at pressures below the phase change is $+ 3.3 \times 10^{-6}$ eV/atm. At 27.5 katm the phase change from hexagonal to cubic form occurs after which the pressure dependence is very weak.[7]

4.4. Defect levels in the forbidden energy gap.

Native defects and impurities present in CdS introduce levels in the forbidden energy gap. Woods and Nicholas[8] used the technique of thermally stimulated currents to investigate the trapping spectrum of levels in the upper half of the energy gap and found levels at 0.05, 0.15, 0.25, 0.41, 0.63, and 0.83 eV below the conduction band. They proposed the following tentative origins of the levels:

0.05 eV	Doubly charged sulphur vacancy
0.15 eV	Associated with a sulphur vacancy
0.25 eV	Singly charged sulphur vacancy
0.41 eV	Unidentified neutral defect
0.63 eV	Singly positively charged cadmium vacancy
0.83 eV	Activation energy for the destruction of a trap complex.

The addition of group III metals (In, Ga, or Al) which substitute for cadmium in the lattice produces donor levels at 0.03 eV below the conduction band[9], and substitution of group VII elements (Cl, Br, or I) for sulphur also produces donor levels at a similar depth.[10]

The investigation of levels in the middle of the forbidden energy gap is difficult, but studies of the infra-red quenching[11] have shown the presence of levels at 0.75 and 1.0 eV above the valence band. Spear and Bradberry[12] measured the variation of the luminescent,

Hall Electron mobility in CdS (Kroger, Vink, and Volger).

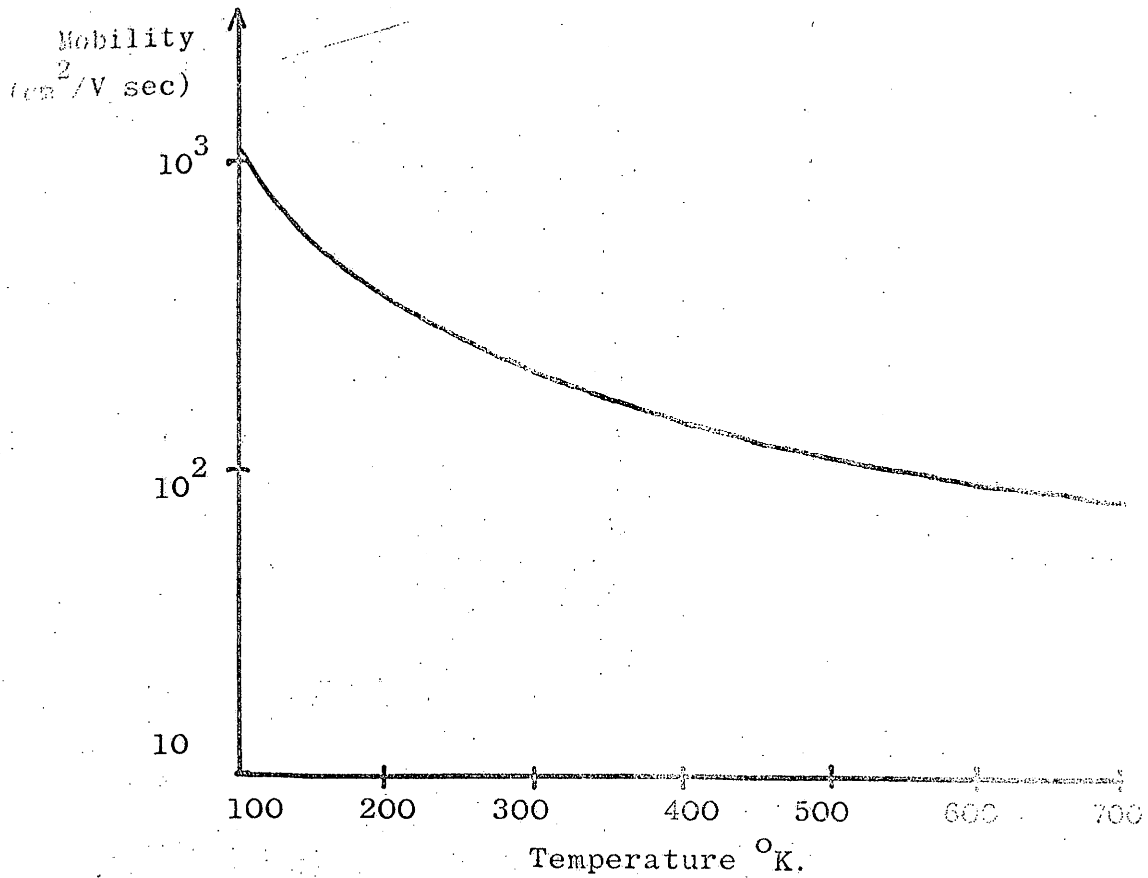

Figure 4.2.

transport, and photoconductive properties of CdS with temperature and intensity of excitation. They deduced the existence of a class II centre ($s_n \ll s_p$) at between 0.13 and 0.15 eV above the valence band. The high activation energy of acceptor levels in CdS makes it virtually impossible to produce p-type material. However Woods and Champion[13] prepared CdS crystals with high copper content (1 to 2 %) in which the current was found to be preponderantly carried by holes. The mechanism has been attributed to impurity band conduction.

4.5. Effective mass and mobility of carriers.

The effective mass of electrons in CdS has been calculated by Kröger, Vink, and Volger[9] from measurements of Hall effect, resistivity, and thermoelectric power. The variation of mobility with temperature is shown in figure 4.2. The theoretical mobility μ_{th} was fitted to this curve by assuming that the scattering was due to a mixture of acoustic mode and longitudinal optical mode phonons. The value of m_e for good fit was in the region $0.2m_e < m_e^* < 0.27m_e$ where m_e is the free electron mass. The values for the mobility are 210 and 10^3 cm^2/V sec at 300 and 100 °K respectively. Zook and Dexter[14] measured the variation of the Hall effect and magneto-resistance with temperature and obtained a value of $m_e^* = 0.25m_e$. They concluded that above 200 °K the mobility was limited by a combination of optical mode and piezo-electric scattering. Cyclotron resonance experiments[15] give an effective mass of $m_e^* = 0.25m_e$.

The effective mass of holes in CdS has been determined by Hopfield

and Thomas[16] who observed changes in the exciton absorption spectrum when the applied magnetic field was reversed. The values of the effective masses parallel and perpendicular to the c-axis for the top valence band were found to be:

$$m^{*}_{h,parl} = 0.7m_e$$

$$m^{*}_{h,perp} = 5.0m_e$$

Their results also indicated that a value of the electron effective mass of $0.2m_e$ was consistent with the conduction band minimum being situated at $\underline{k} = 0$. The drift mobility of holes and electrons in CdS has been studied by Spear and Mort[17] who used a pulse of 40 keV electrons to create free carriers. The drift mobility was then calculated from the measured transit time of the carriers. The electron mobility was found to be 265 cm^2/V sec at room temperature. The hole mobility varied from 10 to 18 cm^2/V sec depending on the crystal. The average value for the hole mobility was approximately 15 cm^2/V sec. The hole lifetime under these conditions was in the range 1 to 3×10^{-7} sec. All their results were obtained with CdS plates so the values quoted are for the direction perpendicular to the c-axis.

4.6. Modulation of the conductivity of CdS.

If a disturbance is applied to a semiconductor so that the density of free electrons and holes increases, then the conductivity increases. The disturbance may be in the form of light or high energy particles

e.g. alpha particles or electrons. The case of optical conductivity modulation or photoconductivity as it is termed is of much interest in CdS since the band gap is sufficiently large for there to be few electrons in the conduction band in pure material at room temperature, so that any disturbance has an appreciable effect, and visible light is sufficiently energetic to excite electrons from the valence to the conduction band. The photoconductive gain G of a material is defined as the number of excess charge carriers passing between the electrodes per second per photon of light absorbed. Thus if ΔI is the photocurrent and F is the number of electron-hole pairs created per second, then

$$G = \Delta I / eF$$

If the mobility ratio, b, is large so that the majority of the current is carried by electrons, then the gain can be expressed as

$$G = \tau_n / t_n$$

where τ_n is the electron lifetime, and t_n is the electron transit time. Thus high τ_n leads to high values of G. In practice the electron lifetime is governed by the presence of recombination centres in the forbidden energy gap. Following Rose[18], the following nomenclature will be used to describe different types of recombination centres:

Class I	$s_n \simeq s_p$
Class II	$s_n \ll s_p$
Class III	$s_n \gg s_p$

where s_n and s_p are the capture cross sections of the centres for

Spectral sensitivity of CdS photocurrent (Bube).

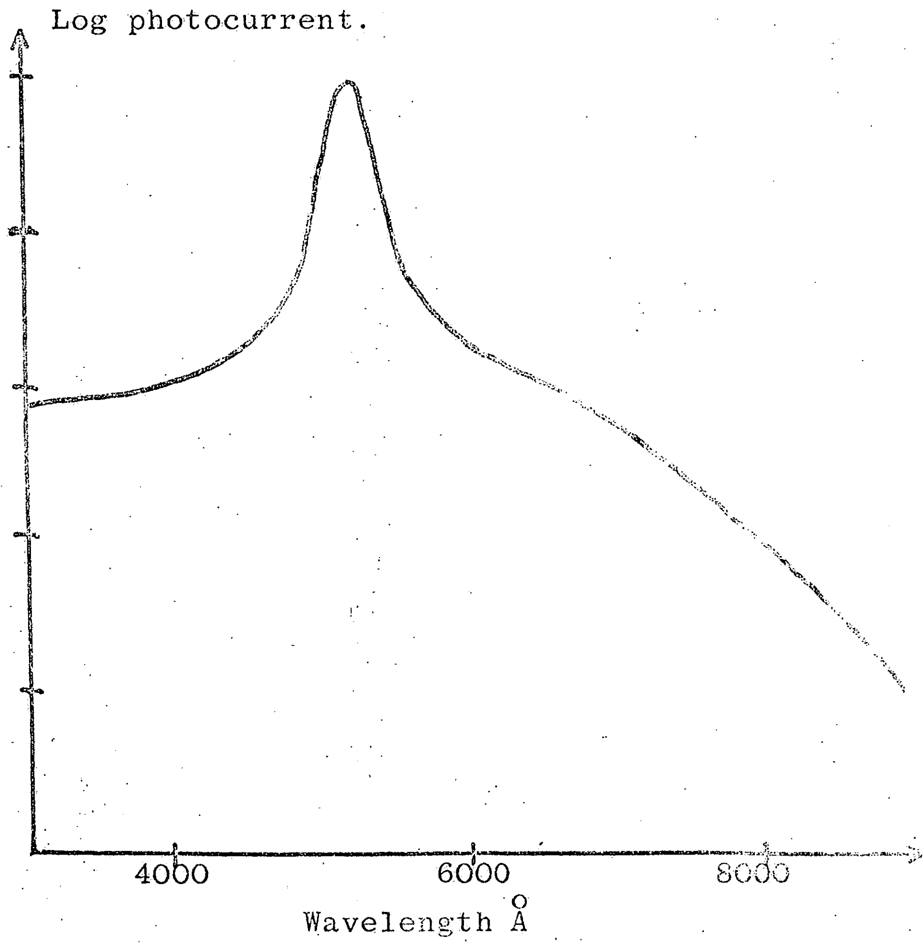

Figure 4.3.

for electrons and holes respectively. In CdS class I centres provide a fast recombination path for electrons, and lead to a small lifetime. However, it is possible to increase the electron lifetime by introducing class II centres into the material. This is known as sensitising the photoconductor. The class II centres trap the holes liberated by the excitation while the class I centres trap the electrons. However in the presence of class II centres there are very few free holes so that once a class I centre has trapped an electron it remains full and does not permit the conduction band electrons to recombine. Thus the incorporation of class II centres increases the electron lifetime and hence the photoconductive gain. The reverse of this process occurs when the photoconductor is simultaneously irradiated with infra-red illumination and visible light. Under these conditions the infra-red illumination raises electrons from the valence band to the class II centres and free holes are left in the valence band. The free holes can now migrate and recombine with conduction band electrons via the class I centres. Thus the application of the infra-red light reduces the electron lifetime and quenches the photocurrent. In CdS infra-red quenching is caused by light of 0.92 and 1.45 microns wavelength at room temperature.

The spectral response of the photocurrent in CdS is shown in figure 4.3.

4.7. Photo-excited luminescence in CdS.

4.7.1. Edge emission.

Edge emission first observed by Kröger[19], is the term used to

describe the recombination radiation which is emitted at 77 °K when CdS is irradiated with light of photon energy greater than that of the forbidden energy gap. The term arises because the emission consists of a series of overlapping bands the maxima of which are equally spaced by 300 cm^{-1} (0.037 eV), the first of which corresponds to an energy close to that of the fundamental absorption edge. The edge luminescence was assumed to be due to recombination via a single impurity level, and the series to arise from the emission of n longitudinal optical phonons ($n = 0, 1, 2, 3, 4.....$). Marshall and Mitra[20] deduced the phonon energies from infra-red transmission measurements and found 6 phonon frequencies due to longitudinal (L) and transverse (T) vibrations of the optical (O) and acoustic (A) modes. Their values were: LO = 295, TO_1 = 261, TO_2 = 238, LA = 149, TA_1 = 79, TA_2 = 70 cm^{-1}. Thus the identification of the edge emission series with longitudinal optical phonons is confirmed. Hopfield[21] has shown that the amplitudes I_n of the emission bands can be described by a Poisson distribution

$$I_n = I_o . N^n / n!$$

where n is the number of phonons emitted and N is the mean number of emitted phonons. In CdS a fit is obtained with $N = 0.87$. By measuring the edge emission of pure and doped CdS at 77 °K, Marlor and Woods[22] have shown that the edge emission series consists of two superposed phonon series due to two separate recombination paths. Their results indicated that sulphur vacancies introduce a level at 0.14 eV

Edge emission from CdS (Klick).

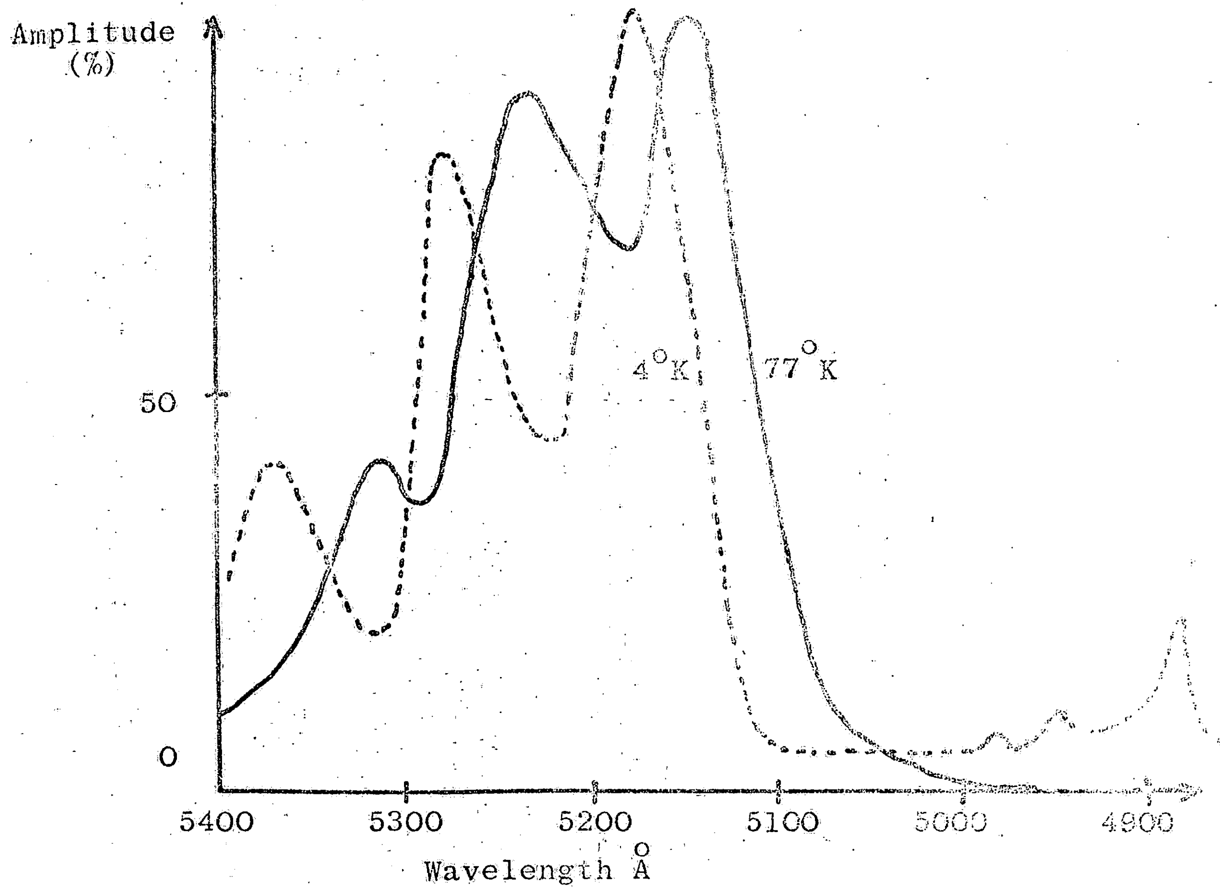

Figure 4.4.

from a band edge, and that sulphur interstitials introduce a level at 0.17 eV from a band edge at 77 °K. The edge emission of a pure CdS crystal is shown in figure 4.4[23].

Spear and Bradberry[12] concluded that the luminescent centre responsible for the green emission was a class II centre at between 0.13 and 0.15 eV above the valence band, and that it was associated with some complex defect which included at least 1 sulphur vacancy. This conclusion is in partial agreement with those of Marlor and Woods.

The nature of the edge emission changes when the CdS crystals are cooled to temperatures below 77 °K and this is shown in figure 4.4. The edge emission become sharper as the temperature is lowered, and shifts to longer wavelengths. Also at the lower temperatures hydrogen like series of lines appear at higher energies almost equal to that of the absorption edge. These are due to excitons, and at temperatures as low as 1.2 °K many of such lines can be observed. The lines are due to several exciton series and the identification of the origin of these lines has been outlined in the comprehensive review paper by Reynolds, Litton, and Collins[24]. The interpretation of the exciton lines is complex and will not be discussed here.

4.7.2. Infra-red emission.

The edge emission from CdS is associated with levels which are close to the conduction and valence bands. There are other possible luminescent transitions which involve levels in the middle of the forbidden energy gap and these give rise to emission in the infra-red.

The infra-red emission bands are centred on 0.75, 1.05, 1.6, 1.8, and 2.05 microns. Bryant and Cox[25] observed changes in the infra-red emission of pure and doped CdS when the material was heated whilst being simultaneously irradiated with visible light of broad band-width. The excitation required for maximum emission in the two bands 0.73 to 0.78, and 1.05 microns was light with wavelength shorter than the absorption edge. For maximum emission in the range 1.5 to 2.2 microns, two excitation bands at 0.6 to 1.05 and 1.3 to 1.65 microns were found. These authors concluded that the centre responsible for the emission was a complex association of defects rather than a single defect.

4.8. Cathodo-luminescence in CdS.

Cathodo-luminescence occurs when a crystal of CdS is bombarded with a beam of electrons. The incident electrons are absorbed within a shallow depth and create free electrons and holes which recombine in a manner similar to that which produces the edge emission. Balkanski and Gans[26] measured the spectral distribution of the cathodo-luminescence in CdS, andshowed that the depth of penetration x_p was given by

$$x_p = 13.9 \times E^{1.46}$$

where E is the energy of the beam in keV, and x_p is given in microns. They found that the spectral distribution of the emission corresponded to that of the edge emission in CdS with an additional high energy component which was due to direct electron-hole recombination across

the forbidden energy gap. Electron bombardment is a convenient way of creating a lerge density of free carriers which corresponds to a wide separation of the quasi-Fermi levels. Lasing action in CdS was first achieved in this way by Basov et al[27] who used 200 keV electrons for excitation. Below threshold the emission consisted of three sharp lines at 5035, 4966, and 4981 Å at temperatures close to that of liquid helium. As the beam current was increased the emission of the 4966 Å line suddenly increased by two orders of magnitude, and the width at half height of the line decreased from 35 to 7 Å. More recently Hurwitz[28] has obtained lasing action in CdS, CdSe and their mixed crystals with 40 keV electrons. He observed Fabry-Perot modes in CdS at 77 °K with a beam current of 7 mA under pulsed conditions. The peak power output was 10 W at 4910 Å with an efficiency of 0.7% at 4.2 °K.

4.9. Injection electro-luminescence in CdS.

Low field electro-luminescence (EL) in thin CdS crystals was first reported by Smith[29] who interpreted the effect in terms of hole injection from formed patches on the anode. The current-voltage characteristics contained a negative resistance region beyond which light emission was observed. The spectral distribution of the light was measured at 77 °K and consisted of two bands. The higher energy band was situated at about 4950 Å which is the wavelength of the absorption edge, and the second band was centred on 5180 Å.

Litton and Reynolds[30,31] have also studied injection EL in CdS.

Energy level model for CdS (Litton and Reynol

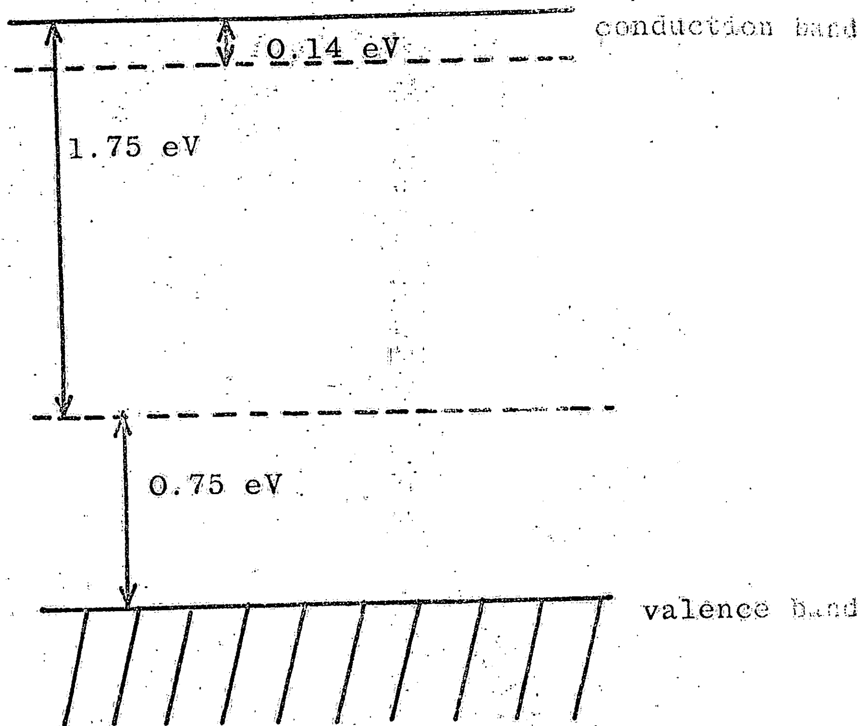

Figure 4.5.

They used silver paint as the anode material and indium as the cathode. The crystals were so called 'tap' crystals which emit light when tapped in the direction of the c-axis after they have been stimulated with light at 77 ^{o}K. The increased conductivity of these crystals is stored indefinitely after optical excitation and the conductivity may increase by up to 11 orders of magnitude on excitation. The edge emission from these 'tap' crystals is unusual in that the second band is more intense than the first. This is similar to the behaviour of doped crystals found by Marlor and Woods[22], and the 'tap' effect is attributed to the high impurity content of the crystals. The energy level scheme for the 'tap' crystals is shown in figure 4.5. The effect of light on such crystals is twofold:

1. The hole traps become filled and the hole lifetime increases.
2. The steady state hole quasi-Fermi level moves into a position more favourable for hole injection.

Since the crystals remain stimulated after the illumination has been removed, the hole trap must be a class II centre with a very small capture cross section for electrons. In all cases the unexcited crystals would withstand fields of several kV/cm without breakdown, whereas excited crystals showed negative resistance with as little as 50 V/cm applied. Litton and Reynolds interpreted the negative resistance using Lampert's theory and obtained a value of $s_p \cong 2s_n$ for the hole trap. Such a low ratio of s_p/s_n is characteristic of a class I centre and does not explain why the increase in conductivity persists

Tunnel injection electro-luminescence (O'Sullivan and Malarkey)

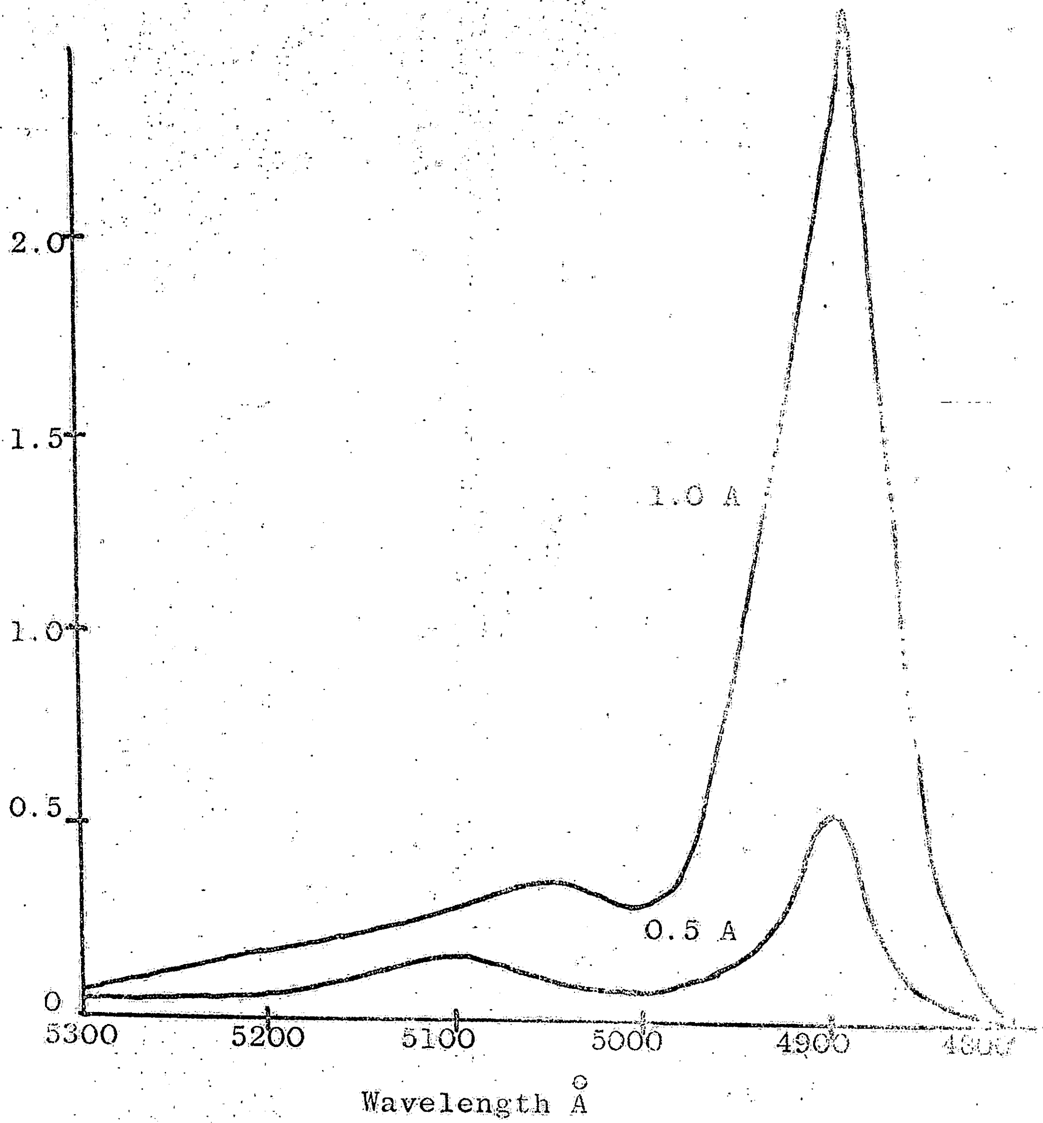

Figure 4.6.

after the illumination is removed.

Injection EL has also been observed by tunnelling holes into CdS through thin films of aluminium oxide[32]. The crystals were about 1 ohm-cm resistivity so that most of the applied voltage was dropped across the oxide film. EL was obtained with as little as 1.3 V applied to the device. O'Sullivan and Malarkey[33] produced tunnel injection EL through thin films of SiO on 0.2 ohm-cm CdS. The emission spectrum was measured at current densities up to 20,000 amps/cm^2 under pulsed conditions. The spectrum is shown in figure 4.6. The narrowing of the 4900 Å line from 100 to 35 Å as the current density is increased could be due to the onset of stimulated emission. In all devices however, destruction or saturation due to heating took place before lasing action could be achieved.

CHAPTER 5

Growth of CdS single crystals

5.1. Introduction.

The use of single crystals for the study of a given material is highly desirable. The chief reason for this is that in poly-crystalline material there is a high surface area to volume ratio compared with that for single crystals. This high ratio means that the bulk properties of the material can be masked by surface effects, and this renders the study of the basic properties of the bulk material difficult if not impossible. Many semiconductors such as germanium, silicon and the III-V compounds have a well established technology so that single crystals can be grown with closely controlled properties. The problem of producing single crystals of CdS is much more difficult, the reasons for which will be seen from the next section. In order to improve the growth techniques applicable to CdS the defects in the available material must be studied. Once the preparation of CdS crystals reaches a state comparable to that already achieved in germanium and silicon, then CdS devices will become good practical commercial propositions.

5.2. Methods of growing CdS single crystals.

5.2.1. Growth from solution.

Provided a suitable solvent exists, crystals with high melting points can often be grown from solution at temperatures appreciably lower than the melting point. CdS single crystals have been grown

by a flux melt method using cadmium chloride as the solvent. Vecht and Apling[1] recrystallised evaporated CdS thin films by dissolving them in a silicone oil which contained copper or silver diethyl-dithio carbamate complexes. These organo-metallic compounds behaved as activators. The crystals produced were either plates or feathers. No optical or electrical properties of these crystals were reported.

5.2.2. Growth from the melt.

CdS can only be melted at high temperature if a sufficiently high pressure is applied. Medcalf and Fahrig[2] melted CdS at 1500 °C under 100 atmospheres pressure of argon. Their crystal growing method was based on the techniques used by Bridgman[3] and other workers. The CdS charge was contained in a graphite crucible surrounded by a furnace. Once the charge was molten the power to the furnace was slowly reduced causing progressive freezing of the melt starting at one end of the charge. Growth started at the bottom of the crucible and proceeded vertically. Fahrig[4] reported a further extension of the work in which crystals 1 cm in diameter and 3 cm long could be grown in 8 hours and larger ingots in up to 16 hours. Doping could be achieved by adding small quantities of metallic salts to the charge before melting. Most dopants were found to distribute uniformly throughout the crystals but with some impurities segregation did occur.

5.2.3. Growth from the vapour phase (sealed system).

Growth of CdS crystals from the vapour phase can be achieved either in a sealed system or by a flow method. In sealed systems

the CdS charge is sublimed down a temperature gradient in an atmosphere of argon, hydrogen sulphide, or in vacuum. The sublimation under these conditions produces a polycrystalline boule, the crystallites of which can be as large as 10 ml in volume. Piper and Polich[5] modified this method by pulling the tube through the furnace and obtained good single crystals of 1 cm^2 cross section and 3 cm long. Clark and Woods[6] of this laboratory have reviewed the methods of growth in closed systems. These authors obtained good results by modifying Piper and Polich's arrangement. The tube was pulled through the furnace whilst an atmosphere of one atmosphere pressure of argon was maintained over the charge. This produced boules 1 cm in diameter and 3 cm long. Clark and Woods concluded that the best results would be obtained with an evacuated tube containing the charge being pulled through a vertical furnace. The important feature of this method is that exact stoichiometry of the charge must be maintained if reasonable transport is to occur. This can be seen from the results of Somorjai and Jepson[7] who showed that the rate of evaporation of crystals of CdS containing an excess of cadmium or sulphur was two orders of magnitude less than that of stoichoimetric crystals. Nitsche[8] increased the rate of transport by introducing a small quantity of iodine into a sealed evacuated ampoule. The iodine transports the CdS down a temperature gradient by reacting to form cadmium iodide and sulphur. At the cold end of the tube the reaction is reversed to give CdS and iodine. The iodine then diffuses

back down the concentration gradient. The method is only useful if contamination of the crystals by iodine can be tolerated. For most experiments on CdS the method is unsuitable since iodine forms shallow donors and conducting n-type material is produced.

5.2.4. Growth from the vapour phase (flow method).

The flow method was reintroduced by Frerichs[9] who reacted streams of cadmium vapour and hydrogen sulphide. The cadmium vapour was carried in hydrogen. The vapours passed through a high temperature region at 1100 °C and the CdS condensed in the cooler part of the furnace on a silica substrate at about 900 °C. Fahrig[4] synthesised CdS from the purified elements. The cadmium and sulphur vapours were transported into the reaction chamber from separate boilers. An inert carrier gas was used. The conditions were such that the growth took place in an atmosphere containing a non-stoichiometric excess of sulphur. Stanley[10] sublimed CdS powder in an oxygen free stream of nitrogen. The CdS powder charge had been prepared by precipitation from solutions of cadmium salts. Fochs[11] modified Stanley's technique by varying the growth temperature during the run. This enabled the crystals to grow separately from one another and thus attain larger dimensions. Vecht, Ely, and Apling have shown that CdS is purified by the partial sublimation process since non-volatile impurities remain in the unsublimed residue, and impurities more volatile than CdS condense beyond the growth region.

Woods[13] has studied the growth habit of CdS crystals grown by

Frerichs' method. The majority of the crystals were found to be rods or rectangular plates with the c-axis in the plane of the plate. Ibuki[14] came to a similar conclusion for CdS crystals grown by Stanley's technique.

5.3. Choice of method for growing CdS crystals for double injection experiments.

The requirements for double injection experiments are such that thin plates of CdS are essential if convenient low voltages (less than 1 kV) are to be employed. The flow methods of Frerichs and Stanley both produce thin plates and are therefore most suitable. The Frerichs technique was not practicable in these laboratories because of inadequate fume extraction facilities. Stanley's method had been used here previously by Clark, Nicholas, and Marlor with considerable success and was therefore selected. Furthermore it had the advantage that the apparatus could be set up quickly and relatively cheaply. The main disadvantage is that stoichiometry of the crystals is difficult to control using this method since growth takes place under non-equilibrium conditions.

5.4. Description of the crystal growing apparatus.

A schematic diagram of the apparatus is shown in figure 5.1, and a photograph of the equipment in figure 5.2. The argon gas was supplied by B.O.C. Ltd. and was 99.995% pure. It was passed via the cylinder reduction valve to a conventional vacuum needle valve. The stability of the flow was such that in a run of 2 hours duration the maximum drift in the flow rate of 180 ml/min was ±5 ml/min. The

Flow chart for crystal growth.

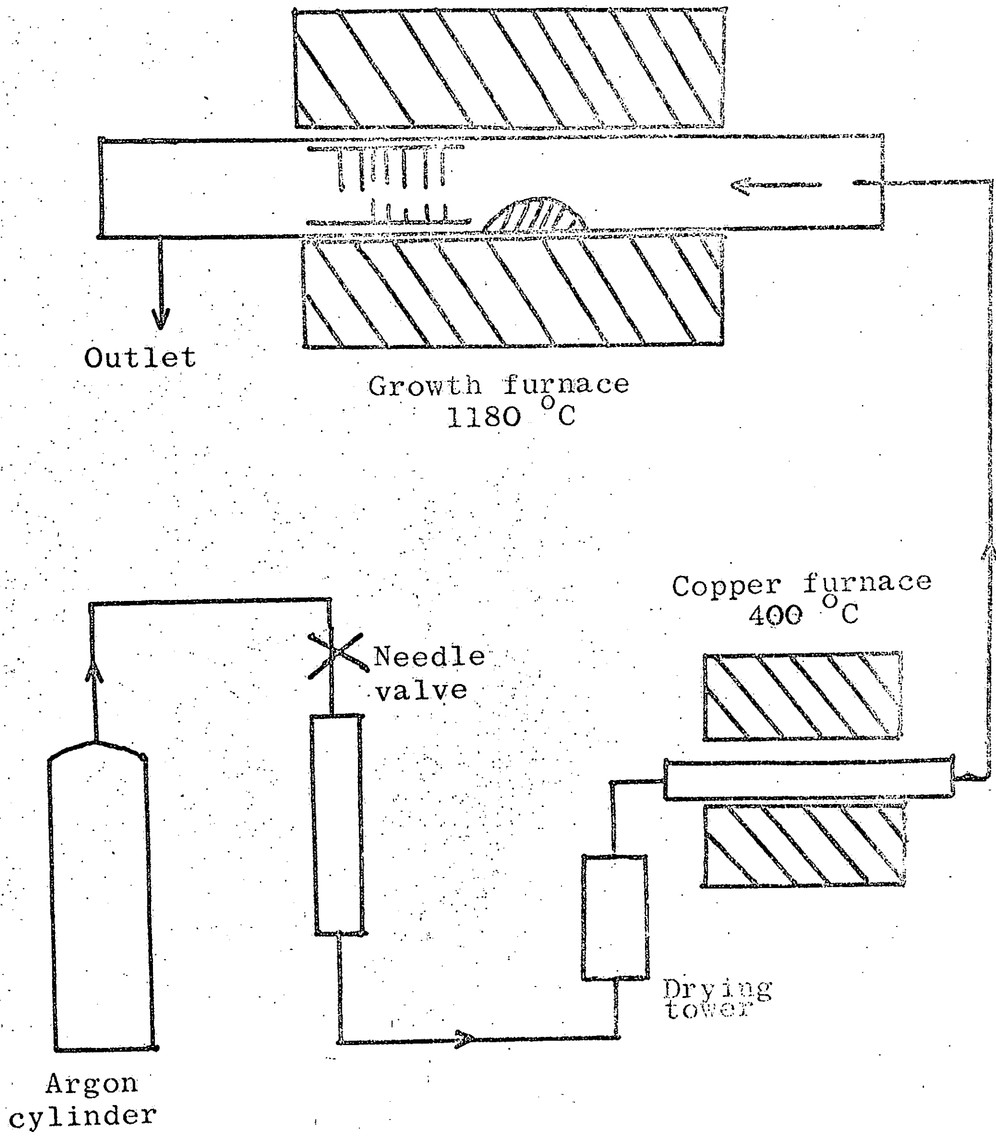

Figure 5.1.

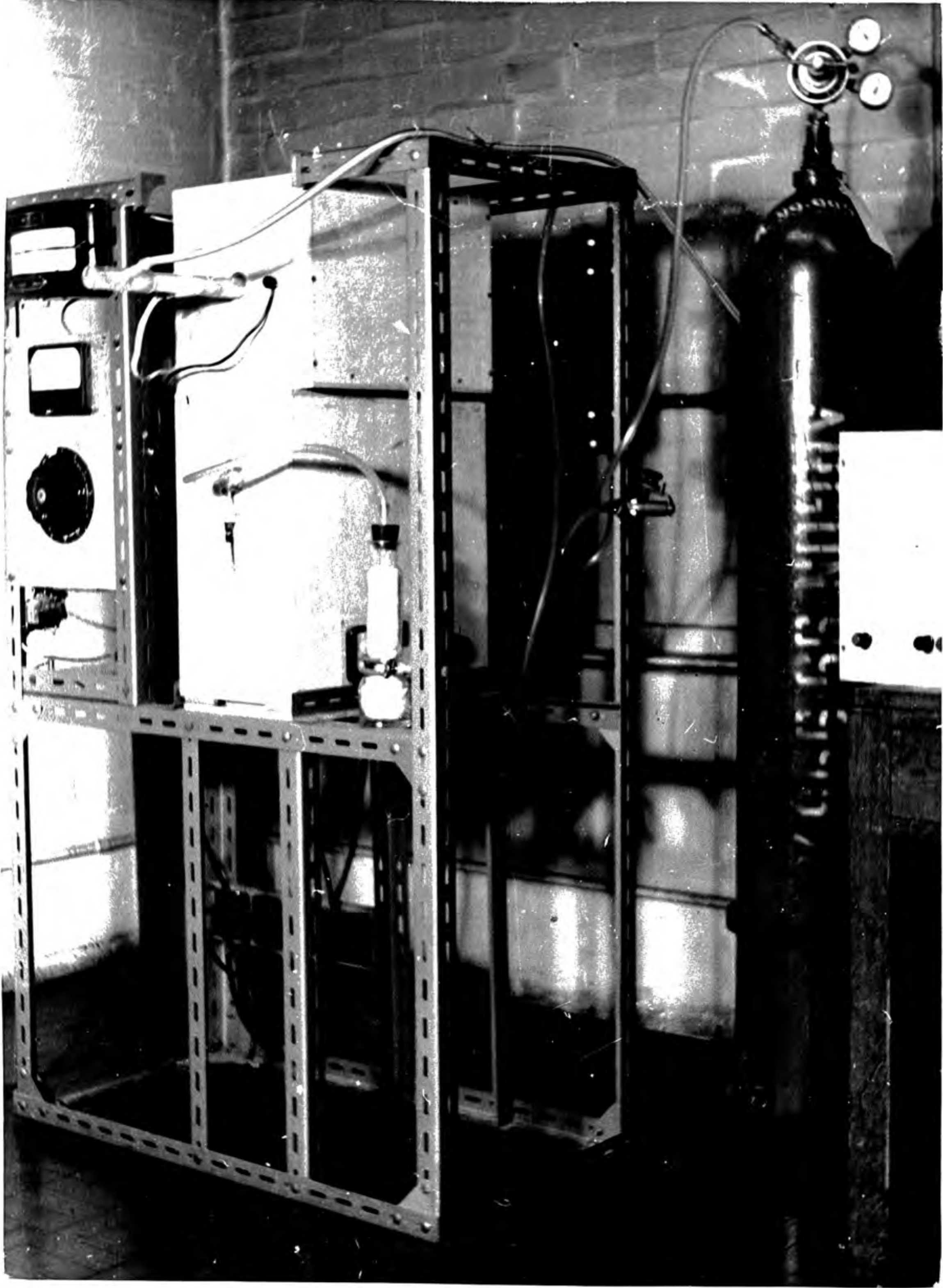

Figure 5.2.

Temperature profile of crystal growing furnace.

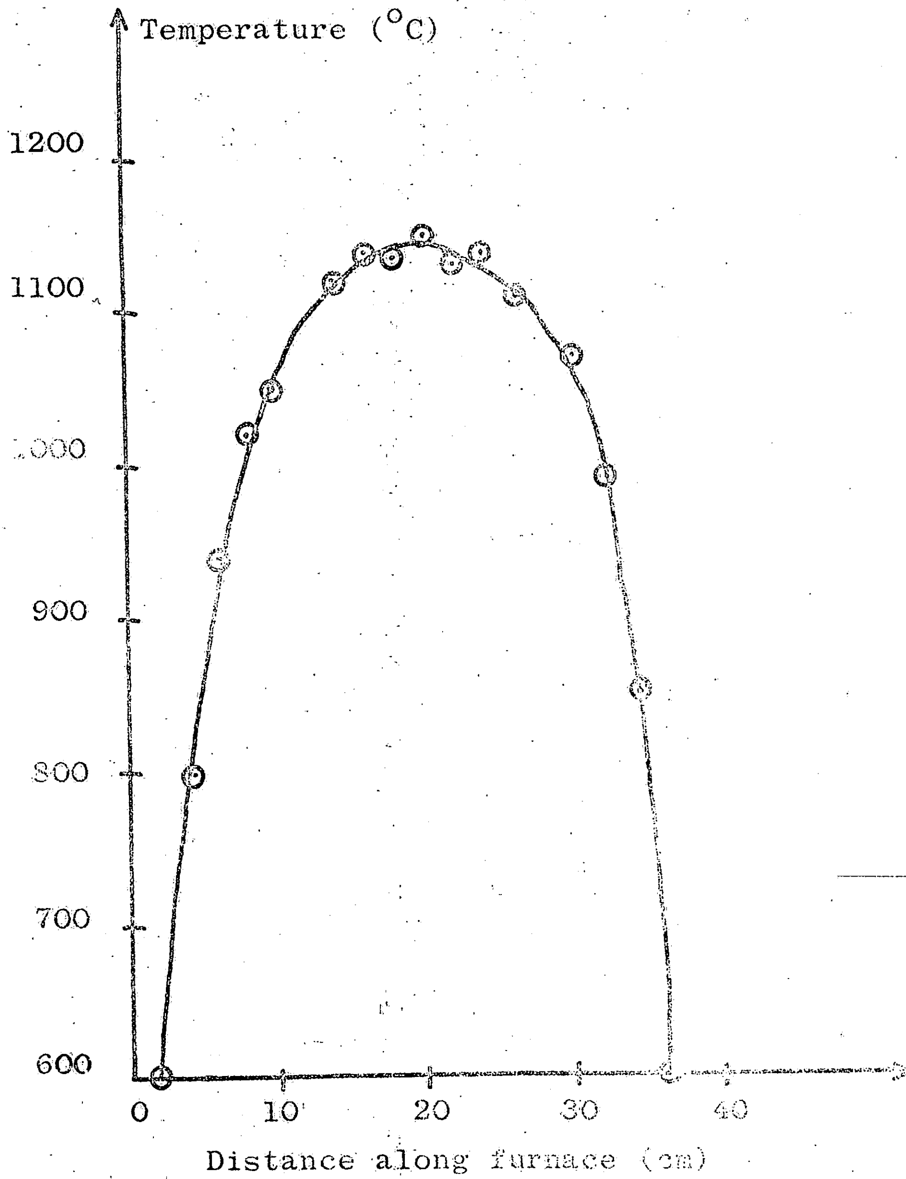

Figure 5.3.

needle valve also enabled fine adjustments to be made. The argon then passed through a drying tower containing calcium aluminium silicate to remove any water from the gas. A Rotameter flow meter was used to measure the flow rate, and heated copper turnings at a temperature of 400 °C removed oxygen from the gas stream. At this stage the purified argon entered the silica growth tube, passed over the heated charge at 1180 °C, and finally left the system via an exhaust pipe into the atmosphere. Growth took place on a split silica liner which was a close fit in the tube. The use of the liner facilitated the removal of the crystals without breaking them. A substrate was present on the liner from previous runs and this also assisted in preventing diffusion of impurities from the silica into the crystals, and at the same time provided nucleation centres for growth[12]. The growth ofthe crystals could be observed through the flat silica end plate connected to the growth tube by a cone and socket joint.

The electric furnace for heating the CdS charge comprised a lagged mullite tube wound with Kanthal A wire in a single untapped winding. The temperature profile of the furnace is shown in figure 5.3. The temperature of the charge was measured with a Pt:Pt 13% Rh thermocouple placed between the growth tube and the mullite tube. The furnace temperature was stabilised with an Ether 991 on/off anticipatory temperature controller which was used to switch a resistance is series with the winding. The resistance reduced the

current through the furnace by 30%. With this arrangement the control was better than 5 °C at 1180 °C.

5.5. Pre-treatment of the starting charge.

Ideally the starting CdS powder should be pure and stoichiometric. Jackson[15] at A.E.I., Rugby has prepared ultra-pure CdS powder with a total metallic impurity content of less than 1 ppm. His method is as follows: cadmium chloride solution and an organo-sulphur compound are purified by ion exchange. The two pure solutions are then mixed together with vigorous stirring. The chemical reaction that takes place gives homogeneous precipitation of CdS which ensures that stoichiometry results. The reaction proceeds at room temperature so that there is no tendency for the CdS to dissociate. Unfortunately the price of such ultra-pure CdS powder is prohibitively high. Suitable CdS can be obtained commercially in less pure form but must be given some initial heat treatment to remove volatile impurities. During this work, the starting material has been bought from two sources namely L.Light and Co., and Derby Luminescent Co. The latter produce powder with better uniformity from batch to batch as judged by the crystal yield from a large number of runs. In both cases the CdS is prepared by precipitation from cadmium chloride solution using ammonium sulphide. As a result the powder can contain as much as 15% of ammonium chloride. The heat treatment is designed to remove the ammonium chloride from the powder so that chlorine doped crystals are not produced. The powder is baked at 500 °C under vacuum whilst

being continuously pumped. A bake of 6 hours duration was found to change the colour of the powder from orange to pale yellow. 500 °C was chosen as the upper limit in temperature for the bake since at higher temperatures significant dissociation of the CdS with the resultant loss of sulphur would occur. The powder was spread over the bottom of a 10 cm diameter pyrex vessel. The pumping was carried out through a 3 cm diameter outlet pipe opposite the large surface area of the powder. The high vacuum was provided by a mercury diffusion pump backed by a conventional rotary oil pump. A liquid nitrogen cold trap was employed to prevent contamination of the powder by mercury vapour. The starting pressure was 10^{-5} torr as measured on a McLeod gauge and never rose above 10^{-3} torr during the whole out-gassing period. This bake was the only pre-treatment given to the CdS powder.

5.6. Procedure for crystal growth.

Some 30 gm of the baked out powder was loaded into the centre of the 27 mm internal diameter silica tube. The 12 cm long split cylinder silica liner was placed adjacent to the charge and extended to the edge of the furnace. The argon flow was then turned on and adjusted to 180 ml/min whilst the copper furnace was brought up to temperature in 30 min. During this time the growth tube was flushed with argon. The growth furnace was then switched on and with 6 amps passing took 30 min to reach the sublimation temperature of 1180 °C. Growth

Figure 5.4.

was observed from time to time through the end window, and the run was stopped when the tube was completely blocked with crystals. This occurred when half to two thirds of the charge had sublimed. The furnace was then allowed to cool (usually overnight) with the argon flowing. The liner and residue were removed from the tube when it was cold. Finally the split cylinder was opened out and the crystals removed with fine tweezers. A good run produces of the order of 20 clear unstriated plates varying in area from 4 to 25 mm^2, and in thickness from 20 to 300 microns. A photograph of some plates is shown in figure 5.4. When undoped crystals were grown, the tube and liner were washed only after about every 8 runs (following reference 12).

5.7. Observations during growth.

As the furnace temperature was raised beyong 600 °C, the last residual volatile impurities remaining from the bake were removed from the charge into the carrier gas. At 600 °C a white smoke could be seen which disappeared at 700 °C. This was probably the last remaining small trace of ammonium chloride. Observation of the gas flow showed that the flow is streamlined in two counter-rotating currents. The longitudinal velocity of the gas was approximately 5 mm/sec which is consistent with streamline flow. At still higher temperatures in the range 700 to 1000 °C the vapour was black indicating that free cadmium was being evolved from the charge. This cadmium was carried in the gas stream and condensed on the cold part of the tube outside the

furnace. Some of the cadmium diffused backwards against the gas flow and condensed on the tube at the entrance to the furnace. Once the temperature reached 1100 °C the gas flow was clear. At this temperature it could be seen that growth had already started. The growth started on the roof of the liner and later proceeded from all parts of it. Plates grew either directly on the substrate, or like flags on flag-poles from thin needles. The growth took place in the temperature range 850 to 950 °C. There was no correlation between the growth temperature and the degree of striation of the plates. Good clear plates could be found at all places in the growth region. One of the most important conditions for the production of good plates was stability of the gas flow. Temperature stability did not seem to have any effect on the quality ofthe plates in agreement with the findings of Fochs[11] who varied the growth temperature deliberately. Rods were produced in all runs even when the conditions favoured the growth of plates.

5.8. Addition of excess sulphur to the starting charge.

The large quantity of cadmium deposited on the cold part of the tube indicated that the starting charge was cadmium rich. Similar conclusions have been reached by Clark. Therefore, in order to improve the stoichiometry of the crystals, 1 or 2% of sulphur was added to the 30 gm charge. The sulphur was 6N purity supplied by L.Light and Co. It was hoped that the sulphur would react with the cadmium before the sulphur boiled away. The result of utilising excess sulphur

was that the yield of plates was improved. Such plates were also less striated and of larger area than those produced without the addition of sulphur. It seems reasonable to conclude that the excess sulphur improved the stoichiometry of the charge which in turn led to the better yield. It follows therefore that stoichiometric growth conditions favour the plate habit. Good electro-luminescent devices were fabricated from the crystals grown from a charge containing excess sulphur.

5.9. Purity of the crystals.

No sensitive analytical facilities were available in these laboratories. However, a mass spectrometer analysis of a small number of crystals was carried out at U.K.A.E.A., Capenhurst. Whilst the results are only accurate to 50%, the trends are shown. The analysis showed that the main contribution to the impurity content was due to 130 ppm of zinc, 8 ppm of silicon, and 4 ppm of nickel. Other metallic impurities were present in small quantities totalling 10 ppm. The values for the starting powder were 60 ppm of zinc, 80 ppm of silicon, 25 ppm of nickel, andothers totalling 30 ppm. Apart from the increase in zinc concentration, the sublimation did purify the CdS to some extent, in agreement with the findings of Vecht, Ely, and Apling[12].

5.10. Doped crystal growth.

Stanley's method is highly suitable for the production of doped crystals. The doped crystals were grown mainly for luminescence

measurements done as a separate piece of work by Guy Marlor. The dopants were introduced into the gas flow prior to its entering the furnace, or were placed in a silica boat in the furnace in front of the charge, or were mixed with the charge itsself. The range of dopants used is tabulated below in table 5.1.

Table 5.1.

Dopant	Group	Method of incorporation
Copper	Ib	Copper sulphide mixed with the charge
Aluminium Indium Boron Gallium Thallium	III	Metal in silica boat
Oxygen	VI	Carrier gas 95% argon, 5% oxygen
Chlorine	VII	Argon bubbled through HCl
Indium: Chlorine	III-VII	Indium chloride mixed with the charge
Copper: Chlorine	Ib -VII	As for copper and chlorine combined

The effect of dopants was to alter the growth rate and to modify the crystal habit. For example oxygen enhanced the growth rate and gave a good yield of plates. On the other hand the group III metals slowed down the rate of growth and produced crystals mostly in the form of hollow cones. Details of the crystal growing runs are listed in Appendix 1.

5.11. Conclusions.

Stanley's method provides plates suitable for double injection

experiments. The addition of 1% excess sulphur to the starting charge enhances the yield of plates with a high degree of crystalline perfection. The sulphur improves the stoichiometry of the charge and this is reflected in the growing conditions. More than 50 runs have been carried out in the course of this work to produce both pure and doped crystals of CdS for the fabrication of electro-luminescent devices.

CHAPTER 6

Measurements of the spectral distribution of the luminescence from cadmium sulphide

6.1. Introduction.

Measurements of the spectral distribution of the luminescence of pure CdS crystals have been made at temperatures close to that of liquid nitrogen. A comparison has been made of the photo-, cathodo-, and electro-luminescent spectra. The wavelength range covered in the measurements was from 4800 to 6000 Å.

6.2. Experimental.

The measurements were made using an Optica CF4-DRNI continuously recording spectrophotometer which has a range from 1850 Å to 4 microns. The instrument is a double beam, grating spectrophotometer with best resolution of about 2 Å. For these measurements the single beam mode was employed. In this mode the input signal is compared with a constant reference signal. The difference between the input and the reference is amplified and read out by a Honeywell potentiometric chart recorder. The light input is converted into an electrical signal by an R.C.A. IP 28 photomultiplier. The results presented in this chapter are not corrected for the spectral response of the photomultiplier. The data from the chart recorder was analysed by translating the graphs into digital form with a d-MAC mechanical digitiser type FD 8 which enabled a large number (of the order of 300 per graph) of points to be printed out onto 5-hole paper tape. The accuracy of

the digitiser is 0.01 cm. The wavelengths of the peaks in the spectra were measured with the digitiser, and a simple computer programme enabled the wavelength, energy, and wave number of each peak to be printed out. The computer programme is shown in Appendix 2. Since many scanning speeds were employed it was necessary for ease of comparison to alter the wavelength scales of the various graphs so that the abscissae were identical and thus a unified presentation could be given. This was achieved by scaling the digitised points with the Elliott 803 computer, and drawing out the scaled graphs with a Benson-Lehner digital incremental graph plotter type 121. The graph plotter joins up the points with a series of straight lines in steps of 0.005 inches. The programme used to scale the points is shown in Appendix 3, and this was used with a pre-compiled graph plotter package. I am most grateful to Mike Holroyd of the Geophysics department for his assistance with graph scaling proceedures. A control test was made to ensure that the wavelengths of the peaks corresponded with the values obtained by measuring the graphs directly. The agreement was better than 5 Å, which is the best accuracy to which the peaks could be located. All wavelength values are quoted to the nearest Angstrom unit.

The photo-luminescence was excited by a high pressure mercury lamp. The current through the lamp was stabilised to reduce noise and the power dissipation was 500 Watts. The 3650 Å excitation wavelength was selected by passing the light from the lamp through Chance glass filters to remove the unwanted mercury lines. The light

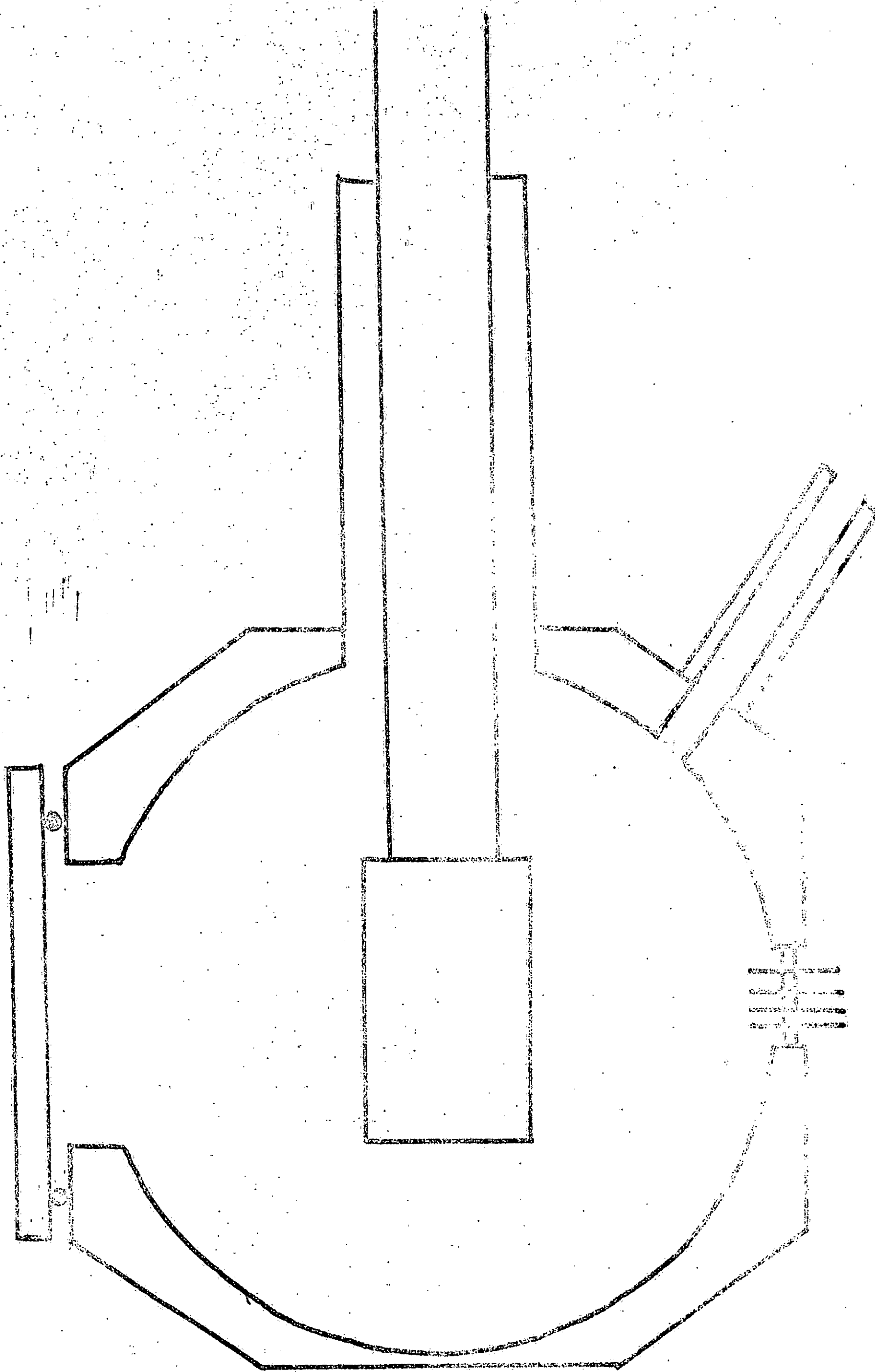

All metal cryostat.

Figure 6.1

Current stabilising circuit.

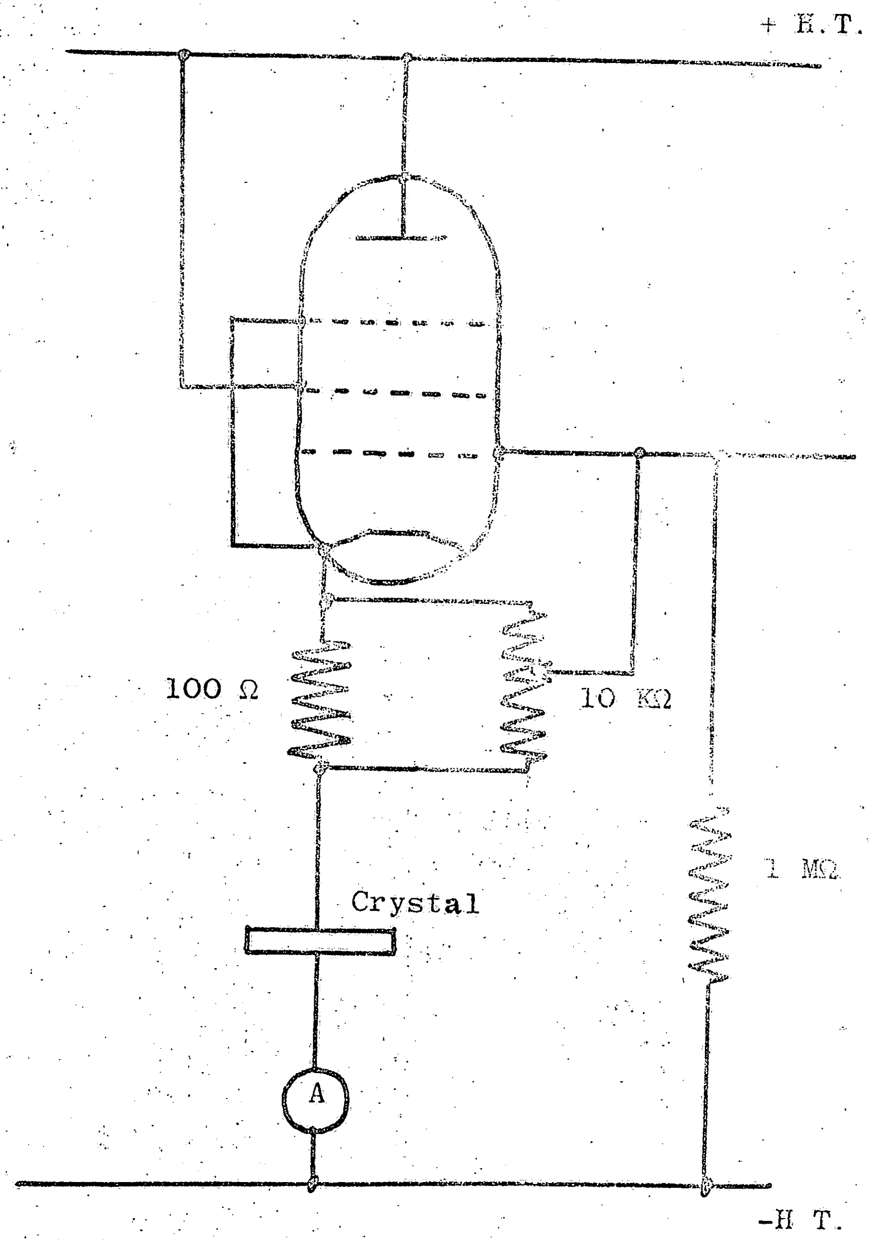

Figure 6.2.

was focussed onto the crystal by a large diameter condenser lens. The devices were mounted on the copper block of an all metal cryostat, the design of which is shown in figure 6.1. The cryostat was evacuated with an Edwards rotary oil pump type ES 35 and the temperature of the crystal was monitored with a copper-constantan thermocouple attached to the copper block close to the crystal. The normal operating temperature of the cryostat was in the region of 100 ^{o}K but temperatures as low as 85 ^{o}K were frequently attained. The electro-luminescent spectra were obtained from the light emitting devices, the construction of which is described in Appendix 4. The D.C. spectra were obtained with the device connected in a circuit designed to stabilise the current flow. The circuit is the simple negative feedback arrangement shown in figure 6.2. For the spectra measured with pulsed D.C. applied across the device, the same experimental arrangement as is described in section 7.2 was employed. For the cathodo-luminescent spectra an all glass cryostat was used. The cryostat was evacuated to a high vacuum by a mercury diffusion pump with a liquid nitrogen cold trap. The G.E.C. electrostatically focussed electron gun had a maximum operating voltage of 14 kV.

6.3. Photo-luminescent spectra of pure CdS crystals.

The photo-luminescent spectrum of a pure CdS crystal is shown in figure 6.3. The crystal was grown with excess sulphur added to the starting charge. Most of the devices examined were made from such crystals. The emission consists of the normal edge emission from CdS with two additional bands centred at approximately 4950 and

Photo-luminescence of device 39

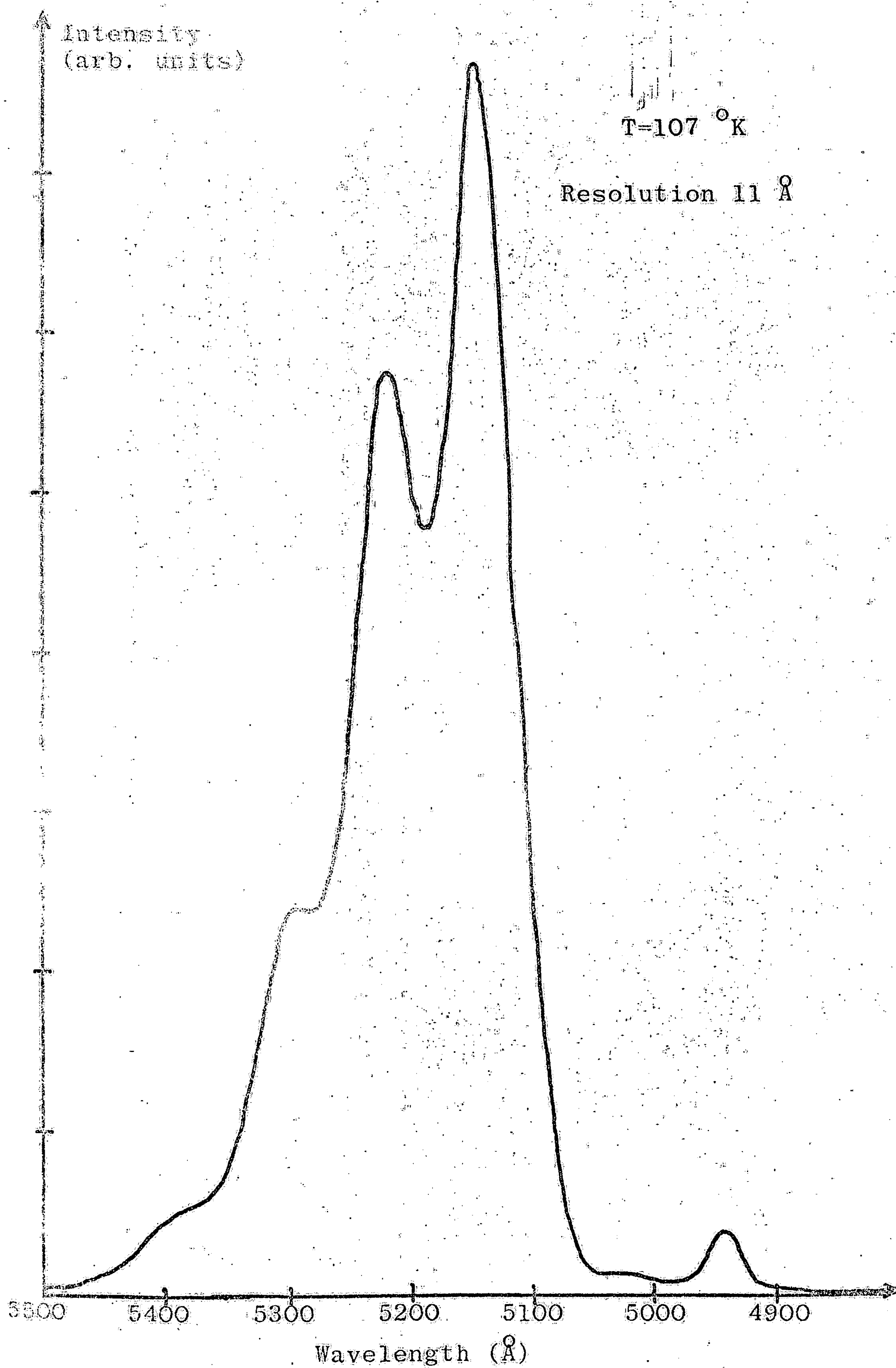

Figure 6.3

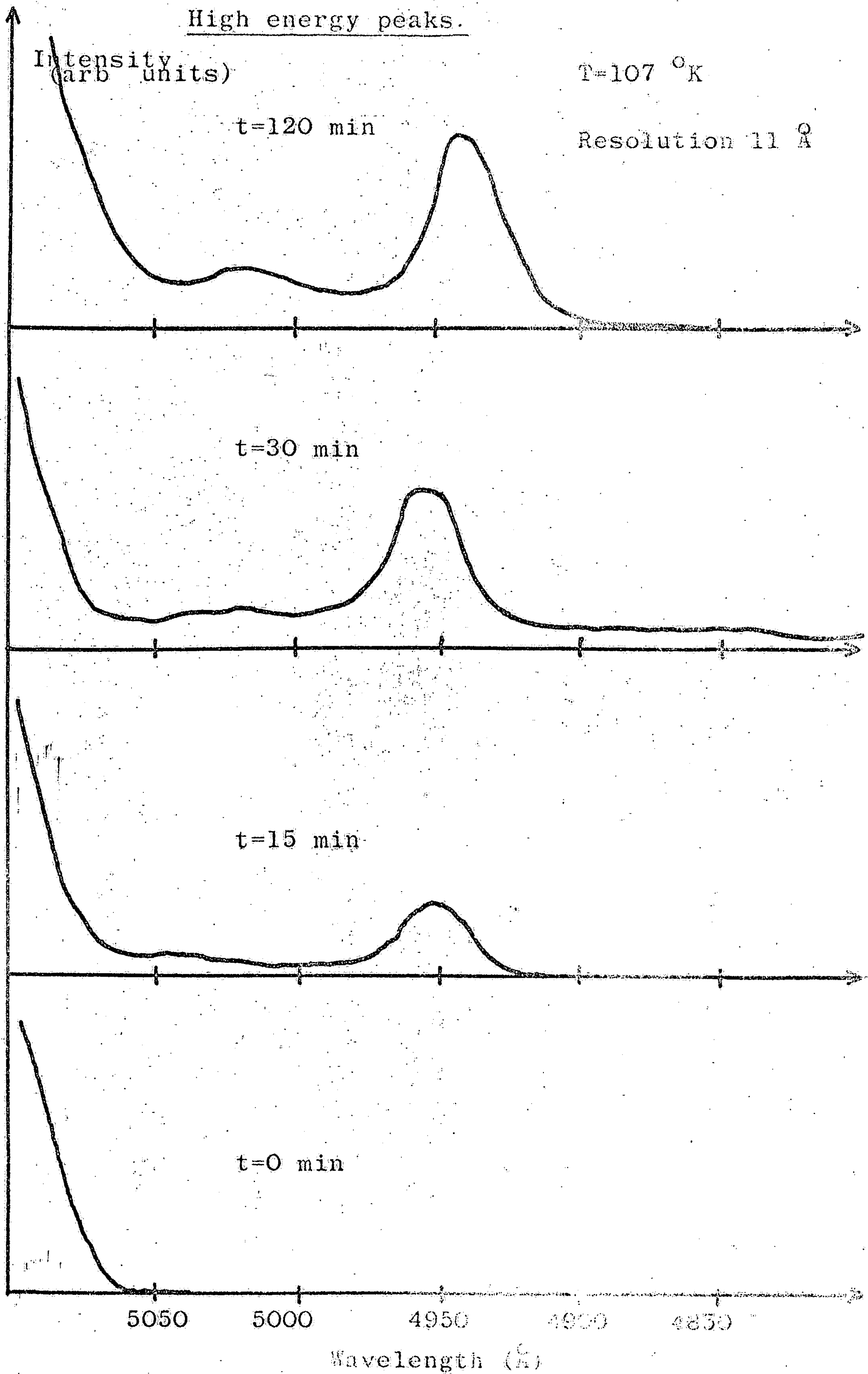

Figure 6.4

5020 Å. These two high energy bands were found to increase in amplitude with time when the crystal was maintained at temperatures close to 100 °K with the ultra-violet light continuously incident on the crystal. Figure 6.4 shows the increase in amplitude of the two high energy bands with time. Their amplitude was initially zero. After 15 minutes the band centred at 4950 Å was clearly visible, and the other band was present but of smaller magnitude. After about 2 hours the amplitudes of both bands reached saturation values equal to those of figure 6.4.4. Whenever these two bands were observed the one centred at 4950 Å was the larger. The spectrum beyond 5500 Å is not shown. In sulphur rich crystals there was no emission detectable beyond 5500 Å. In crystals grown without the addition of excess sulphur a weak, broad, structureless band centred on approximately 5800 Å could sometimes be seen. Discussion of the spectral measurements is deferred until chapter 8.

6.4. D.C. electro-luminescent spectra of CdS devices.

As was stated in the introduction to this thesis, one of the initial aims of this work was to improve the light output of the devices so that sufficient intensity could be obtained in order that the spectral distribution of the electro-luminescence could be measured. The first device to be bright enough for this to be achieved was device 15 which was prepared from a crystal grown without the addition of excess sulphur to the charge. The measurement was carried out by Guy Marlor, and the spectrum he obtained is shown in

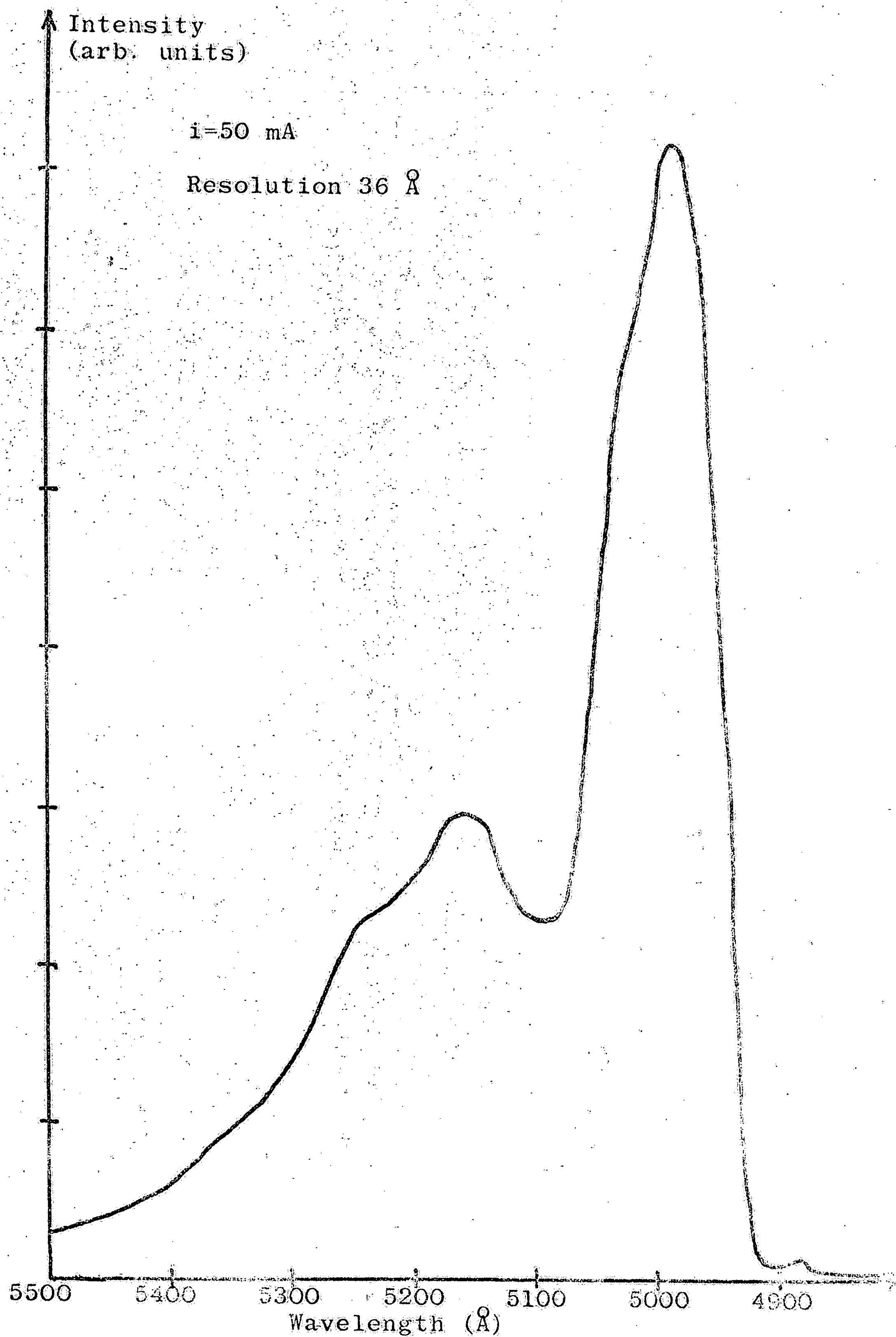

Figure 6.5

Electro-luminescence of device 39.

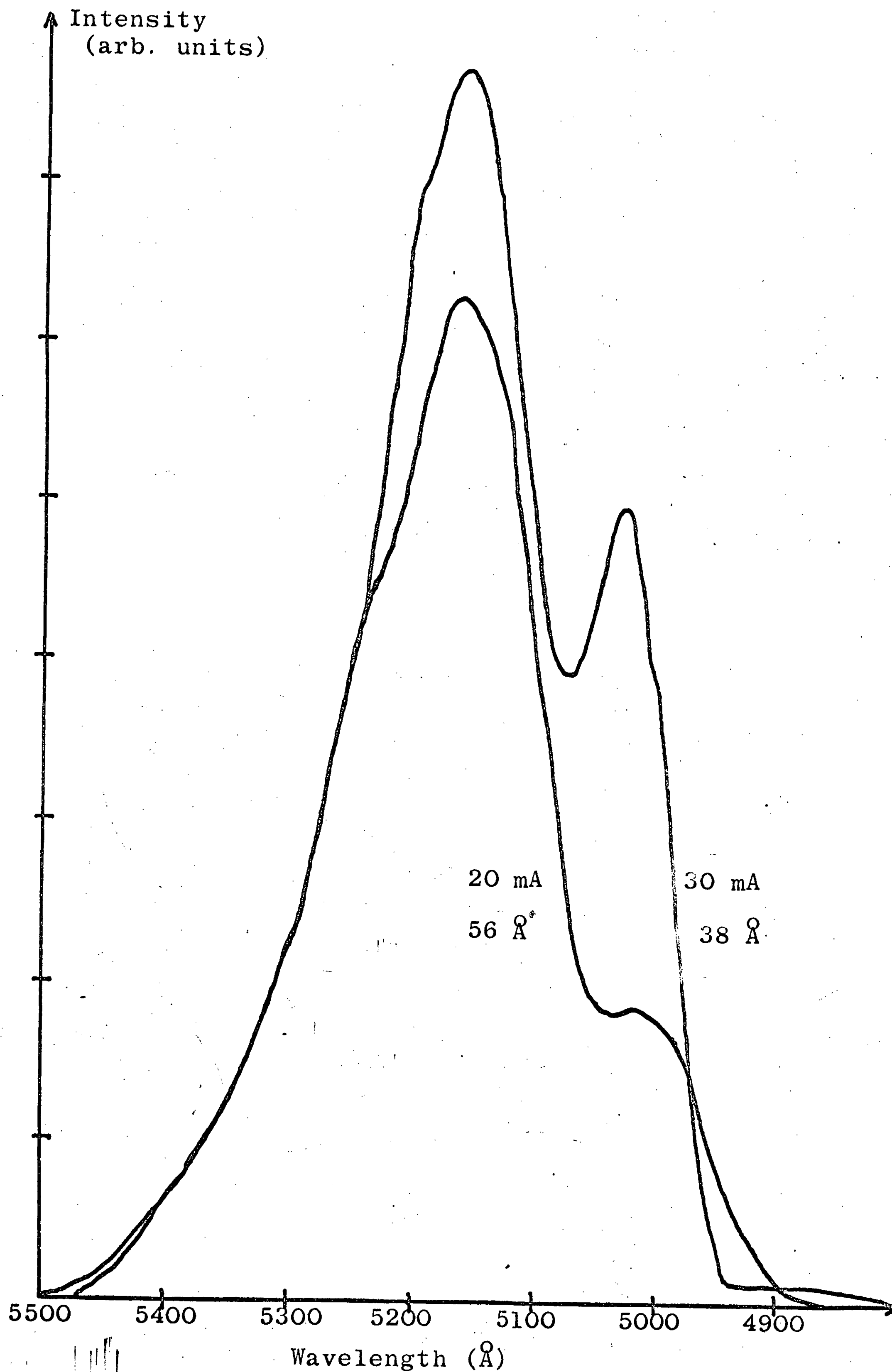

Figure 6.6.

Electro-luminescence of device 39.

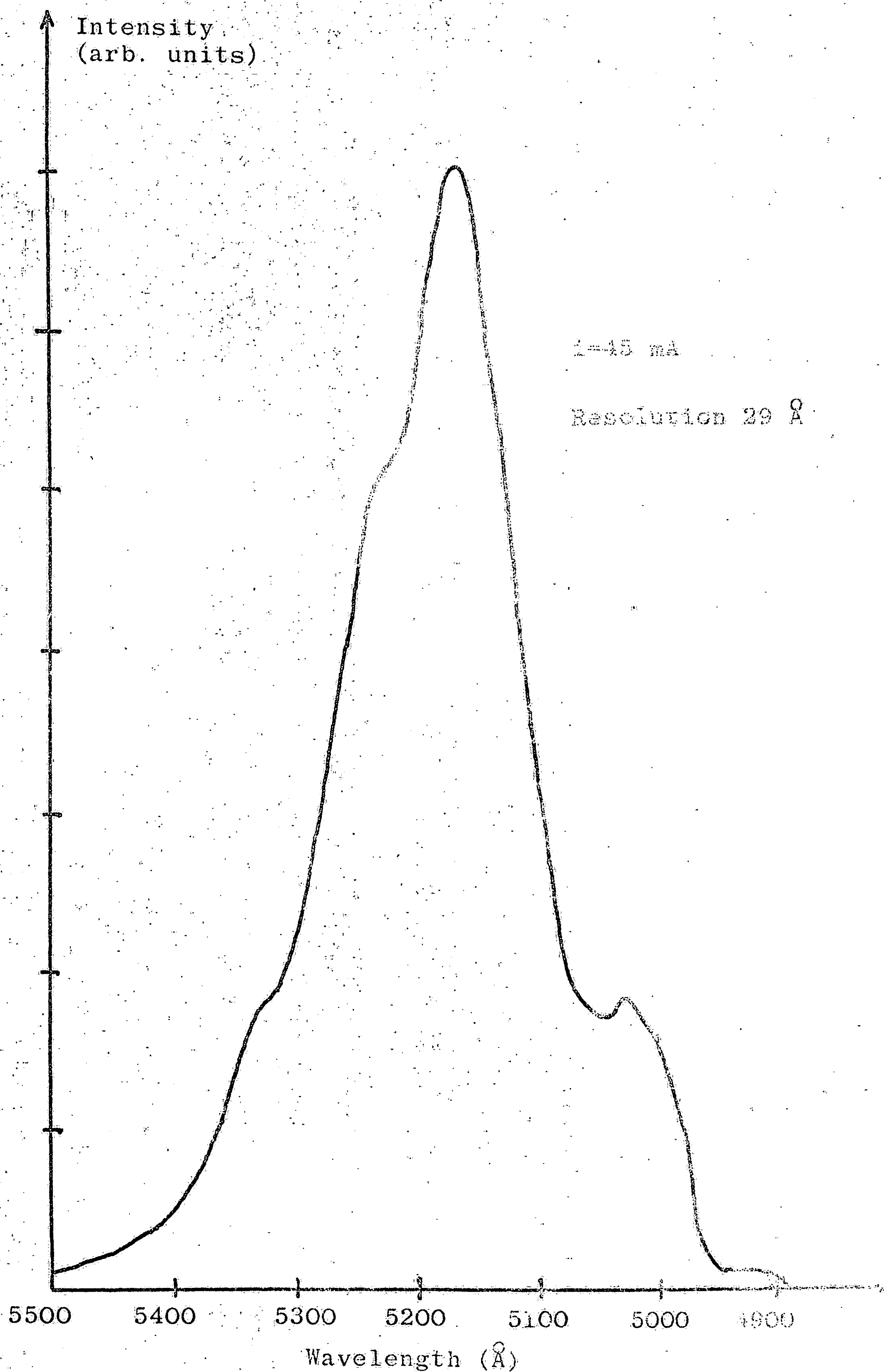

Figure 6.7.

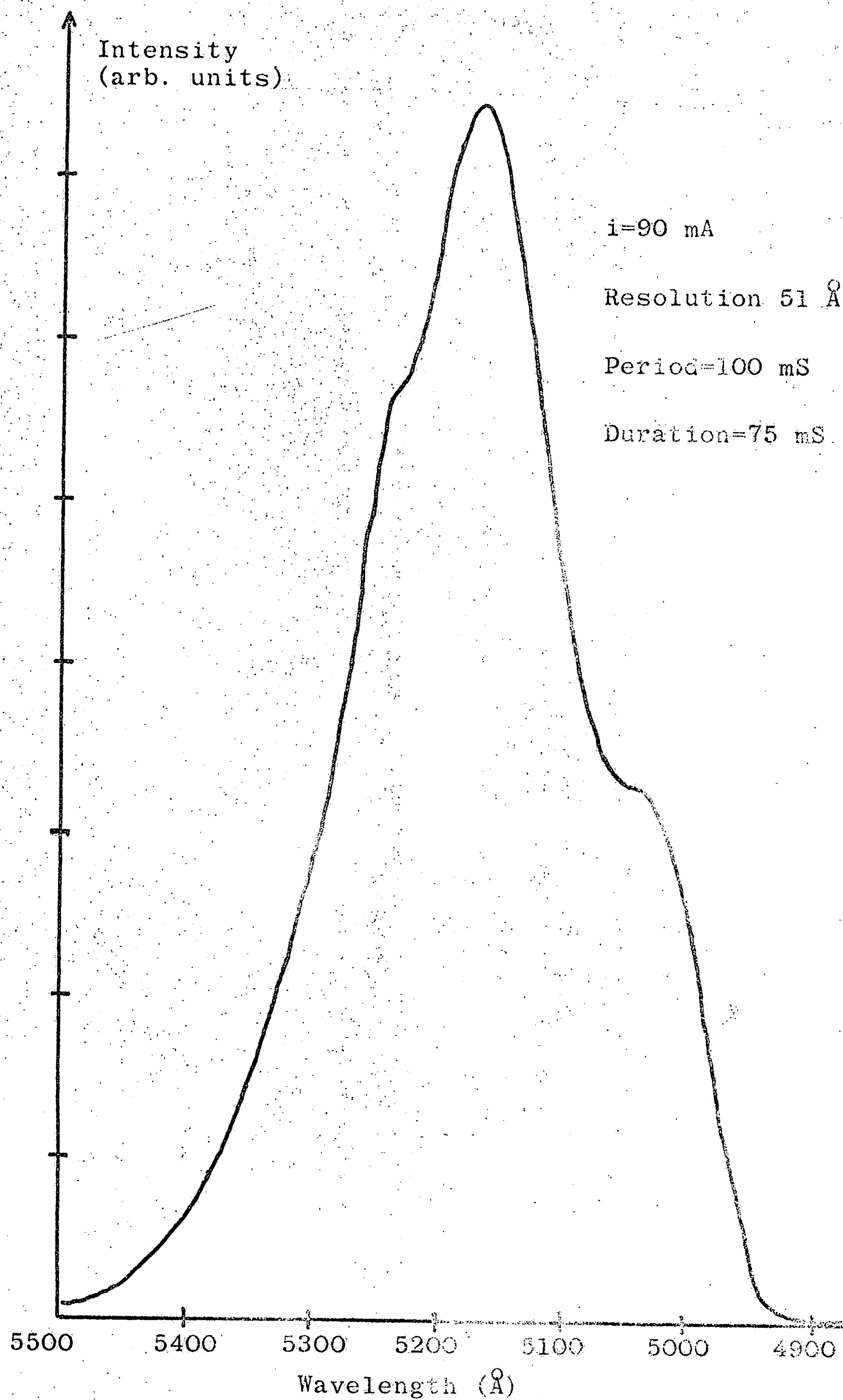

Figure 6.8.

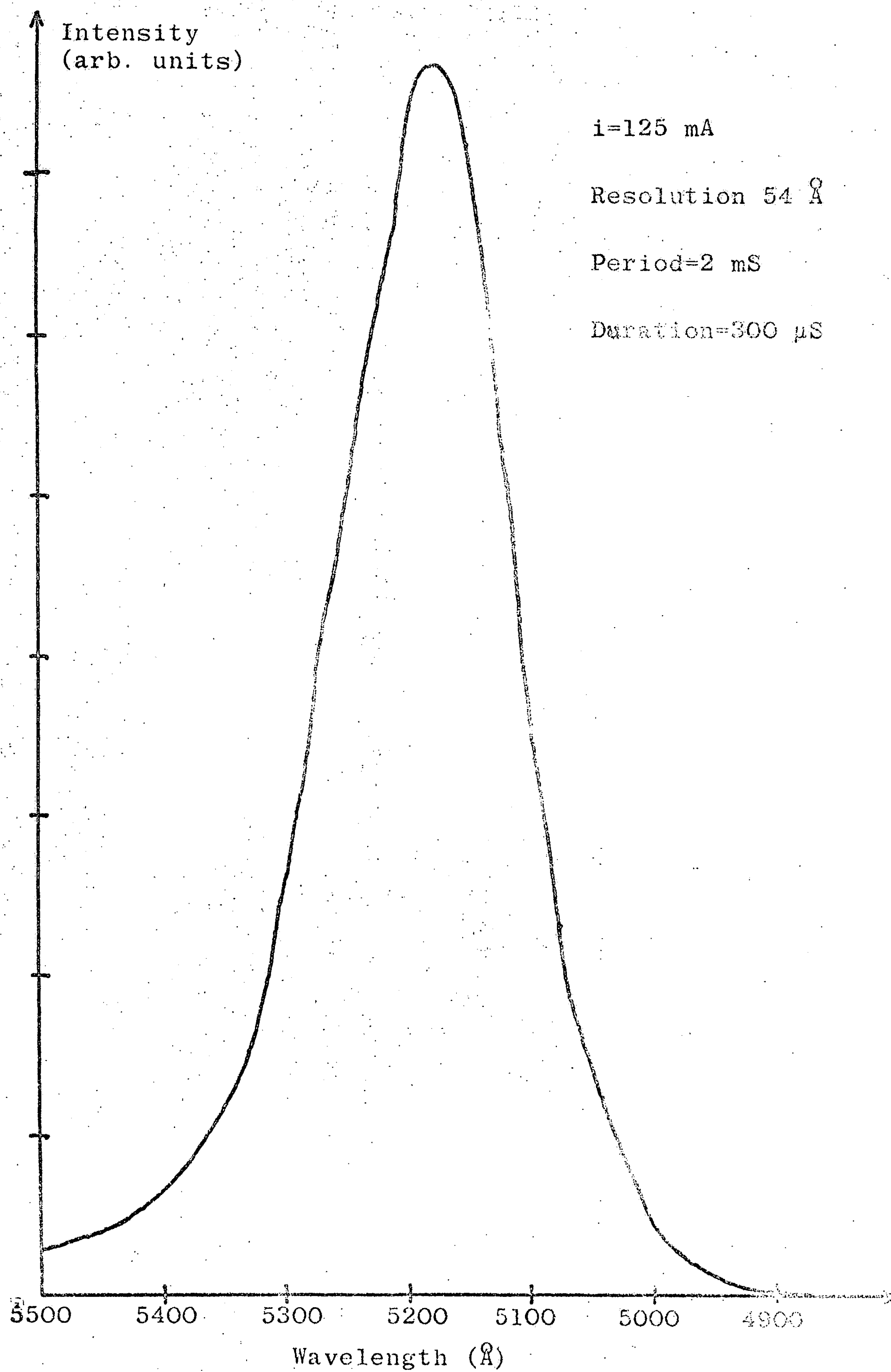

Figure 6.9.

figure 6.5. In contrast to the photo-luminescence the main contribution to the light output lies in the high energy region. The main peak at 4988 Å has a shoulder at 5025 Å, and then at longer wavelengths the edge emission series follows. This device also showed a weak band at 5800 Å corresponding to thephoto-luminescence band present in these crystals at that wavelength. The spectra of a device made from a sulphur rich crystal is shown in figures 6.6 and 6.7. Three different current densities were used. With this particular crystal the edge emission was the dominant process, but the high energy emission was much more intense than in the corresponding photo-luminescence curve shown in figure 6.3.

6.5. Pulsed D.C. electro-luminescence of CdS devices.

Two spectra were obtained when pulsed D.C. voltages were applied to the devices. Figure 6.8 shows the spectrum of device 39 which was pulsed with square wave voltage pulses of 100 mS period and 75 mS duration. The curve obtained was similar to that of the D.C. spectrum. With this device it was not possible to obtain a spectrum at very low duty cycles so that the heating of the device could be reduced. Device 43, however, was sufficiently bright for a low duty cycle to be measured and the spectral distribution of the emission is shown in figure 6.9. The period was 2 mS and the duration was 300 microseconds. The emission was all in the edge emission region with no high energy components. The high energy components were also absent from the photo-luminescent spectrum of this crystal.

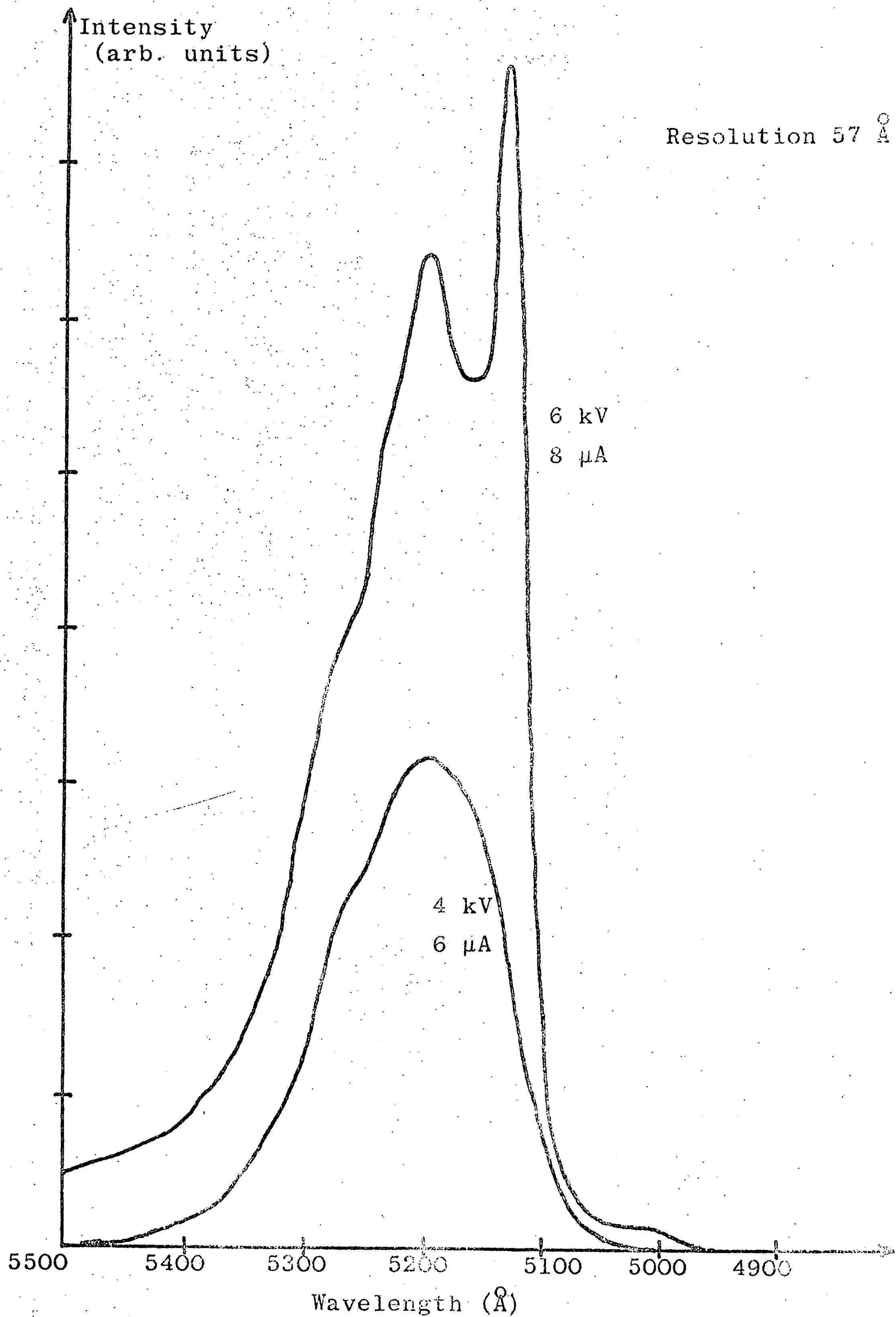

Figure 6.10.

6.6. Cathodo-luminescence of pure CdS.

The cathodo-luminescent spectrum of a pure CdS crystal was measured for comparison with the photo-, and electro-luminescence. Excitation was provided by a D.C. electron beam, the intensity and energy of which could be varied by altering the control grid bias and the accelerating potential respectively. The emission intensity was found to decrease in about 20 minutes from a bright visible green light (of comparable intensity to the electro-luminescence) until it was no longer visible with the naked eye. This was thought to be due to parts of the cryostat charging up, thus deflecting the beam away from the crystal. A small permament magnet placed close to the crystal outside the cryostat was found to keep the electron beam incident on the crystal. However the light output was now amplitude modulated at a frequency of about 0.5 c.p.s. These oscillations were not only visible to the naked eye but of sufficiently low frequency for the spectrophotometer to respond to them. The frequency of the oscillations was found to be virtually independent of the beam energy and intensity. In order to display the spectra, these oscillations were averaged out. Figure 6.10 shows the spectra measured at two excitation levels. The lower intensity spectrum exhibits no structure, but the edge emission series is apparent at the higher intensity. Luminescence at temperatures above liquid nitrogen temperature was also visible. At room temperature, the luminescence appeared to the eye to be more yellow than at 77 °K but the intensity was too low

for the spectral distribution to be measured.

CHAPTER 7

Electrical and optical double injection effects

7.1. Introduction.

This chapter describes the variations in the current through CdS crystals as a function of applied voltage and external illumination. The current flow is determined to a large extent by the hole lifetime which in turn is governed by the occupancy of a recombination centre which is situated near the middle of the forbidden energy gap. This recombination level is a class II centre ($s_p \gg s_n$) so that once a given centre has captured a hole there is only a small probability that it will then capture an electron. With low D.C. voltages applied to the crystals Ohm's law is obeyed, as predicted by the model of Ashley and Milnes which was discussed in section 2.5. At some higher voltage V_o significant electron injection takes place and the current varies as the square of the voltage. A transition region is observed at still higher voltages and at a voltage V_B electrical breakdown occurs. At the breakdown voltage, the hole transit time is approximately equal to the hole lifetime, and the breakdown corresponds to the onset of two carrier current flow. After breakdown the the current rises almost vertically at constant voltage V_M. In all crystals measured in the dark, the breakdown was followed by negative resistance so that $V_B > V_M$.

When external illumination of photon energy greater than E_R, the energy required to raise an electron from the recombination centre

to the conduction band, is incident on the crystal, the hole lifetime increases as the recombination centres become filled with holes. Thus if a voltage V in the range $V_M < V < V_B$ is applied across the crystal, then in the dark a low current will flow. In this condition application of light of photon energy greater than E_R of sufficient intensity can increase the hole lifetime to a value equal to the hole transit time and two carrier current flow commences. Once two carrier current flow has been initiated, the higher current persists even when the illumination is removed. The action ofthe light therefore is to switch the device from a low one carrier current to a high two carrier current state. This effect will be termed optical switching.

Measurements have also been performed with A.C. and pulsed D.C. voltages applied across the samples.

7.2. Experimental.

7.2.1. D.C. measurements.

The D.C. current-voltage characteristic measurements were carried out with the device mounted in the all metal cryostat described in section 6.2. Light could not be completely excluded from the cryostat so it was enclosed in an aluminium light tight box. The voltage across the crystal was measured with a Philips valve voltmeter tyoe GM 6020 which has a range from 10 mV to 1000 V and an input impedance of 10^8 ohms. The lowest current measured was 10^{-6} amps. A Sangamo-Weston meter type S 82 was used over the range 10^{-6} to 10^{-3} amps. For higher currents up to 10 amps an AVO meter mark 8 II was employed. The light output was measured with an EMI 9541

photomultiplier which operated with 1250 V between the cathode and the collector. I am grateful to Derek Ellis of this department who designed and built the stabilised supply for the photomultiplier. The D.C. voltages applied to the samples were obtained from a 0 to 300 V, 0 to 100 mA stabilised power supply. The optical threshold wavelength, and infra-red quenching measurements were performed with the cryostat in front of the exit slits of a Hilger and Watts monochromator type D 285.

7.2.2. A.C. measurements.

The A.C. drive for the modulation of the current through the crystals was provided by setting a steady bias current through the crystal with the circuit employed in the spectral measurements described in section 6.4. The circuit is that shown in figure 6.2. For the A.C. measurements the voltage on the control grid was sine wave modulated with a Venner oscillator type TSA 625/2. At all times the amplitude of the modulation of the current through the crystal was less than the standing D.C. bias current. The current and light waveforms were displayed on a Tektronix 545A oscilloscope with a dual beam plug-in unit type CA. In one experiment the light was transmitted along a light pipe 1 metre long and 8 cm in diameter. The pipe was a pyrex cylinded coated on the inside with an opaque film of silver obtained by precipitation from ammoniacal silver nitrate.

7.2.3. Pulsed D.C. measurements.

The pulses were supplied by Solartron pulse generators types

GO 1101 and OPS 100 C. The former had a wider range of pulse durations (10^{-6} to 10^{-1} sec) but had a high output impedance (2500 ohms), whereas the latter had an output impedance of 140 ohms but a maximum duration of 250 microseconds. Both generators had a maximum voltage output of 100 V. The voltage, current, and light pulses were displayed on a Tektronix 545A oscilloscope. The B timebase of the oscilloscope was employed to trigger the pulse generator, and the A timebase displayed the signal. The period could thus be varied from 20 microseconds to 10 seconds. When required, the trace was photographed with a Schackman 35 mm oscilloscope camera type AC 2/25.

7.3. D.C. measurements.

In the course of the work it was found that many crystals, particularly those thicker than 100 microns, were very photo-sensitive. These samples were of very high resistivity in the dark where the current was typically less than 1 microamp with 100 V applied. Investigation of the photoconductivity revealed that under certain conditions , the increase in conductivity when the sample was irradiated could be stored at liquid nitrogen temperature. The effect was initially investigated with light from a microscope lamp passing through a Chance glass filter OGr 1, which transmits light in the visible range between 4500 and 6000 Å. Any given crystal was found to have a breakdown voltage V_B below which only low currents were observed, and above which the current increased with decreasing

Current-Voltage characteristic for device 46.

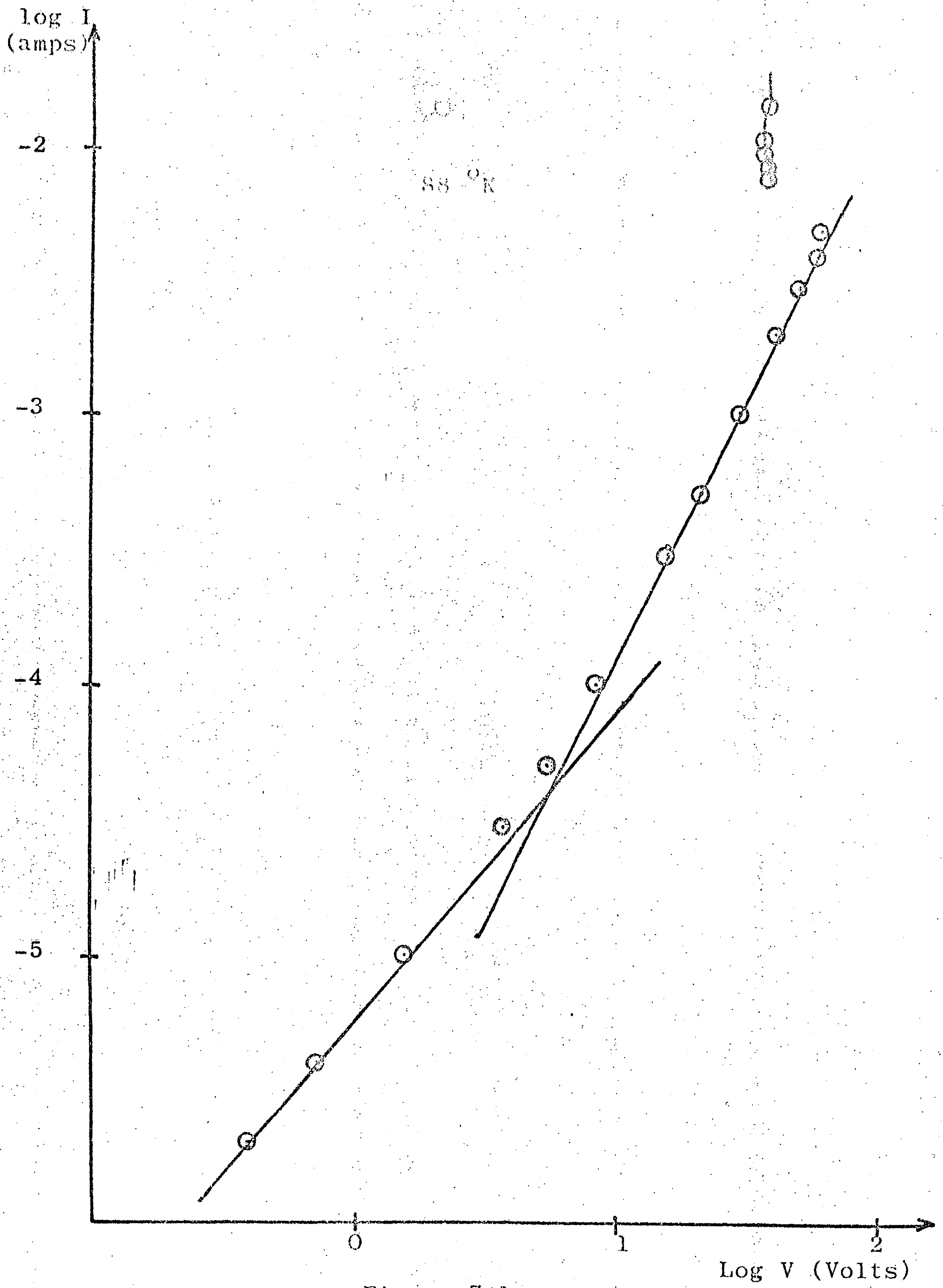

Figure 7.1.

voltage. Finally the current rose with almost constant voltage, V_M, across the crystal. It was necessary to incorporate a current limiting mechanism into the circuit or the current rose to such a level that the device was destroyed. If a voltage in the range $V_M < V < V_B$ was applied to the crystal, then in the dark a low current flowed. Illumination with the green light could now raise the current to a high value as observed in the post breakdown region of the characteristic measured in the dark. When the illumination was switched off, the current remained at the higher level and did not return to its original low level in the dark. Thus the crystals may be considered as a switch which can be triggered by applying a sufficiently high voltage or by illuminating them with light. Investigations of both kinds of triggering were carried out.

The current-voltage characteristic for a crystal at 88 °K is shown in figure 7.1. The characteristic consists of an ohmic region at low voltages followed by a square law dependence of the current on voltage above about 6 Volts. The square law dependence continues until a transition region is reached at 50 volts. Between 50 and 65 volts the current rises very steeply until at 65 volts breakdown occurs. At breakdown the current through the crystal rises to 8 mA and the voltage across the crystal falls to 40 volts. In the post-breakdown region, the current rises practically vertically with almost constant voltage across the sample. The post-breakdown region was

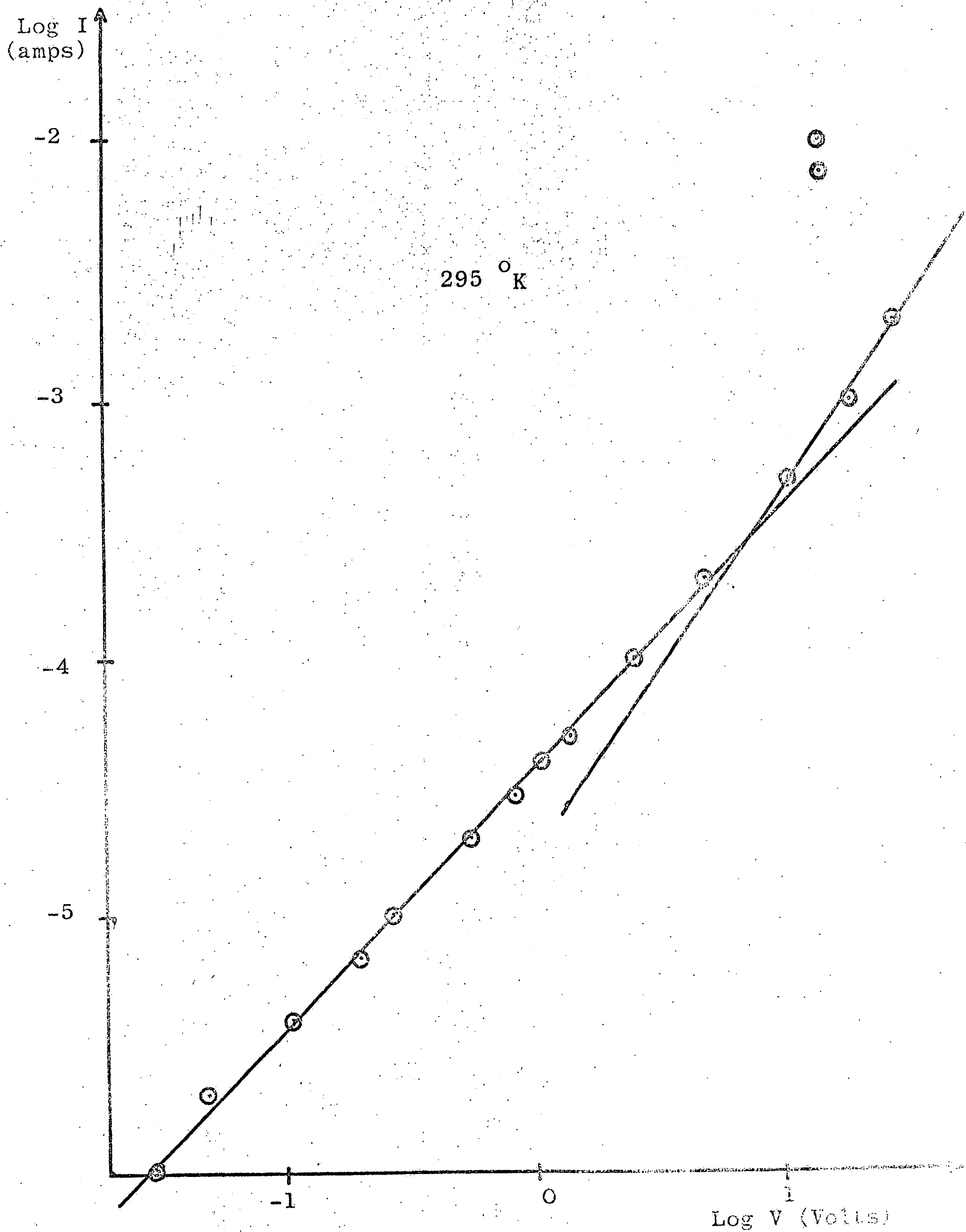

Figure 7.2

Linear current-voltage characteristic for device 46

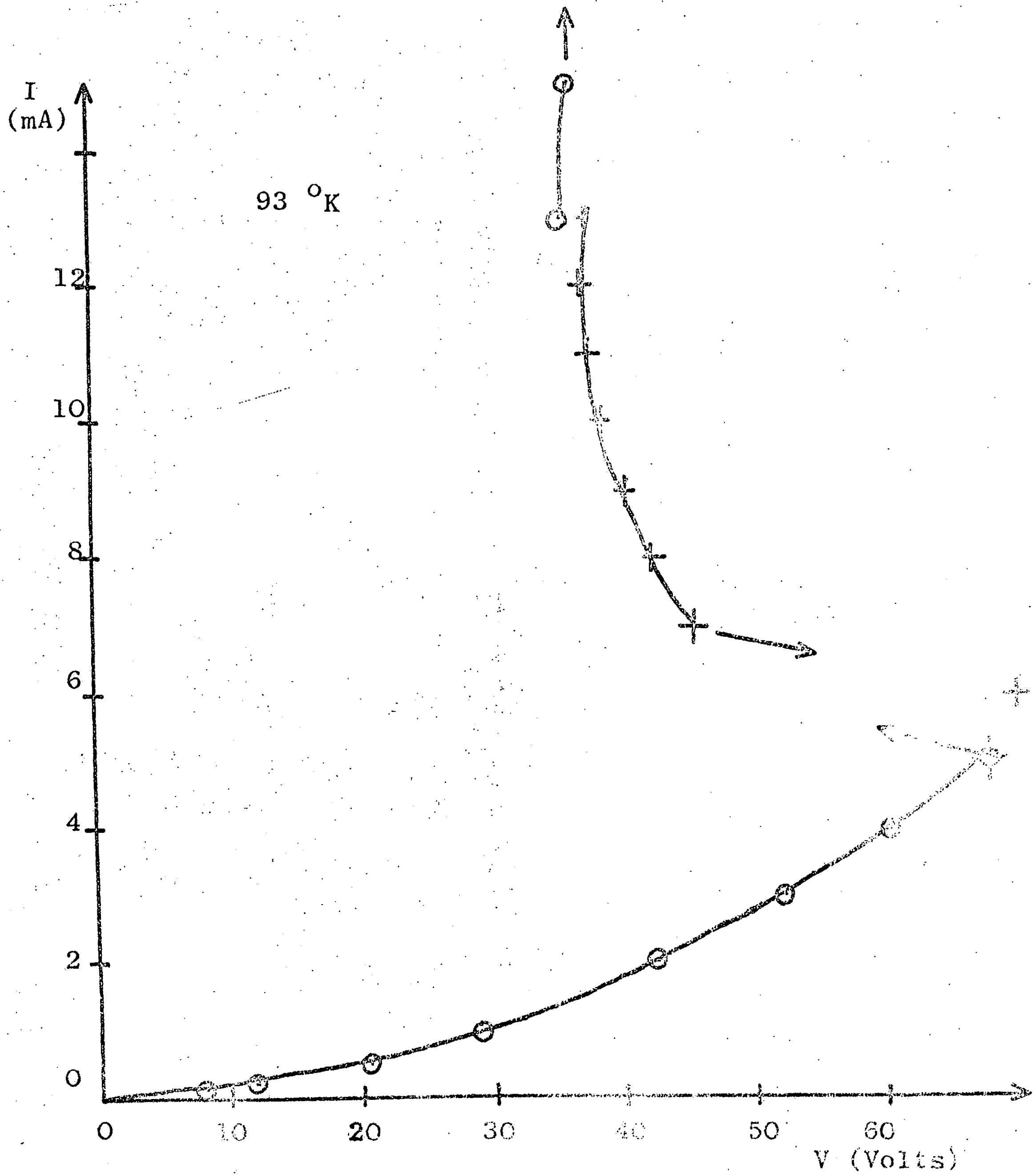

Figure 7.3

not explored beyond 15 mA because of the danger of the crystal being destroyed by thermal runaway. For reasons discussed in section 7.5, the higher current section of the characteristic was not explored with pulse techniques.

The switching effect could be obtained at temperatures up to room temperature. Figure 7.2 shows the room temperature characteristic where the ohmic region extends over a wide current range up to 200 microamps, and the square law dependence is not observed. At 7 volts the current starts to rise superlinearly with the current varying as the voltage to the power 1.4, and breakdown takes place at 27 volts compared with 65 volts at 88 ^{o}K. In the post-breakdown region a vertical rise in current at constant voltage occurs.

The post-breakdown current is dependent on the resistance in series with the device, and hysteresis is observed when the characteristic is taken with the current increasing and with it decreasing. The current-voltage characteristic is shown on a linear scale in figure 7.3 to emphasise the post-breakdown region. The resistance in series with the crystal was 4700 ohms. As the breakdown voltage is reached, the device switches on to pass a current of 13 mA with 35 volts across the crystal. At 15 mA the voltage across the sample is 35.5 volts. As the total applied voltage is reduced, the current falls and can be reduced below 13 mA with the high current state remaining. The current could be reduced to 7 mA before switching occurred and the voltage across the crystal rose to 70 volts. The

Breakdown voltage against device thickness.

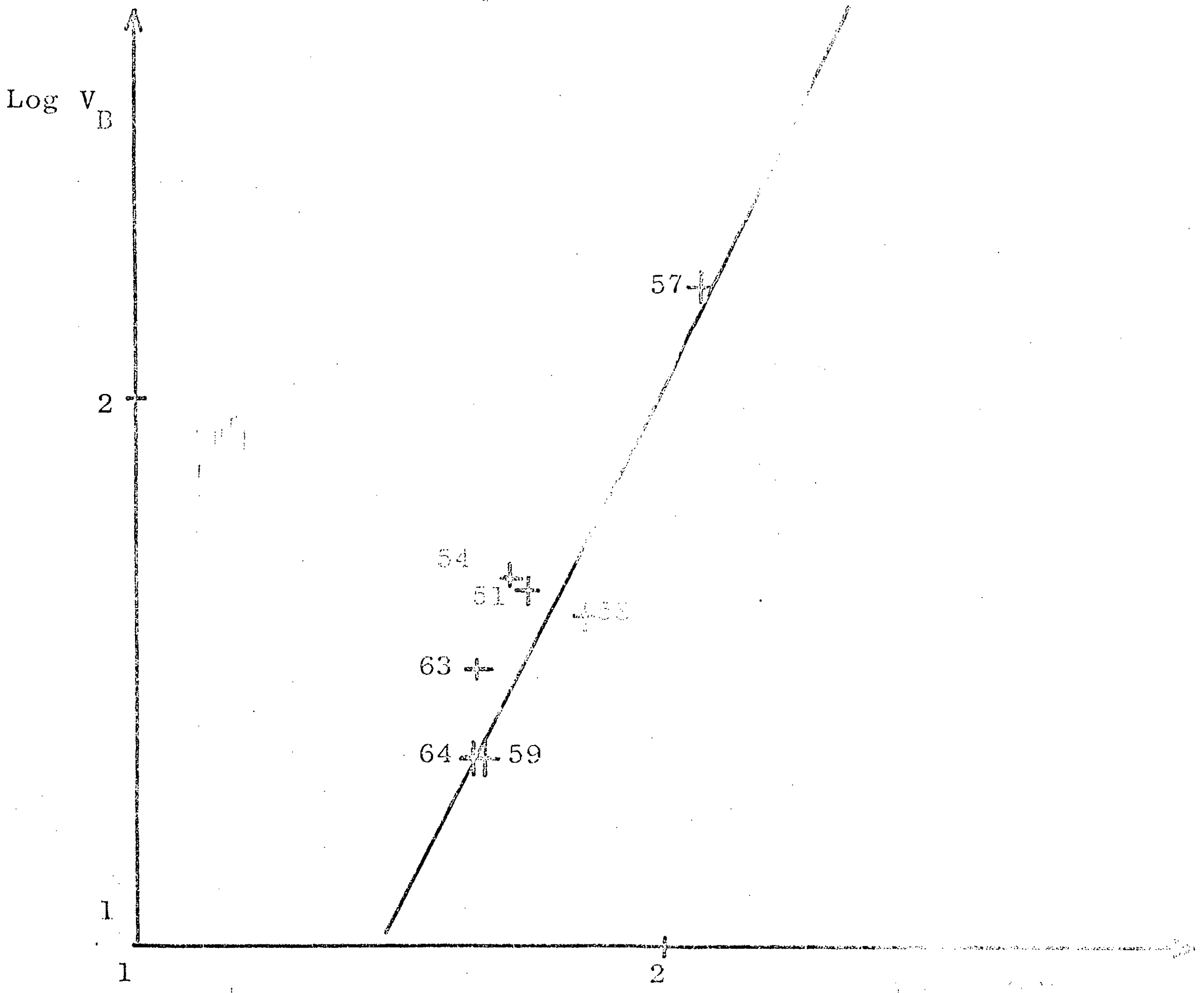

Figure 7.4

change in impedance of the device between the off and the on state is approximately a four-fold reduction. With between 35 and 65 volts across the crystal in the off state, a transition to the on state could be produced by applying a voltage pulse in addition to the D.C. bias. Switching took place if the total voltage across the sample during the pulse was greater than the 65 volt breakdown threshold.

The pre-breakdown characteristics just described are in agreement with the theory of Ashley and Milnes for a partially compensated semiconductor. However, not all devices showed this kind of characteristic. Some crystals had extremely high power law dependences of current on voltage and no ohmic regime was observed at the lowest currents measured.

The theory of Ashley and Milnes predicts that the breakdown voltage should vary as the square ofthe crystal thickness for crystals of a given material with identical doping levels. Figure 7.4 shows the log-log plot of breakdown voltage against thickness for 7 samples from the same crystal growth run. The smooth line has slope 2 ~~is the square law dependence~~ as predicted by Ashley and Milnes. The agreement with the square law variation is good, particularly since the crystals must have shown slight variations in defect concentrations. Crystals from other growth runs were never more than an order of magnitude away from the smooth line.

The effect of a bias light on the current-voltage characteristic was investigated for one crystal. The characteristic is shown in

Current-voltage characteristic with illumination.

Device 50

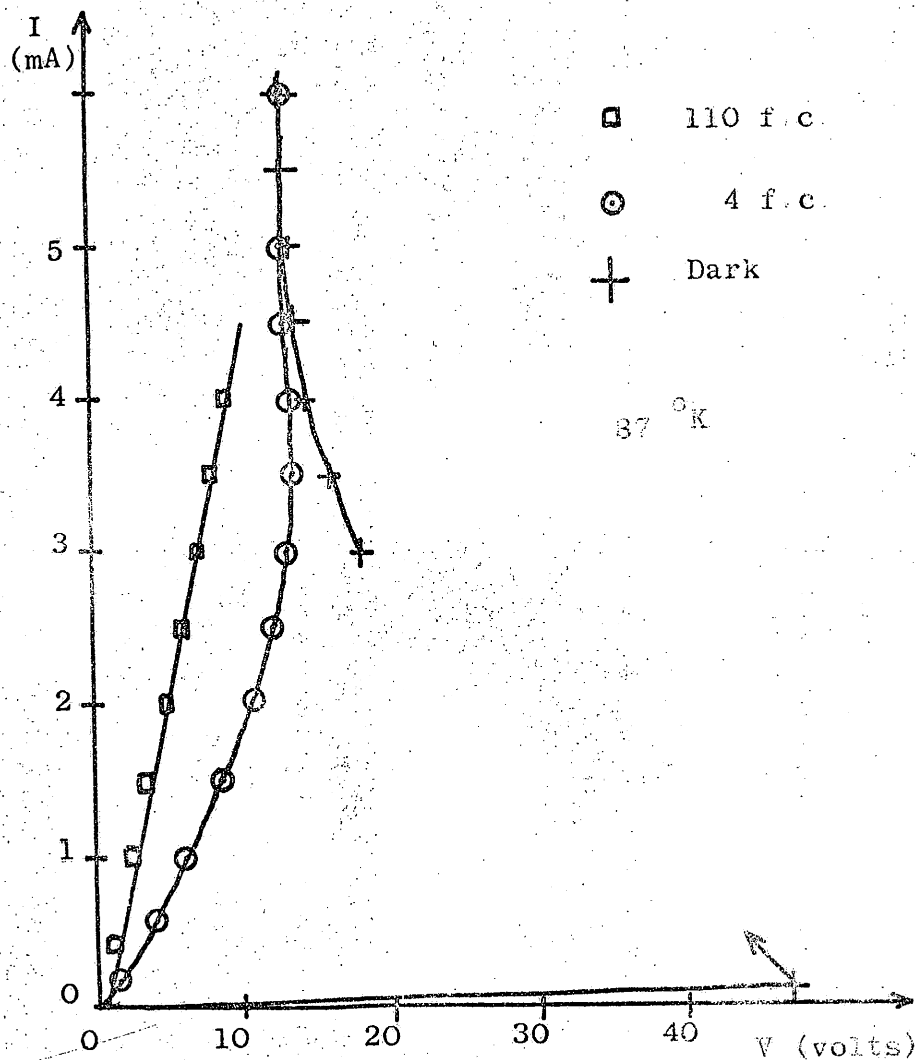

Figure 7.5

figure 7.5. The bias light was obtained by passing the output from a microscope lamp through a Chance glass filter OGr 1. Curve 1 is the characteristic obtained with the sample in the dark. With light of 4 f.c. intensity incident on the crystal, a switching effect is not observed. The current-voltage curve shows a slight negative resistance as seen in curve 2. The negative resistance disappears completely in curve 3 where the intensity of illumination was 110 f.c.

The switching effect observed when a crystal biased below the breakdown voltage was irradiated with green light was investigated further using light from a monochromator. The crystal was placed infront of the exit slits of a Hilger and Watts monochromator with a tungsten filament lamp as source. The crystal was biased just below threshold at close to 100 °K, and attempts were made to observe the switching effect with light of wavelength in the range 4500 Å to 2 microns. With light of photon energy much greater than the fundamental absorption edge no switching occurred, but when the wavelength was increased to 4880 Å, the crystal switched to the high current state. All light in the wavelength range 4880 to 8100 Å produced switching, but no light of wavelength greater than 8100 Å could switch the current even with thetungsten lamp giving maximum output. With very low light intensities spurious thresholds were obtained because a shorter wavelength of light was required to make the crystal switch.

Since the switching on of the devices was thought to be due to

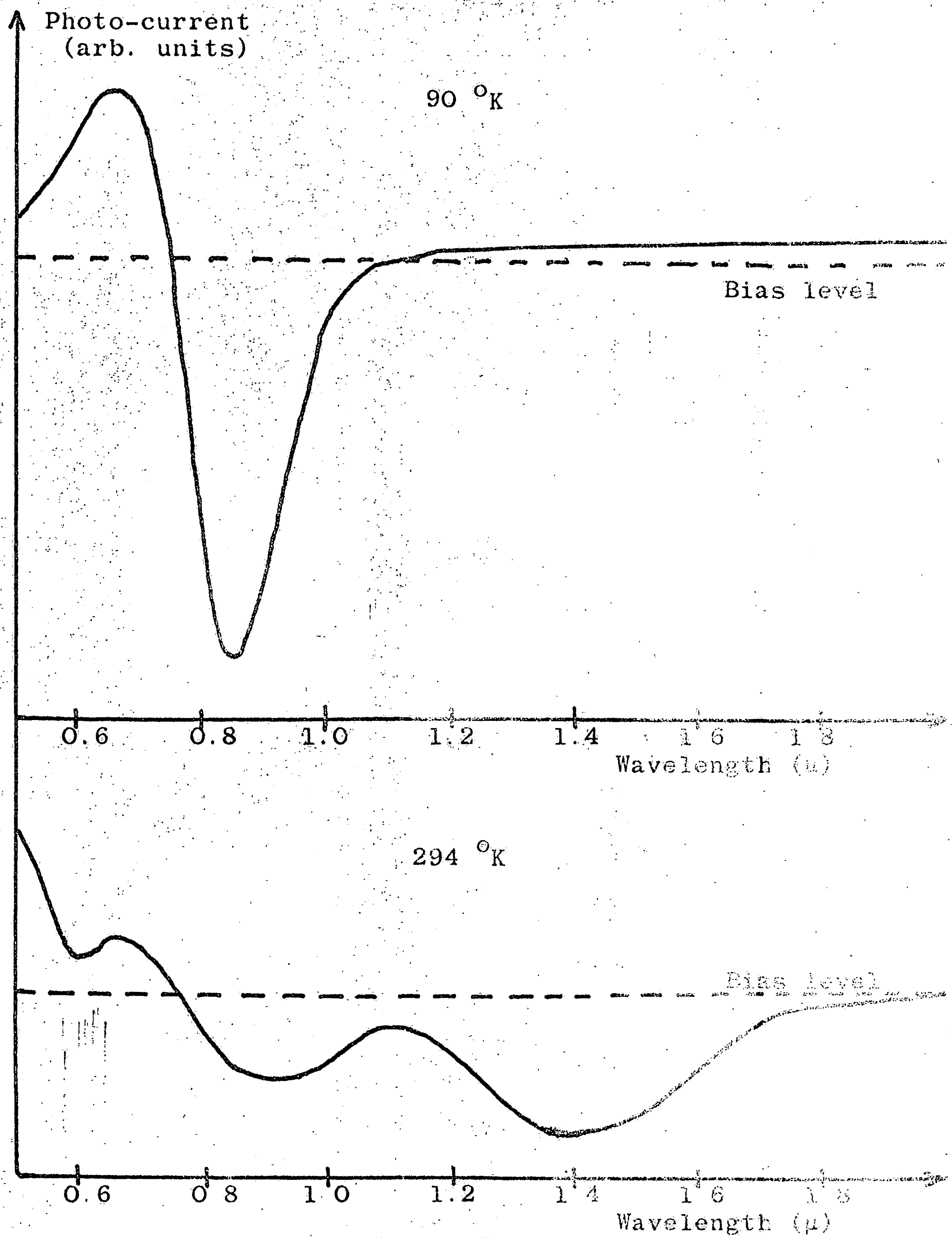

Figure 7.6

increasing thehole lifetime by ejecting electrons from a recombination centre, attempts were made to switch the current from the high to the low state by raising electrons from the valence band to the recombination centre. The raising of electrons from the valence band to levels in the forbidden energy gap is known to be responsible for the infra-red quenching of the photocurrent in CdS. It was first verified that the infra-red quenching effect took place in the crystals used in this work. The infra-red quenching bands were investigated by irradiating the sample with a bias light to produce a photocurrent, and with quenching light from a monochromator. The photocurrent was excited by the emission from a microscope lamp passing through a Chance glass filter OGr 1. The infra-red quenching spectrum was measured at 90 and 294 ^{o}K. The results for device 50 are shown in figure 7.6 and are not corrected for the variation of the monochromator output with wavelength. At the temperature in the region at which the switching threshold was investigated a strong quenching band centred on 0.85 microns is present, and at room temperature there are two bands centred on 0.92 and 1.45 microns. The bias light was now removed , and with the crystal in the on state light from the monochromator was used to try to switch the current into the low state. No switching was observed with light in the wavelength range 0.45 to 2.0 microns.

With the crystals in thelow current state, no light output was observed even at temperatures below 100 ^{o}K. In the high current state visible green light was emitted at all temperatures below approximately

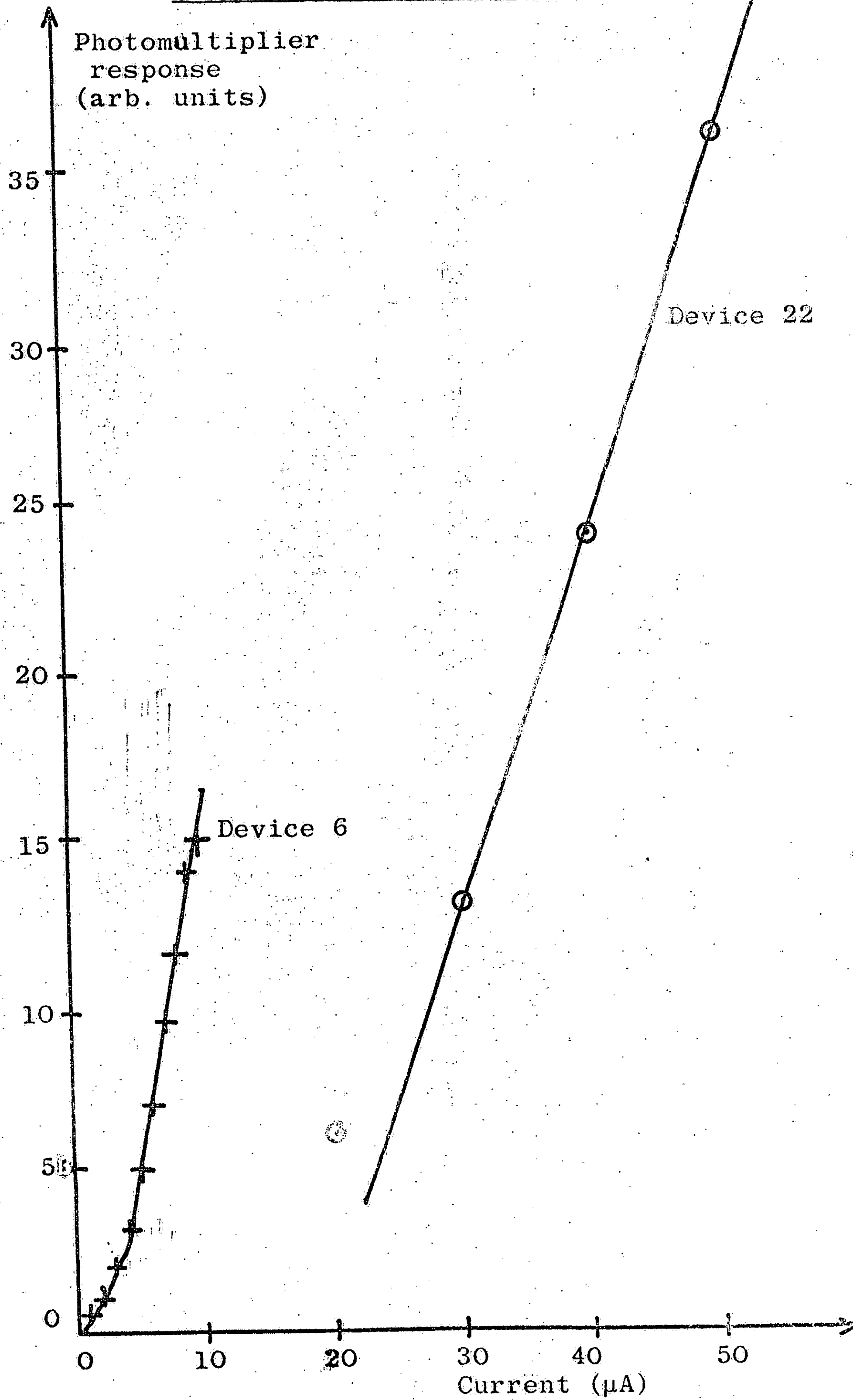

Figure 7.7.

Current-light output characteristic for device 43.

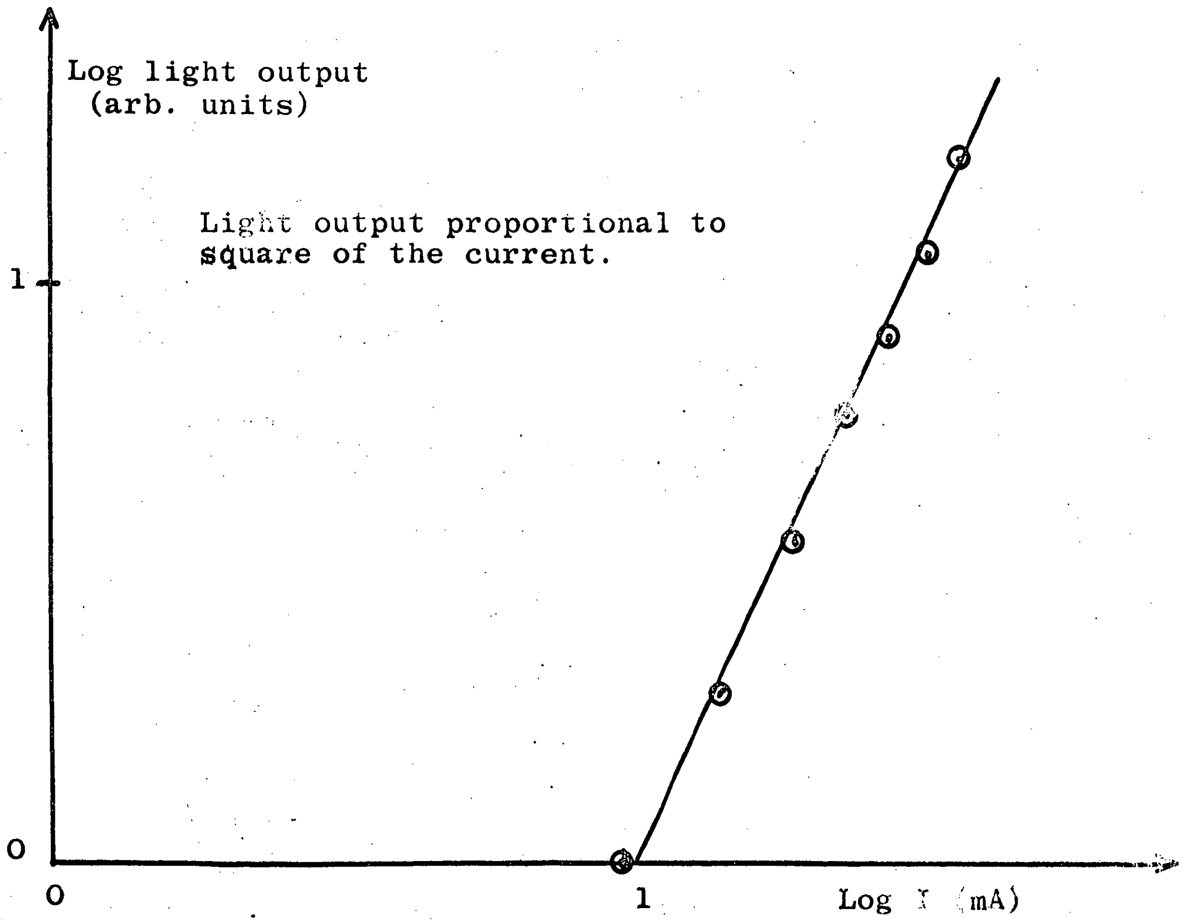

Figure 7.8.

Current-light output characteristic for device 50.

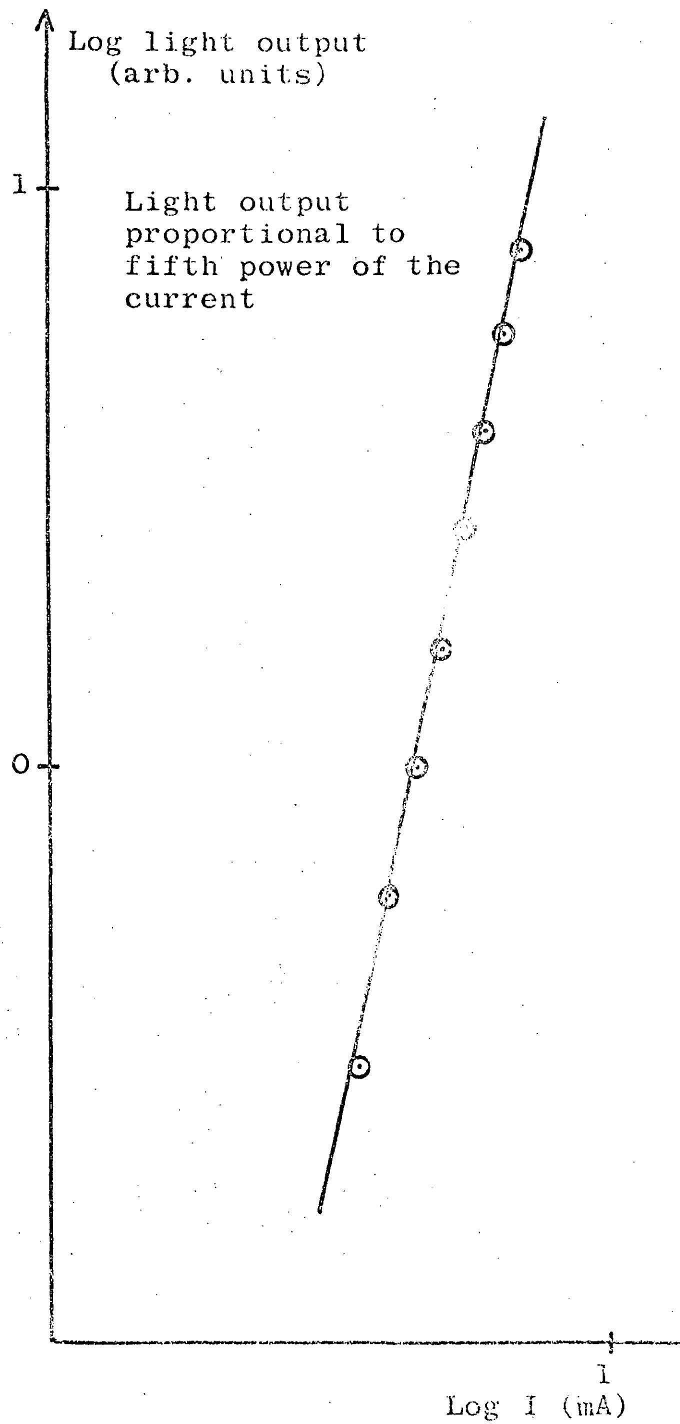

Figure 7.9.

A.C. Modulation of light output.

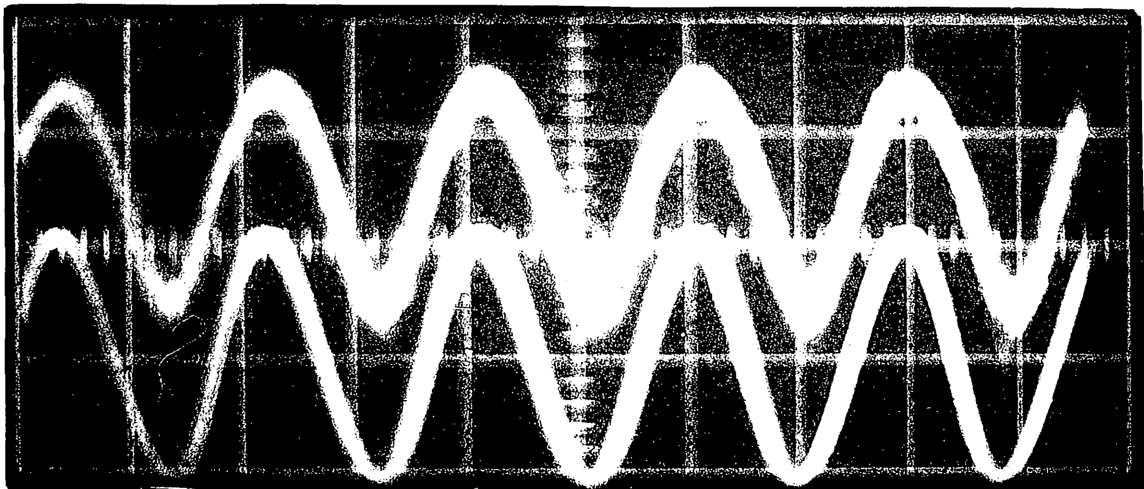

Upper trace: Light.
Lower trace: Current.

Figure 7.10.

A.C. Light output against current.

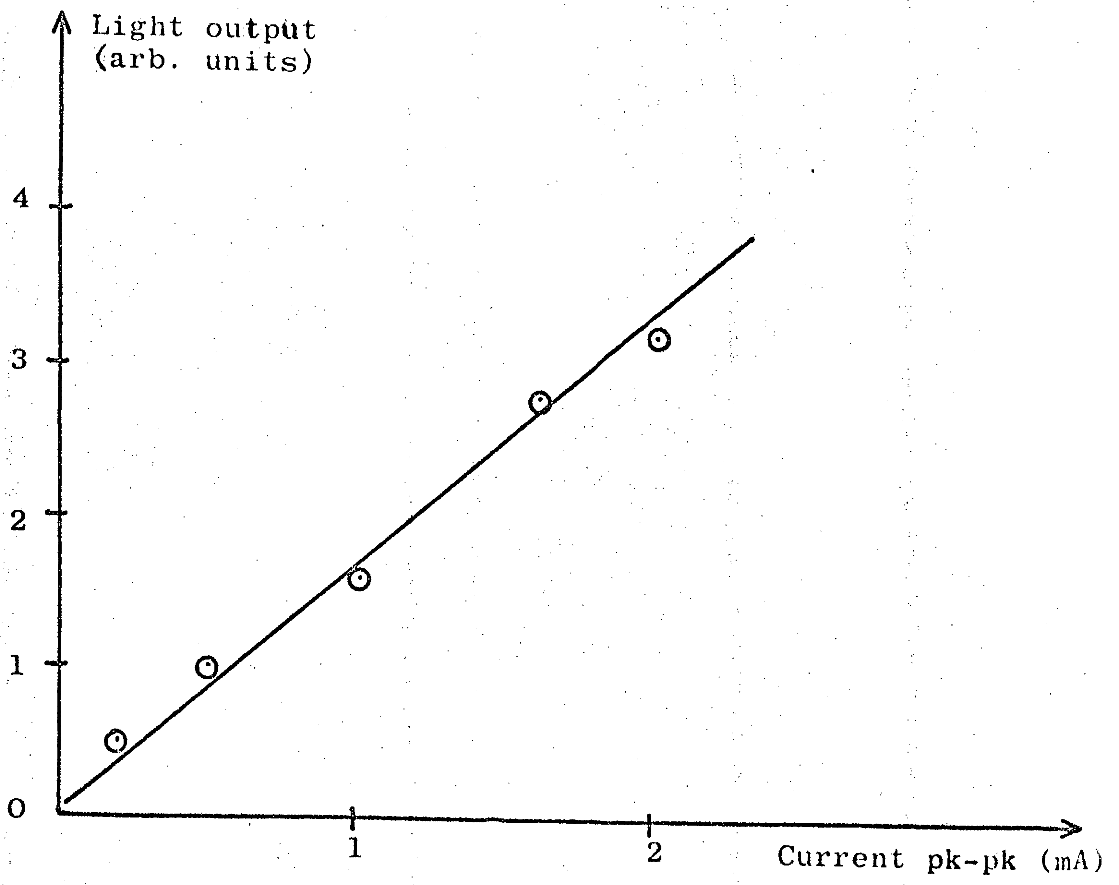

Figure 7.11.

A/C. Light output against frequency.

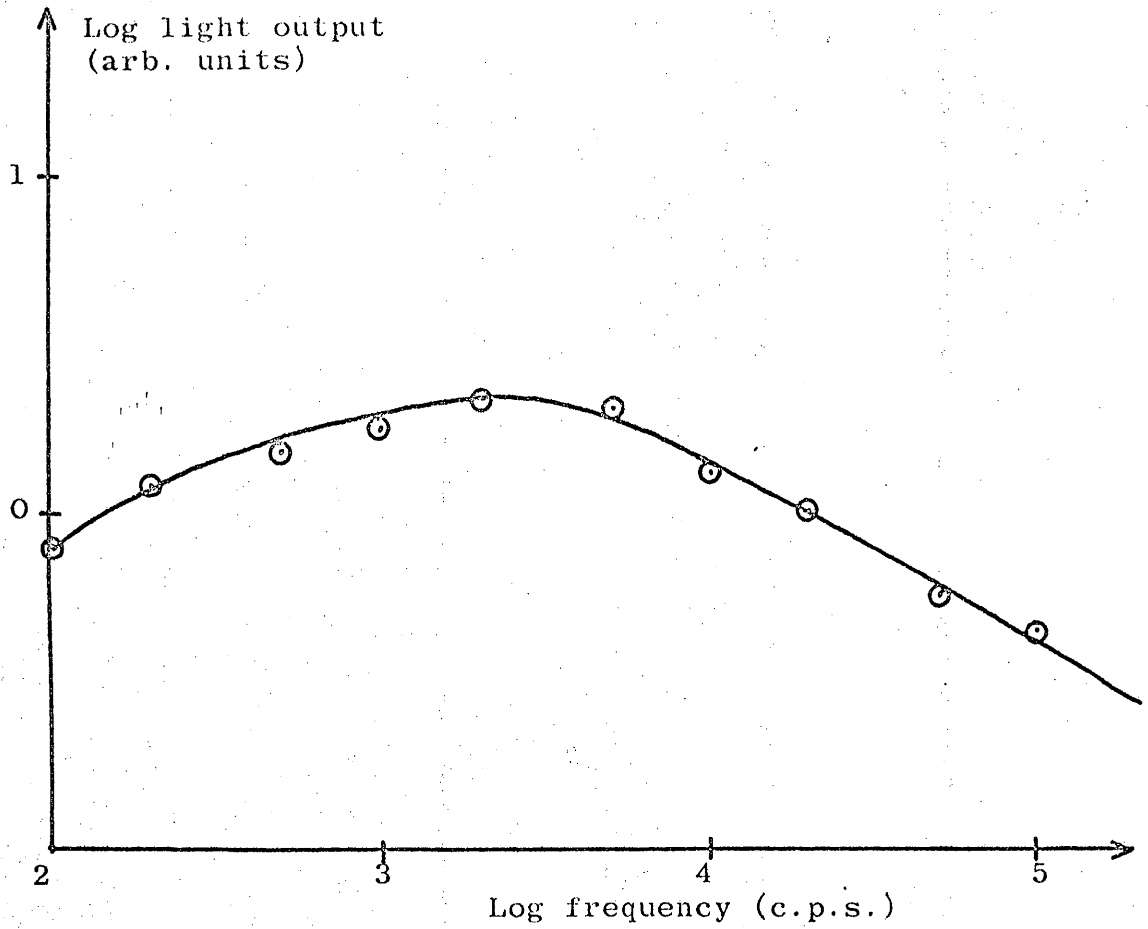

Figure 7.12.

140 °K. The light output-current characteristics have been measured for several samples and are linear over a wide range. Figure 7.7 shows the characteristics for two crystals and indicates the wide variation in the output from sample to sample. Two ~~anomalous~~ other power law dependences were observed. The characteristic of device 43 shown in figure 7.8 is a square law, whilst that of device 50 displayed in figure 7.9 is a fifth power law.

7.4. A.C. measurements.

When A.C. modulation is superimposed on a steady D.C. current through the crystal, the light output is also A.C. modulated. A photograph of the oscilloscope trace showing sine wave modulation of both the light and the current waveforms is shown in figure 7.10. Theupper of the two traces is the light, and the lower is the current waveform. The A.C. light output-A.C. current characteristic is shown in figure 7.11, and is linear. The frequency response of the light output is shown in figure 7.12. Thecurrent was also frequency dependent and the curve in figure 7.12 was corrected by normalising the current. The output varies by less than a factor 5 over the range 100 c/s to 100 kc/s. No measurement was possible at frequencies above 100 kc/s because the noise on the signal became of the same order as the sine wave amplitude.

Any source of light whose output can be modulated directly by modulating the current through it has potential for use in telecommunication systems, since if the light can be modulated at a

very high frequency then a large amount of information can be transmitted along a single beam. Thus with a light source that can be modulated at up to 1 Gc/s, of the order of 10^6 telephone channels could be carried down a single light pipe. The light pipe experiment was tried with the CdS light emitting devices. The path length was 1 metre and was chosen to demonstrate the feasibility of the experiment as well as to determine its limitations. The current through the crystal was A.C. sine wave modulated on top of a steady D.C. current. The light from the sample was directed down a silvered pyrex tube and then detected at the other end with a photomultiplier. The output from the photomultiplier was either displayed on a Tektronix oscilloscope type 545A, or amplified and passed through a loudspeaker coil. The maximum frequency of modulation before the signal was obliterated by noise was 500 kc/s. This was the highest frequency of modulation of any device constructed in the course of this work. This low frequency of cut-off coupled with the low intensity of output compared to injection lasers in other materials means that the CdS light emitting device is unlikely to have any telecommunications applications.

One extra experiment performed out of interest rather than for gaining information about CdS was to modulate the current through the device with audio frequency signals from a commercial record player. The light pipe transmitted the music as would be expected from the sine wave modulation experiments, and after amplification the signal from thephotomultiplier was easily recognisable as music with noise

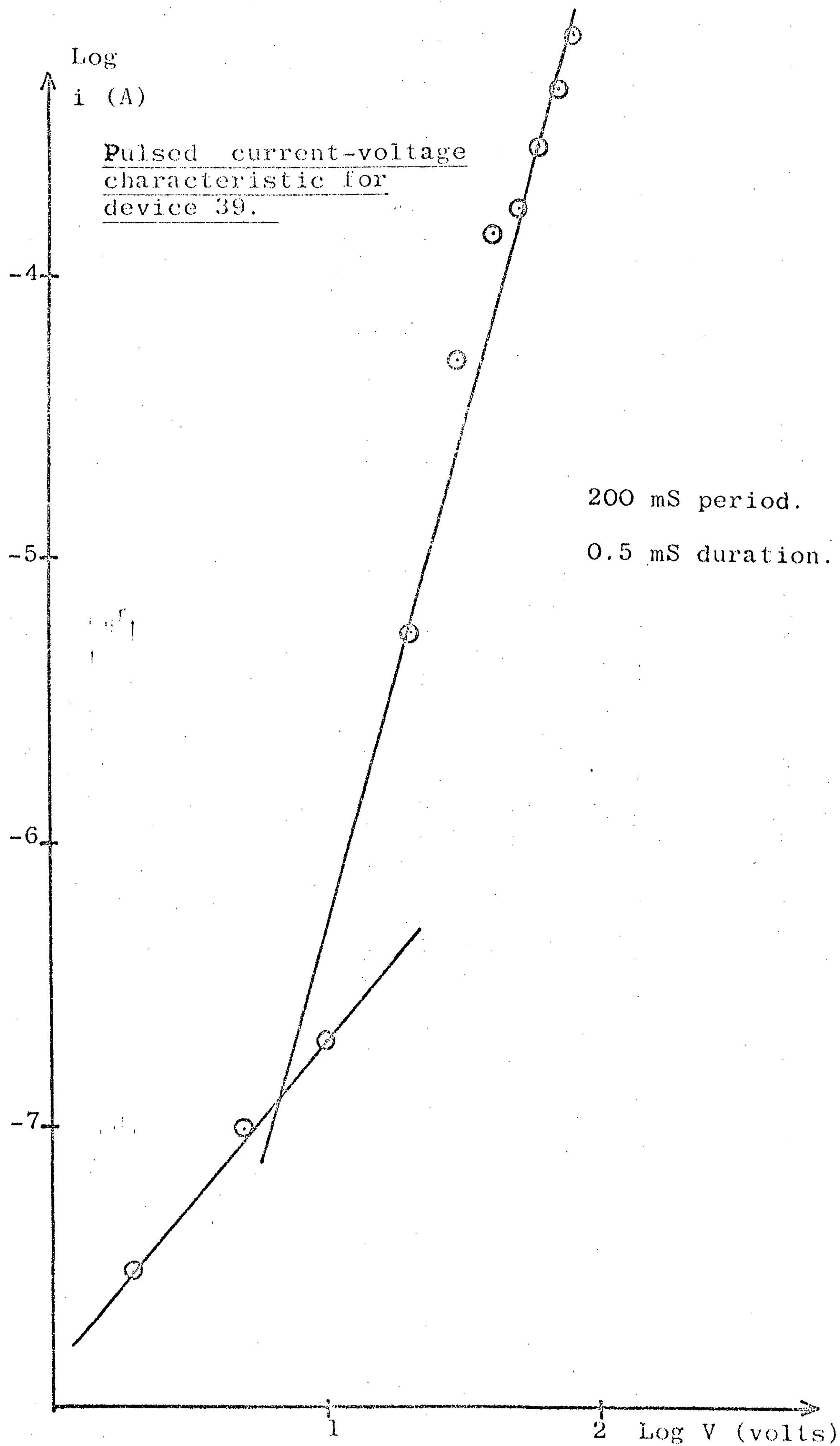

Figure 7.13.

UPPER TRACE : LIGHT, LOWER TRACE : CURRENT, TIMEBASE : 5mS/div

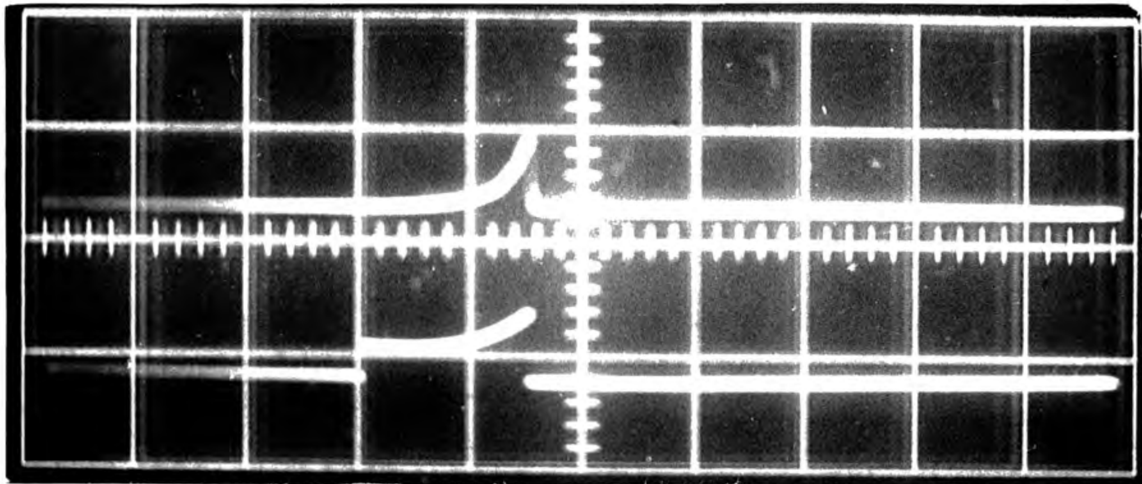

(1)

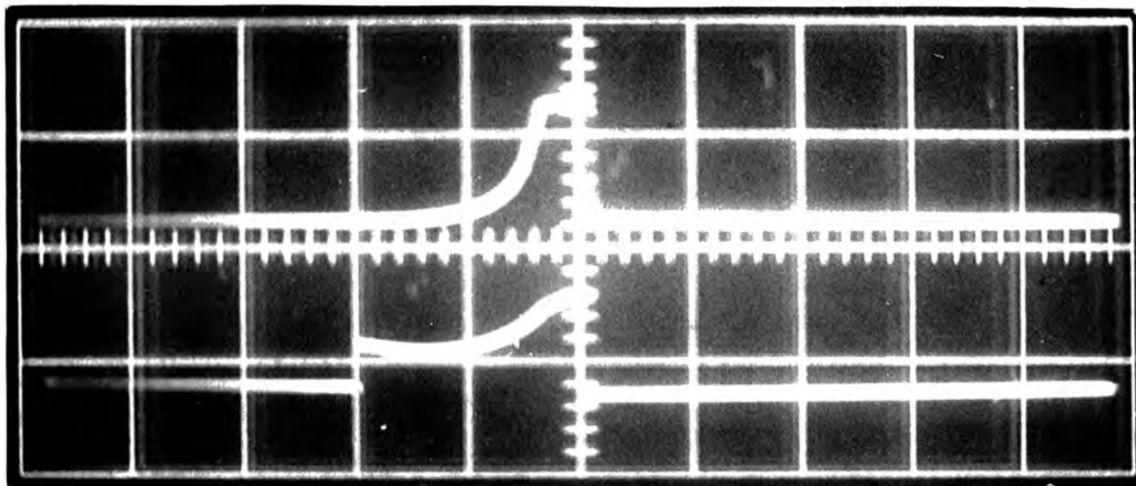

(2)

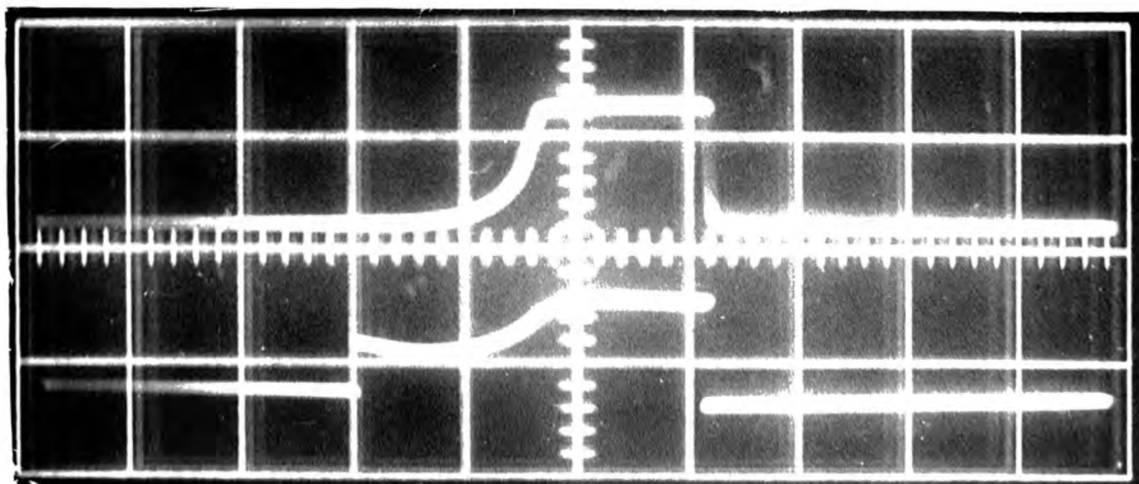

(3)

Figure 7.14.

and distortion superimposed.

Observations of the sine wave modulation showed that there was a phase difference between the light and current waveforms, the current leading the light. No measurements were made of this phase relationship because it was found to be too complex.

7.5. Pulsed D.C. measurements.

Measurements have been made with rectangular pulses applied to CdS crystals. During the pulse, the voltage across the sample was forward bias as for the D.C. measurements, and after the pulse duration had expired the voltage across the crystal was zero. When pulses are used a new range of phenomena occur. When the pulse amplitude is less than the D.C. breakdown voltage V_B a low current flows and the current waveform is that of a diferentiating circuit which corresponds to the crystal behaving like a capacitor. The current-voltage characteristic of a crystal measured under these conditions is illustrated in figure 7.13. The pulse duration was 0.5 mS and the period was 200 mS. At low voltages the characteristic is ohmic while above 7 volts the current increases as the cube of the applied voltage.

When the pulse amplitude exceeds V_B, the current is much larger than before, the difference being similar to that observed when D.C. switching occurs. The important feature of the pulse measurements is that when the voltage pulse amplitude is greater than V_B the current pulse waveform contains a step. This effect is shown in figure 7.14. Three pairs of waveforms illustrate the current and light waveforms

at constant voltage and period but with the duration increasing from 8 mS in 7.14.1 to 16 mS in 7.14.3. Theperiod was 200 mS. In 7.14.1 the step is not fully developed, but the back end of the current pulse is rising from the initial plateau. Figure 7.14.2 shows the step with the back of the pulse flattening off to another level hgiher than the plateau, and in 7.14.3 the second level extends over nearly half the duration of the pulse. Since the light is not emitted during the initial plateau but only when the current starts to rise, it is clear that the back end of the pulse where the light is emitted corresponds to the D.C. on state ofthe crystal, and is therefore associated with high hole lifetime and complete filling of the class II recombination centre with holes. The explanation of the step in the current pulse is deferred until Chapter 9.

The length ofthe initial plateau is dependent on the following parameters:

1. The temperature.
2. The pulse duration and period.
3. The external illumination.
4. The initial plateau height (which in turn depends on the voltage pulse amplitude.).

The measurements of the variation of the initial plateau length were hampered by the necessity to keep all the other parameters constant, and the plateau length itsself jittered under constant conditions of the parameters under control (temperature, period,

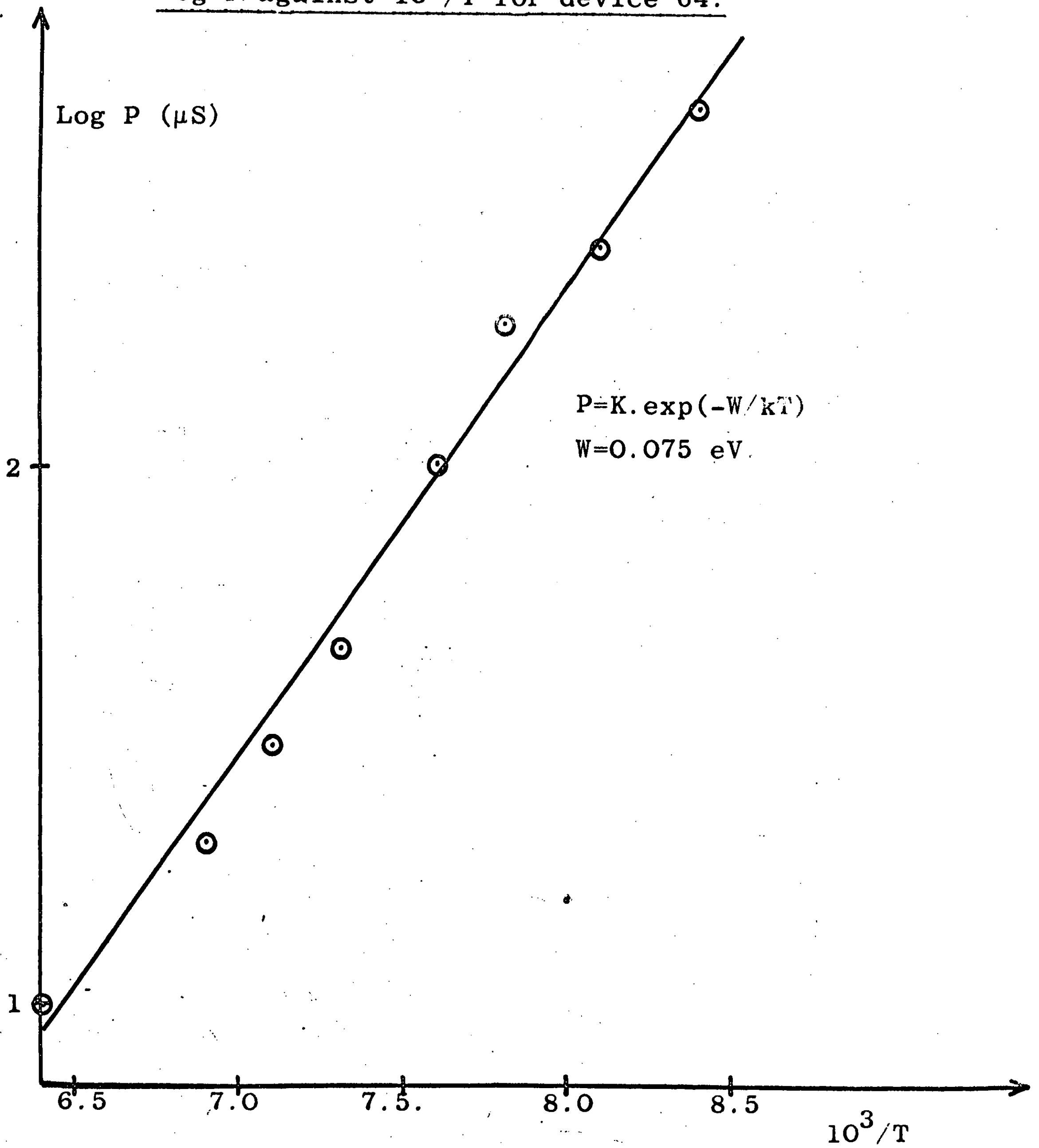

Figure 7.15.

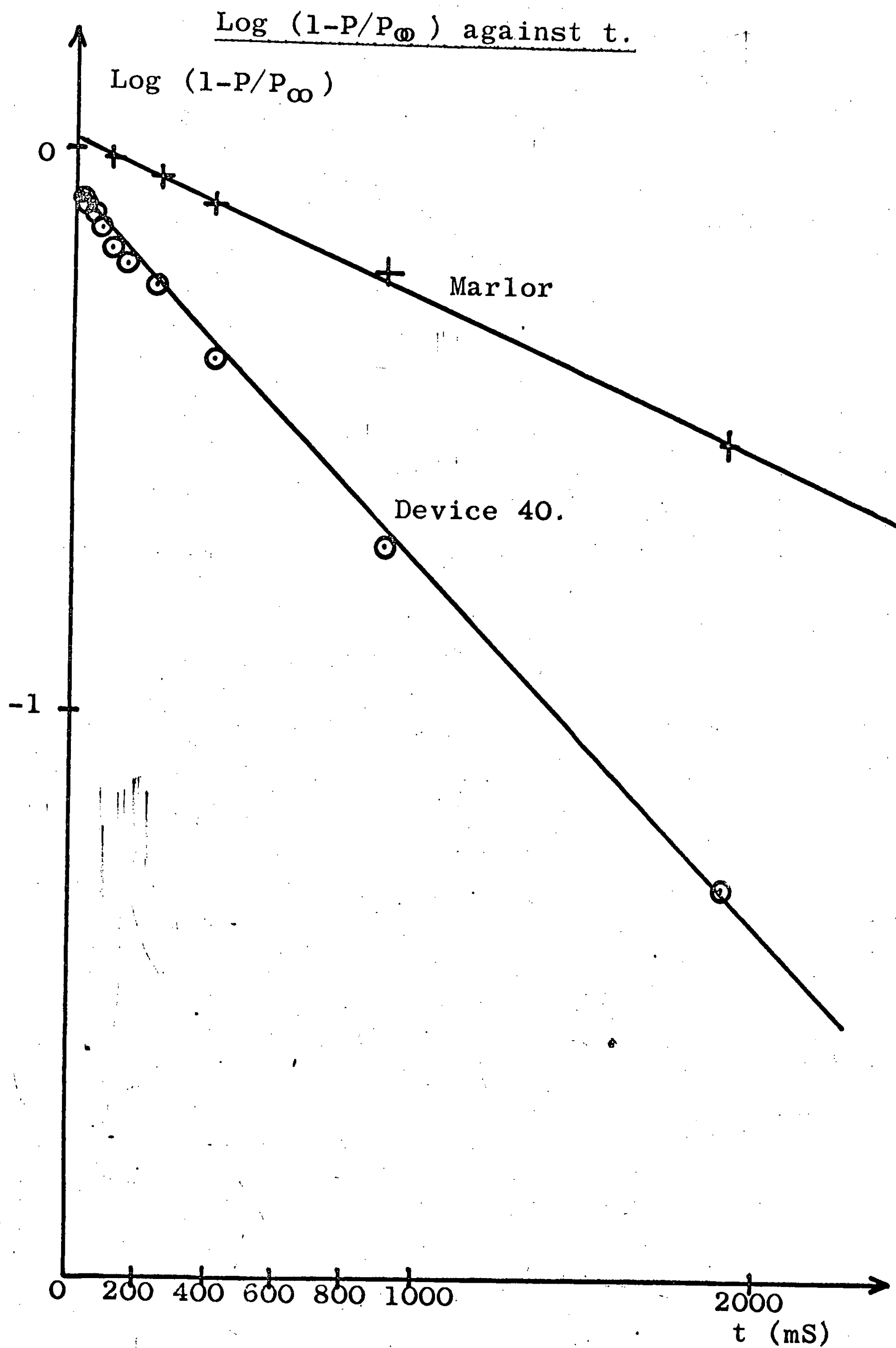

Figure 7.16.

duration, illumination, pulse amplitude). The variation of the plateau length with temperature is shown in figure 7.15. The pulse duration was 1 mS and the period was 100 mS. Figure 7.15 indicates that if the plateau length is P then it can be expressed in the form

$$P = K.\exp(-W/kT)$$

where K is a constant, and W is the activation energy for the process. In figure 7.15, W = 0.075 eV.

The variation of the plateau length P with repetition rate was measured on a crystal which showed a relationship which can be explained on a simple model. The model is described in chapter 9, and predicts that a plot of $\log(1-P/P_\infty)$ against t should be linear. t is the time that the pulse is off (i.e. t period-duration). A plot of $\log(1-P/P_\infty)$ against t is shown in figure 7.16 for device 40 and for a crystal previously mounted up and measured by Marlor. The difference in the slopes of the lines is due to the measurements being carried out on different crystals at different temperatures. Both are good straight lines but the intercepts differ from unity predicted by theory by about 5% for Marlor's crystal, and by 15% for that used in this work.

The change in the plateau length when external illumination is incident on the crystal has also been observed. With the Hilger and Watts monochromator and tungsten lamp, insufficient intensity could be obtained so the effect was studied using a microscope lamp and Chance glass filters. With red, yellow, and green light the plateau

Efficiency of light output against temperature.

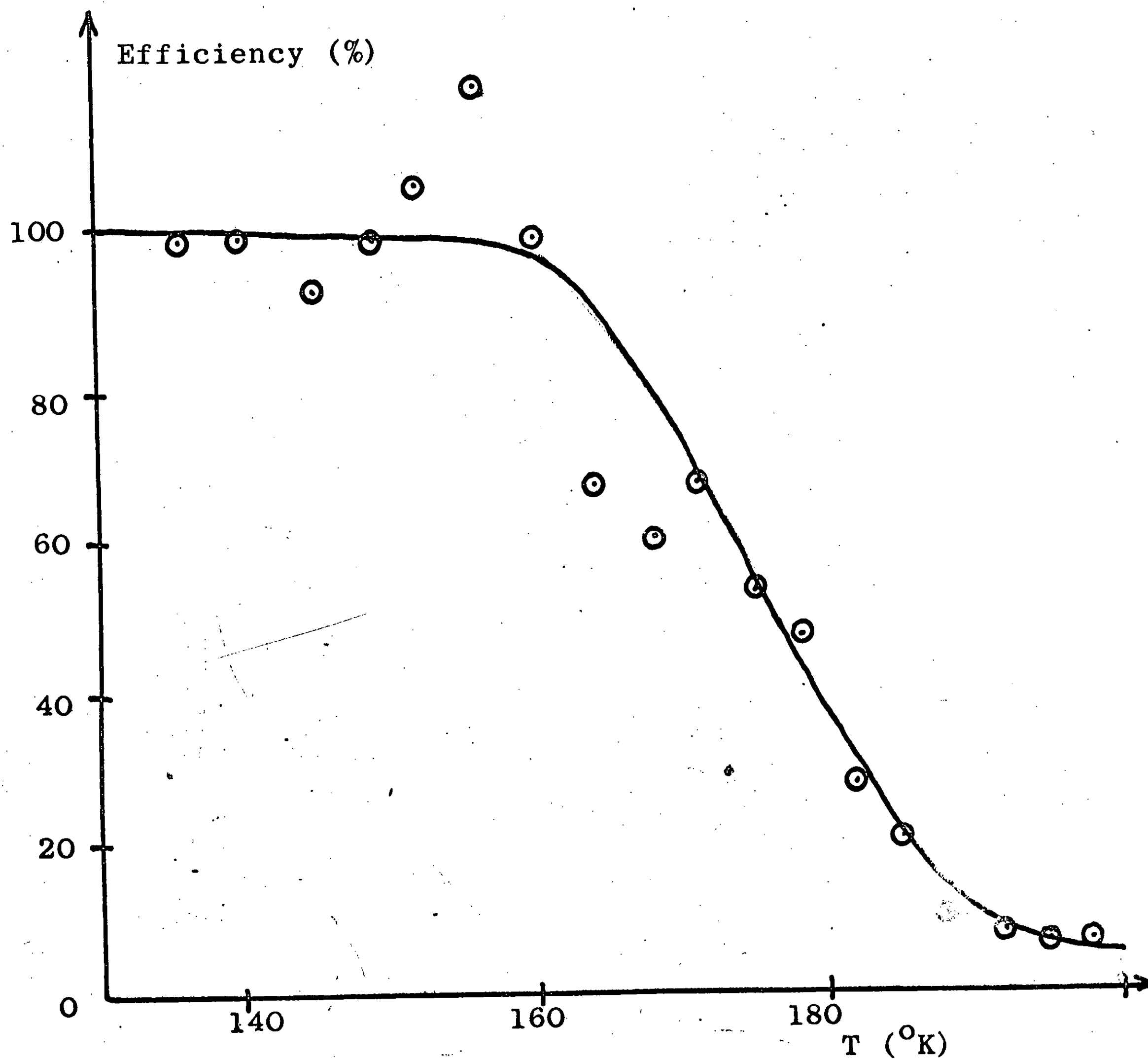

Figure 7.17.

Log (1/Eff. -1) against $10^3/T$.

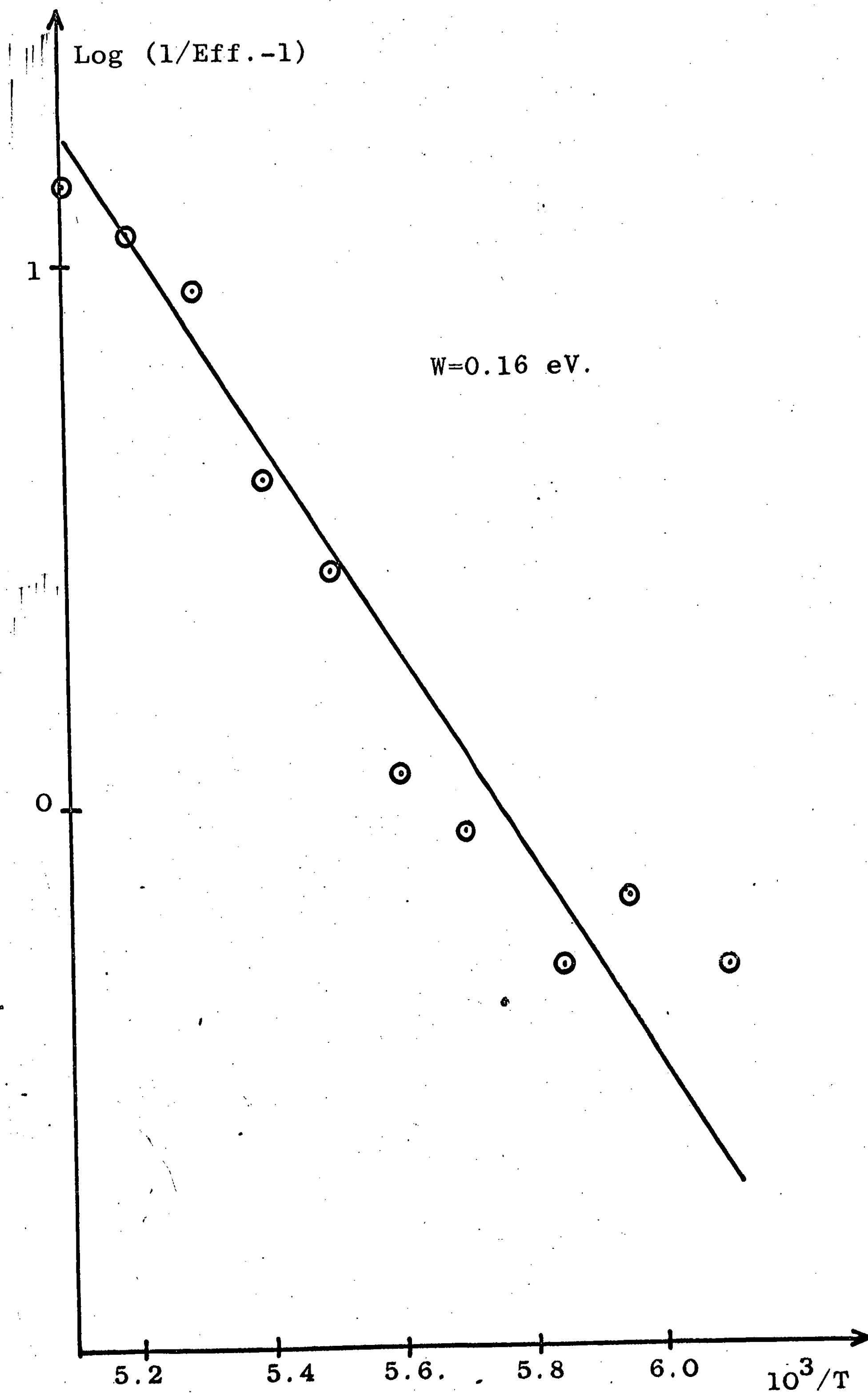

Figure 7.18.

length decreased when the illumination was applied. With blue light however an anomalous effect was observed. Let the initial plateau length be P_i. As the intensity of the blue light was increased, the plateau length increased from P_i until it was equal to the duration of the pulse and no step was visible. As the light intensity was increased still further, the plateau length suddenly shortened to a value P_f where $P_f < P_i$. Removal of the illumination increased the plateau length to a value slightly greater than P_f but still less than P_i. If the pulsed voltage was removed for a few seconds, and then re-applied, the plateau length was restored to its original value P_i.

The variation of the light output under pulsed conditions with temperature is plotted in figure 7.17. The efficiency was assumed to be 100% at 130 °K and below. The large jitter on the readings is not due to experimental error but because the light output jittered with time. The noise on the signal also increased as the temperature was raised. If the Schon-Klasens model of thermal quenching as described in section 3.3 is assumed to hold, then a linear relationship between $\log(1/\eta - 1)$ and $1/T$ is expected. Figure 7.18 shows that the relationship is linear for points in the range 160 to 195 °K. The activation energy for the process is 0.16 eV.

Although the light output falls off as the temperature is raised, and noise on the light waveform increases, light output at room temperature has been detected with a photomultiplier although it was not

Room temperature light output.

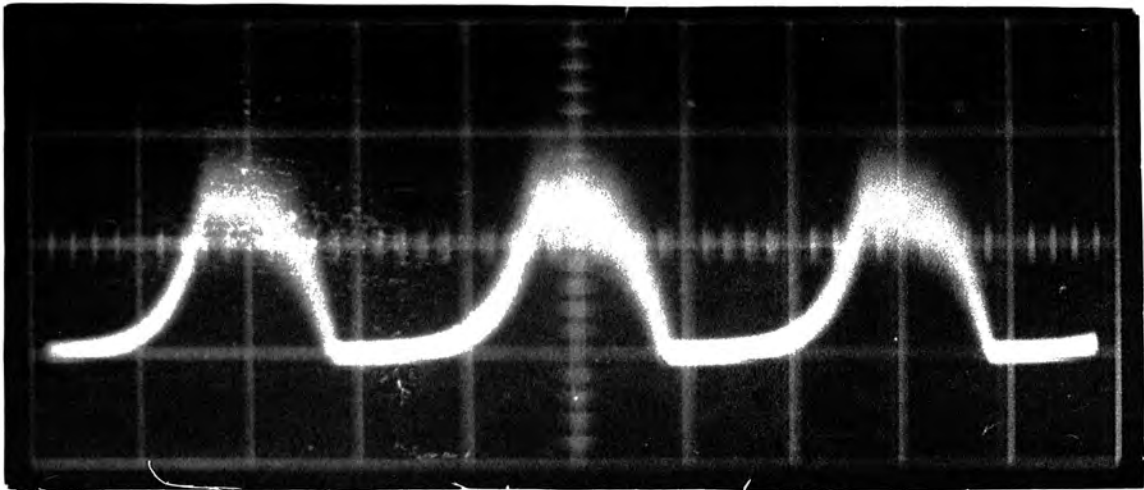

Horizontal scale: 200 μS/division.

Figure 7.19.

visible to the naked eye. Figure 7.19 is a photograph of the oscilloscope trace when the device was maintained at room temperature. A check was made to ensure that the signal was not spurious. The insertion of a shutter removed the signal and the insertion of filters indicated that the light was in the wavelength range 4500 to 6000 Å.

CHAPTER 8

Discussion of the spectral distribution measurements

8.1. Analysis of the photo-luminescent spectrum.

8.1.1. The edge emission.

The values of the wavelengths of the maxima of the bands which form the edge emission spectrum of CdS are tabulated in figure 8.1 for two sets of measurements performed on the same crystal on separate occasions. The photon energy and wave number corresponding to each maximum is also shown in figure 8.1. The agreement between the two runs is better than 10 Å except for the fifth maximum which was only tentatively identified and therefore difficult to locate accurately. The separation between the positions of the maxima is of the order of 300 cm^{-1} which is consistent with the series being due to recombination via a defect with the emission of 0, 1, 2, 3,.... longitudinal optical phonons (wave number 295 cm^{-1} from section 4.7). If it is assumed following Marlor and Woods[1] that the first maximum is due to a centre 1, and that the rest of the series is due to recombination via a separate centre 2 with the emission of 0, 1, 2..... phonons, then the photon energies of the two transitions involved in the luminescence are 2.407 and 2.373 eV respectively. The forbidden energy gap of CdS at 77 °K is 2.52 eV, and the shift of band gap with temperature is -5×10^{-4} eV/°K, so that the band gap at 107 °K is 2.505 eV. Thus the centres 1 and 2 are 0.10 and 0.13 eV from a band edge at 107 °K. This result is consistent with the findings of Reynolds[2] and of Marlor and Woods[1].

Photo-luminescence of device 39 (see fig 6.3).

Run 7 107 °K

	Wavelength (Å)	Energy (eV)	Wave number (cm^{-1})	Separation (cm^{-1})
1	5150	2.407	19,420	
				280
2	5223	2.373	19,140	
				250
3	5294	2.342	18,890	
				300
4	5379	2.305	18,590	
				250
5	5451	2.274	18,340	

Run 12 105 °K

	Wavelength (Å)	Energy (eV)	Wave number (cm^{-1})	Separation (cm^{-1})
1	5153	2.406	19,410	
				290
2	5230	2.370	19,120	
				260
3	5302	2.338	18,860	
				280
4	5381	2.304	18,580	
				180
5	5436	2.281	18,400	

Figure 8.1.

Energy levels in CdS at 77 and 107 ^{o}K.

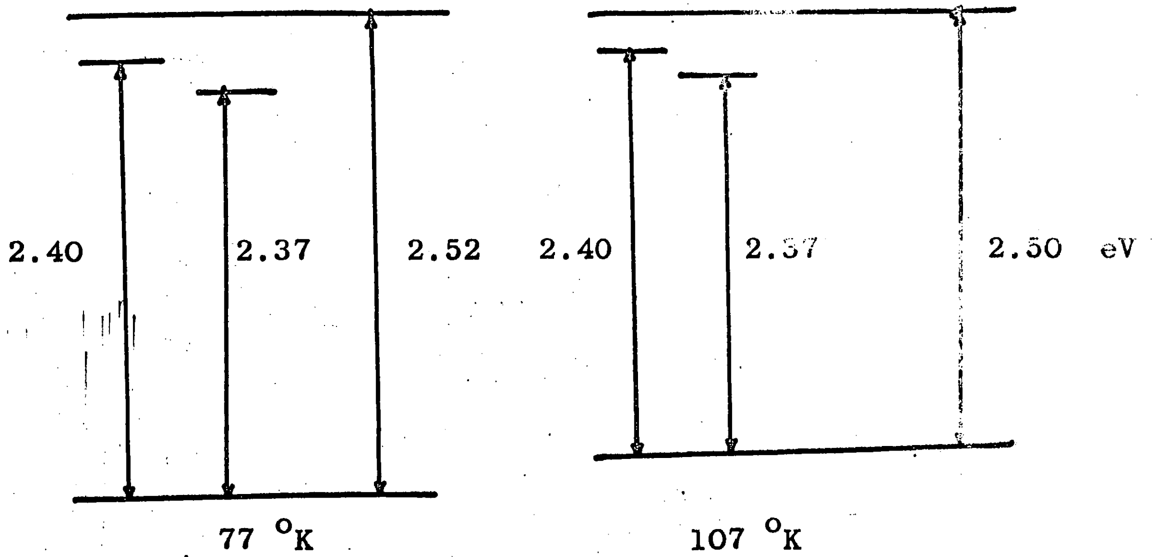

Figure 8.2.

Positions of high energy peaks (see fig 6.4).

		Wavelength (Å)	Energy (eV)	Wave number (cm^{-1})
t=15 min	1	4941	2.509	20,240
	2	5026	2.467	19,900
t=30 min	1	4959	2.500	20,160
	2	5021	2.469	19,910
t=120 min	1	4942	2.509	20,240
	2	5019	2.470	19,[illegible]

Figure 8.3.

Reynolds found that the wavelength of the green emission shifted little with temperature. In agreement with this Marlor and Woods obtained 2.404 and 2.369 eV for the luminescent photon energies at 77 ^{o}K compared with 2.407 and 2.373 eV at 107 ^{o}K measured in the present work. Thus the energy separation of centre 1 from its band shifts from 0.12 to 0.10 eV, and that of centre 2 from 0.15 to 0.13 eV when the temperature is raised from 77 to 107 ^{o}K. Since both centres shift by the same amount, the tentative suggestion is that both levels are associated with the same band. For illustration purposes the levels are assumed to be close to the conduction band, and the energy level scheme of the present work is compared with that of Marlor and Woods in figure 8.2.

8.1.2. The high energy bands.

As stated in section 6.3, the two emission bands with maxima at energies greater than the edge emission series appear when the crystal is maintained at low temperatures whilst being illuminated with light. This implies that the two high energy bands are associated with a surface or bulk photo-chemical effect or with photo-adsorbtion of impurities onto the surface of the crystal. The positions of the two maxima of the two bands are tabulated in figure 8.3 for the three cases illustrated in figure 6.4. The maximum 1 islocated at a wavelength corresponding to a photon energy almost equal to that of the forbidden energy gap of CdS at the temperature at which the measurement was made, and is due to either direct electron-

D.C. Electro-luminescence of device 15 (see fig 6.5).

	Wavelength (Å)	Energy (eV)	Wave number (cm^{-1})	Separation (cm^{-1})
1	4988	2.485	20,050	150
2	5026	2.467	19,900	510
3	5158	2.403	19,390	320
4	5243	2.365	19,070	350
5	5343	2.320	18,720	1,470
6	5800	2.140	17,250	

Figure 8.4.

hole recombination or to recombination via a level which is almost merged into one of the bands.

Reynolds[2] found emission bands centred at 4880, 4927, and 5012 Å at 77 °K which shifted by the same amount as the band gap with temperature, therefore these wavelengths correspond to 4910, 4957, and 5042 Å at 107 °K. Thus the second two bands observed by Reynolds correspond to the two high energy bands observed in the present work. The energy associated with the second maximum is 2.47 eV which places the energy level responsible 0.03 eV from a band edge. This is of the order of the depth of shallow donor levels below the conduction band in CdS[4]. Thus it may be postulated that the high energy emission observed by Reynolds and in this work is due to the same two recombination mechanisms, and that the higher energy band is due to a transition which produces the emission of photons with energies almost exactly equal to that of the forbidden energy gap, and that the other band is a result of recombination between a free hole and an electron trapped at a donor level 0.03 eV below the conduction band.

8.2. Analysis of the D.C. electro-luminescent spectra.

8.2.1. Device 15.

The spectral distribution of the emission from device 15 was shown in figure 6.5, and the wavelengths of the maxima of the bands are tabulated in figure 8.4. The temperature of the crystal was not monitored but other measurements have shown that with 50 mA flowing through the sample, the temperature is approximately 130 °K. The crystal had

D.C. Electro-luminescence of device 39 (see figs 6.6 and 6.7).

		Wavelength (Å)	Energy (eV)	Wave number (cm^{-1})	Separation (cm^{-1})
20 mA	1	5017	2.471	19,930	
105 °K	2	5164	2.401	19,370	
30 mA	1	5033	2.463	19,870	
116 °K	2	5170	2.398	19,340	
45 mA	1	4935	2.512	20,260	
					380
	2	5029	2.465	19,880	
					530
	3	5169	2.398	19,350	
					240
	4	5233	2.369	19,110	
					340
	5	5327	2.327	18,770	
					110
	6	5359	2.313	18,660	

Figure 8.5.

an air dried, silver paint anode and evaporated indium as cathode.

In contrast to the photo-luminescence the emission was mainly in two bands centred at 4988 and 5026 Å. The 5026 Å maximum is at the same wavelength as the second maximum identified in section 8.1.2 and therefore is probably associated with the same defect, but the band centred at 4988 Å does not correspond to any emission band previously observed. The edge emission series although weaker than in the photo-luminescence still has the same 300 cm^{-1} spacing and despite the high temperature shows no shift in wavelength from the photo-luminescence at 77 °K, adding further confirmation to Reynolds findings. The feeble band at 5800 Å corresponds to recombination which takes place via a level approximately 0.4 eV from a band edge.

8.2.2. Device 39.

The photo-luminescent spectrum discussed in section 8.1 was that of the crystal from which device 39 was constructed. The wavelengths of the maxima of the electro-luminescence of device 39 for the three current densities used for the measurements shown in figures 6.6 and 6.7, are tabulated in figure 8.5. For the two spectra measured with 20 and 30 mA passing through the crystal there is in each case one band at high energy and one band corresponding to the edge emission. The high energy band centred at a mean position of 5025 Å is the same band as the second band observed in the photo-luminescent spectrum. The edge emission series is not resolved but

Pulsed D.C. electro-luminescence of device 39 (see fig 6.7).

	Wavelength (Å)	Energy (eV)	Wave number (cm^{-1})	Spacing (cm^{-1})
1	5040	2.460	19,840	
				500
2	5169	2.398	19,340	
				240
3	5234	2.368	19,100	
				250
4	5306	2.336	18,850	

Figure 8.6.

the maximum of the bands with 20 and 30 mA passing is displaced to longer wavelength than the first band of the edge emission series in the photo-luminescence.

The spectrum measured at a current of 45 mA was obtained just before the crystal was destroyed by thermal runaway. The two high energy bands are centred at 4935 and 5029 Å, which is in good agreement with the location of the band maxima in thephoto-luminescent spectra. The edge emission series has the first band maximum displaced to longer wavelength relative to the photo-luminescence, but the second maximum is located at about 5230 Å in both the electro-, and the photo-luminescence.

8.3. <u>Analysis of the pulsed D.C. electro-luminescent spectra.</u>

8.3.1. Device 39.

The spectral distribution of the light output from device 39 was measured when pulsed D.C. voltages were applied. The spectrum is shown in figure 6.8, and the locations of the band maxima are tabulated in figure 8.6. The pulse duration was 75 mS and the period was 100 mS. There are two important features of the spectrum:

1. There is a high energy maximum located at 5040 Å which is common to all spectra analysed so far.

2. The first band in the edge emission series is centred at 5169 Å as in the D.C. electro-luminescent spectra, which is a displacement to longer wavelength of 20 Å compared with the photo-luminescence.

The second maximum in the edge emission is not significantly displaced.

8.3.2. Device 43.

The spectrum of device 43 is shown in figure 6.9. The pulse duration was 300 microseconds, and the period was 2 mS. A current of 125 mA flowed during the pulse. The spectrum is different from all the other electro-luminescent spectra in that there is no high energy component. The maximum emission is centred on 5178 Å which represents a displacement of the main edge emission band by about 25 Å from the corresponding photo-luminescent band. In addition there is a slight shoulder at approximately 5267 Å. The absence of high energy structure could be explained by associating a slow rise time with the high energy bands so that during 300 microseconds the emission would not have time to build up to a detectable level. Alternatively, the surface states responsible for the emission could be absent from this crystal. The second explanation is the more likely since the high energy bands were absent from the photo-luminescence, nor did any high energy emission appear in the electro-luminescent spectrum after the crystal had been exposed to ultra-violet light at low temperature.

8.4. <u>Analysis of the cathodo-luminescent spectra.</u>

The cathodo-luminescent spectra of a pure CdS crystal measured at two excitation levels is shown in figure 6.10. The positions of

Cathodo-luminescence of CdS (see fig 6.10).

Low excitation.

	Wavelength (Å)	Energy (eV)	Wave number (cm^{-1})	Spacing (cm^{-1})
1	5200	2.384	19,230	
				240
2	5265	2.355	18,990	

High excitation

	Wavelength (Å)	Energy (eV)	Wave number (cm^{-1})	Spacing (cm^{-1})
1	5133	2.415	19,480	
				250
2	5199	2.385	19,230	
				[illegible]
3	5230	2.370	19,120	
				120
4	5264	2.355	19,000	
				150
5	5306	2.337	18,850	

Figure 8.7.

the maxima of the bands are tabulated in figure 8.7. The errors in the positions of the maxima are greater than the errors in the location of the maxima of the photo-, and electro-luminescence already described, because as was stated in section 6.6 the cathodo-luminescent spectra were obtained after the sine wave modulation had been averaged out. No high energy components are present in the two cathodo-luminescent spectra. The explanation for this could lie in the atmosphere surrounding the crystal. In the photo-, and electro-luminescent spectral distribution measurements the crystal was effectively a cold finger in a vacuum of 0.05 torr provided by a backing pump of the conventional kind. In the cathodo-luminescent measurements however the vacuum of 10^{-5} was achieved by the use of a mercury diffusion pump and a liquid nitrogen cold trap. Thus in the former case any volatile component in the vapour surrounding the crystal would condense onto the crystal as soon as the refrigerant was poured into the cryostat. In the latter case, the liquid nitrogen cold trap would condense the residual volatile vapours before the crystal was cooled down.

The edge emission series is resolved at the high excitation level and has the usual maxima situated in this case at 5133, 5230, and 5306 Å. However both the cathodo-luminescent spectra have unusual bands centred on 5200 and 5265 Å which remain unexplained.

Positions of photo-luminescence peaks.

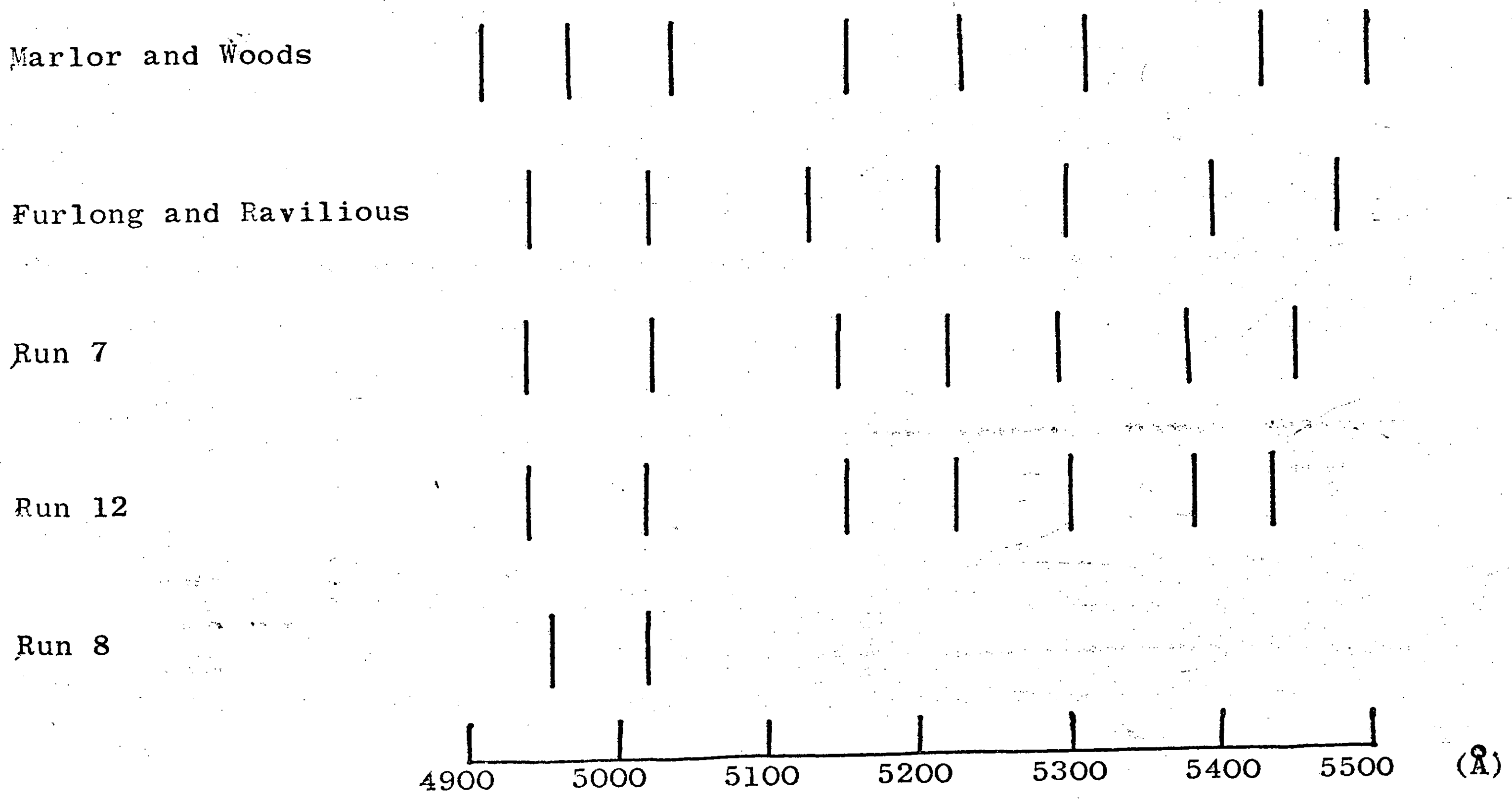

Figure 8.8.

8.5. Comparison of photo-, electro-, and cathodo-luminescent spectra.

8.5.1. Comparison of the photo-luminescence in the present work with the results of other workers.

The photo-luminescent spectra described in this thesis will be compared with the results of Marlor and Woods[1], and with those of Furlong and Ravilious[5]. Figure 8.8 shows a comparison of the high energy and the edge emission band maxima. In the high energy region there is good agreement between the results of the present work and those of Furlong and Ravilious. Furlong and Ravilious showed that the high energy bands disappeared if the crystal was baked whilst the cryostat was pumped. The bands could be restored if the crystal was exposed to the atmosphere. Thus it was concluded that the high energy bands were due to gas adsorbed on the surface of the CdS. The agreement between the two sets of results despite the difference in the temperature at which they were measured is in contradiction with the results of Reynolds who found that the bands shifted in energy by 5×10^{-4} eV/°C.

The values of the positions of the band maxima for the edge emission series obtained in the present work show fair agreement with those obtained by Marlor and Woods, and Furlong and Ravilious. The difference between the location of any given maximum between the three sets of results is never worse than 20 Å for the first five maxima.

Photo-and electro-luminescence spectra of device 39.

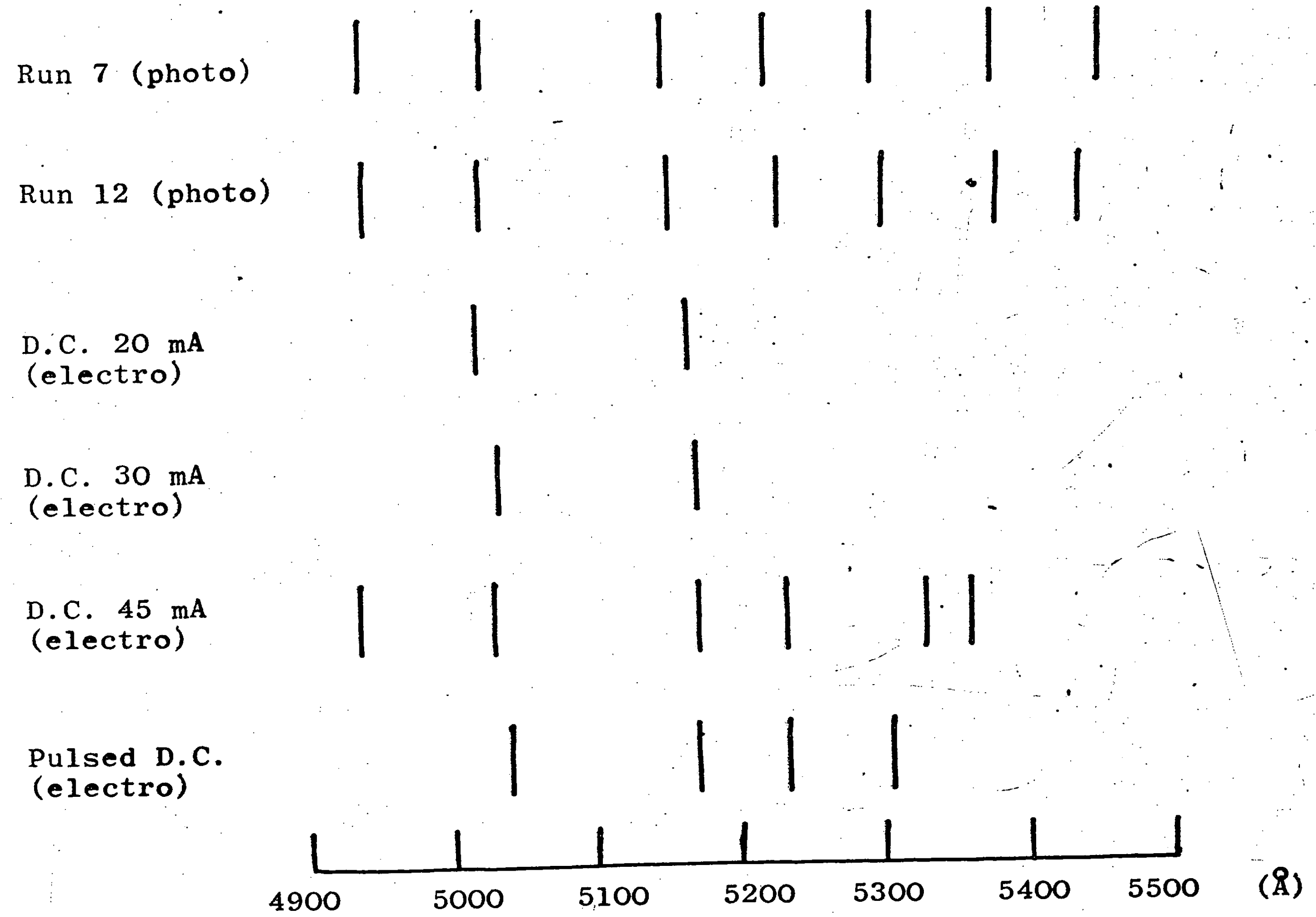

Figure 8.9

8.5.2. Comparison between all the luminescent spectra of device 39.

Figure 8.9 shows the wavelengths of all the maxima of the bands in the photo-luminescence, and in the D.C. and pulsed D.C. electro-luminescence of device 39. Whichever form of excitation was used, the location of the maxima of the two high energy bands coincided to within 10 Å which is of the order of the limit of the experimental accuracy of the measurements. Thus the average values of the wavelengths on which the two bands are centred are 4939 and 5028 Å.

The three edge emission series show good agreement for the second and third maxima when they were resolved. However, the first band of the edge emission series in all the electro-luminescent spectra is shifted to longer wavelengths relative to the photo-luminescent band. The average values are 5152 and 5168 Å for the photo-, and electro-luminescence respectively. This shift could be additional evidence for associating the first maximum of the series with a different centre from the rest of the series. Thus the first maximum could be the luminescence excited primarily by the ultra-violet light as it is absorbed close to the surface of the crystal. The rest of the series could then be excited by the absorption of the radiation associated with the first maximum in the bulk of the crystal. Any change in the state of the surface of the crystal, for example the shallow diffusion of the anode during mounting up of the crystal would affect the position of the first maximum but not the rest of the luminescence. However, the difference may not

Photo-, electro-, and cathodo-luminescence spectra.

Device 39 (photo)

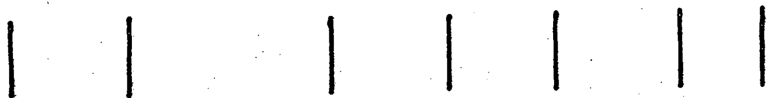

Device 39 (electro) D.C. 45 mA

Device 39 (electro) Pulsed D.C.

Device 43 (electro) Pulsed D.C.

Cathodoluminescence

Cathodoluminescence.

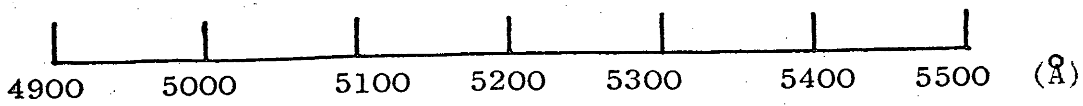

Figure 8.10.

be significant and might be accounted for in the different temperature variations of the two types of luminescent process.

8.5.3. Photo-, electro-, and cathodo-luminescent spectra.

Figure 8.10 shows a comparison between:

1. All the luminescent spectra obtained from device 39.
2. The cathodo-luminescent spectrum of pure CdS.
3. The pulsed D.C. electro-luminescent spectrum of device 43.

In both the pulsed measurements the highest energy maximum is missing and in the spectrum of device 43, the other high energy maximum is also absent. The cathodo-luminescent spectrum shows good agreement with the edge emission series of the photo-luminescence except for the first peak which was badly defined by the averaging process already described. Both the cathodo-luminescent spectra have additional maxima at 5200 and 5265 Å. The 5265 Å band is also observed in the spectrum of device 43, but the band centred at 5200 Å has not been observed in any spectrum other than the cathodo-luminescence. No explanation for these two bands can be offered at this stage.

The difference in the position of the first edge emission band of the electro-luminescence and the photo-luminescence is most marked in the pulsed electro-luminescent spectrum of device 43. The evidence is thus in favour of the shift to longer wavelengths in the electro-luminescent spectra being due to heating of the crystal. The current during the pulse whilst the spectrum of device 43 was being measured

was 125 mA and it seems likely that this caused Joule heating of the crystal during the pulse, and that the thermocouple did not respond to the increase in temperature fast enough to give a true indication of the actual crystal temperature during the time throughout which the light was being emitted. Thus it must be deduced that in all the electro-luminescent spectral measurements the actual temperature of the crystal was greater than that registered by the thermocouple. It could therefore be concluded that the wavelength of the first edge emission peak is temperature dependent above about 110 °K, but as was shown in section 8.1.1, the wavelength does not shift with temperature between 77 and 107 °K. Since the second and third maxima of the edge emission series do not show a similar shift, it must be concluded that the first maximum is associated with one centre whilst the rest of the series is associated with a different centre.

8.6. <u>Summary of the conclusions from the luminescent spectra.</u>

8.6.1. The origin of the high energy bands.

The maxima of the two high energy bands occur at 4940 and 5030 Å in both the photo-, and electro-luminescent spectra. The amplitudes of both these bands are enhanced if the crystal is illuminated with ultra-violet light at temperatures in the region of 100 °K, and saturates after a period of illumination of 2 hours. In the spectra of some crystals the bands were absent no matter how long the radiation was incident on the crystal. With the photo-luminescence, the band centred on 4940 Å was always found to be of greater amplitude than that

centred on 5030 Å, whereas for the electro-luminescence the reverse was true. The energy corresponding to the photon energy of the shorter wavelength band is almost exactly equal to that of the forbidden energy gap of CdS at 100 °K (2.51 eV) and is probably due to recombination at the surface of the crystal via an extremely shallow level, and the photon energy of the other band maximum (2.47 eV) corresponds to a level 0.03 eV from a band edge, and is therefore probably due to recombination between a free hole and an electron trapped at the shallow donor level 0.03 eV below the conduction band. The two bands occur at wavelengths almost exactly equal to those observed by Furlong and Ravilious (4946 and 5027 Å) at 77 °K and if these are due to the same surface processes as seems likely, then the positions of the maxima do not shift with temperature in the range 77 to 107 °K. Since the high energy bands do not appear in all crystals their origin must be more complicated than mere adsorption of gas onto the surface of the CdS. Photo-chemical effects are well known to occur in CdS[6,7], and a surface photo-chemical reaction coupled with the adsorption of gaseous impurities may be necessary to produce the effect.

8.6.2. The nature of the edge emission series.

The edge emission series observed in the photo-luminescent spectrum of CdS is observed in the electro-luminescent spectra under both D.C. and pulsed D.C. excitation, and also in the cathodo-luminescent spectra. The first three bands of the series have

maxima which can be located with reasonable accuracy in the electro-, and cathodo-luminescence, but beyond the third maximum the resolution has been inadequate to enable location of the remainder of the maxima to be made with accuracy. In the photo-luminescent spectra, the first three peaks lie at worst less than 15 Å, and at best less than 10 Å within the values obtained by Marlor at a temperature 30 °K less than that employed in the present work. Thus in agreement with Reynolds findings, it is clear that the edge emission wavelengths do not shift in the temperature range 77 to 107 °K. Therefore the levels responsible for the emission must shift relative to the band in whose proximity they lie at the same rate as the band gap shifts with temperature (5×10^{-4} eV/°C). Further Marlor and Woods have shown that the first peak is of a different origin to the rest of the series, so that centre 1 as defined in section 8.1.1 shifts from 0.12 to 0.10 eV, and centre 2 shifts from 0.15 to 0.13 eV from a band edge as the temperature is raised from 77 to 107 °K. Since both levels shift by the same amount, it seems reasonable to postulate that they are associated with the same band. Further evidence that there are two levels involved is provided by the electro-luminescent spectral measurements. In all the electro-luminescent spectra, the first maximum of the edge emission series is displaced to longer wavelength by as much as 20 Å, whereas the second and third maxima are essentially at the same wavelengths as in the photo-luminescence. The mechanism of the shift could be either the Stark effect or heating of the crystal. Further work is necessary to distinguish between these hypotheses but

the heating of the crystal seems the more likely explanation. This latter explanation would mean that the first band of the series would be temperature dependent above 110 ^{o}K whereas the rest of the series would have wavelengths independent of the temperature over the range investigated. In order to verify this theory it will be necessary to construct devices with built-in thermocouples of low thermal inertia. This has not been possible with the device structure employed in the course of this work.

The assignment of longitudinal optical phonons as being responsible for the edge emission series after the first maximum has not been completely confirmed by the present work. It is possible from the spacings observed in the photo-luminescence of device 39 that transverse optical mode phonons may be responsible for some of the maxima since spacings of the order of 250 cm^{-1} were found and these correspond to the wave numbers of the TO phonons (TO_1 261, and TO_2 238 cm^{-1}). Further work with better resolution at lower temperatures is required to clarify the situation.

CHAPTER 9

Discussion of the electrical measurements

9.1. D.C. current-voltage characteristics.

The current-voltage characteristic of device 46 measured at 88 ^{o}K in figure 7.1 corresponds closely to the type of characteristic predicted by the theory of Ashley and Milnes (section 2.5). The low voltage region is ohmic , whereas for voltages in excess of a transition voltage V_t, a square law is obeyed. After the square law regime, the current rises vertically at the breakdown voltage V_B. According to Ashley and Milnes, the value of V_t. ~~and V_B are~~ is :

$$V_t = \frac{L^2}{\mu_n \tau_n} \qquad 9.1.$$

and

$$V_B = \frac{L^2 n_{RO} . s_p . v_{tp}}{\mu_p} \qquad \text{following Lampert} . \quad 9.2.$$

where the symbols have the same significance as in section 2.5. For device 46, the values are $V_t = 6$ V, $V_B = 65$ V, and $L = 130$ microns. Taking an electron mobility of 250 cm^2/V sec, equation 9.1 gives a value of the electron lifetime of 1.1×10^{-7} seconds. The solution of equation 9.2 would be possible if either the capture cross section for holes, s_p, or the electron density in the recombination centres in thermal equilibrium n_{RO} were known. In the model applicable to CdS, $n_{RO} \simeq N_R$. Thus from equation 9.2, $N_R . s_p = 10^{-2} cm^{-1}$. Thus if s_p is assumed to be 10^{-18} cm^2, then the density of recombination centres N_R is 10^{16} cm^{-3}.

The square law dependence of the breakdown voltage, V_B, on device

Hole lifetime in CdS (fig 7.5).

Device	L(μ)	V_B(Volts)	τ(nS)
51	55	51	40
54	51	47	37
57	116	164	55
58	68	40	77
59	47	22	67
63	44	32	40
64	43	22	58
46	130	65	173

Mean hole lifetime=53 nS.

Figure 9.1.

Hole lifetime in CdS.

Workers	Method of measurement	Value (Sec)
Spear and Mort[2]	Drift	10^{-7}
Keating[3]	Double injection	1.5×10^{-8}
Friedrich[4]	P.E.M.	10^{-7} to 10^{-4}
Rushby	Double injection	5×10^{-8}

Figure 9.2.

thickness, L, was tested on several crystals from the same growth run where the variation in N_R from crystal to crystal should be a minimum. Figure 7.5 shows the log-log plot of breakdown voltage against device thickness, and a reasonable agreement with the square law dependence predicted by the theory of Ashley and Milnes is found. Since breakdown occurs when the transit time for holes is of the same order as the hole lifetime, the values of V_B can be used to calculate the values of the hole lifetime. The hole lifetimes are tabulated in figure 9.1. A mean value of the hole lifetime of 5.3×10^{-8} sec is obtained for the devices whose breakdown voltages were plotted against thickness in figure 7.5. The values of the hole lifetime are within an order of magnitude of the results of other workers on CdS which are summarised in figure 9.2 for comparison purposes.

In contrast to the characteristic at 88 °K, the room temperature characteristic has an extended ohmic region which is dueto the higher thermal density of electrons. In the characteristic shown in figure 7.2, the square law region is not observed since the breakdown region is reached before the transition from ohmic to square law dependence has taken place. This implies that the product of the electron lifetime and the electron mobility must be less at 295 °K than at 88 °K. The value of V_B is less at the higher temperature despite the thermal velocity of holes v_{tp} being approximately $(3)^{1/2}$ greater. The difference is accounted for by the increase

in the hole mobility with temperature. Mort and Spear[2] found that the hole mobility was 5 times greater at room temperature than at 88 °K, and the factor $\left(\frac{3}{5}\right)^{1/2}$ is within 20% of the value required to explain the difference in V_B between 88 and 295 °K.

The hysteresis in the post-breakdown characteristic is also consistent with the theory of Ashley and Milnes which requires that for negative resistance to be observed, the capture cross sections of the recombination centre for electrons, s_n, and for holes, s_p, must obey the innequality

$$s_p \gg s_n$$

Thus once the recombination centre has captured a hole, there is only a small probability that it will recapture an electron, and the high lifetime state for holes can be maintained with lower hole injection rates than those initially required to switch the device into the high current state. As a result the device will stay on at lower currents than are necessary when switching occurs. Once the rate of hole injection is no longer sufficient to populate the recombination entirely with holes, the hole lifetime decreases by several orders of magnitude and the device switches off.

9.2. Optical switching effects.

The switching from a low to a high current state, when the device is biased below the breakdown voltage, by irradiation with light of suitable wavelength is due to the depopulation of the recombination

centres of electrons. This increases the hole lifetime because the recombination centres have a much greater capture cross section for holes than for electrons. When the hole lifetime is increased to a value of the order of the hole transit time, switching occurs. Once the device has switched, it will remain in the high current state with the illumination removed. The switching is a bulk effect as shown by the fact that light which is absorbed close to the surface will not switch the device. The long wavelength threshold (8100 Å) corresponds to a photon energy of 1.53 eV, which gives the position of the recombination centre 1.53 eV below the conduction band or 0.98 eV above the valence band, if the band gap is taken to be 2.51 eV at 100 °K. A similar switching effect has been observed in silicon by Marsh, Baron, and Mayer.[5] They ascribe the effect to the same type of process as described above. Further these authors were able to switch the device off by irradiating the device with light of suitable wavelength. In CdS this corresponds to light of photon energy sufficient to raise an electron from the valence band to the recombination centre, but insufficient to raise an electron from the centre to the conduction band. With the CdS devices all attempts to switch the current from the high to the low state by optical means failed. The switching effect is ~~thus~~ Probably not associated with the levels responsible for the infra-red quenching band centred at 8500 Å (1.45 eV), which is easily observable.

The reduction in the breakdown voltage V_B when the crystal is irradiated is shown in figure 7.4. As the light intensity is increased, the negative resistance range decreases and at the highest light intensity shown disappears completely. Similar characteristics have been obtained from Ge, Si, and GaAs devices by Holonyak et al[6]. These workers applied Lampert's theory (section 2.4) to obtain

$$\frac{s_p}{s_n} \simeq \frac{V_{th}}{V_M}$$

For most CdS crystals this would give a maximum value for the ratio s_p/s_n of 3, which is far too small for the strong asymmetry of the centre, $s_p \gg s_n$, required by Lampert's theory.

9.3. A.C. characteristics.

Figure 7.7 shows that the D.C. current-light output characteristic is linear over a wide range. As would be expected, A.C. modulation of the current about a standing D.C. bias current, to keep the device on at all times, also produces a linear A.C. current-A.C. light output characteristic. The phase difference between the current and the light is complex with the current leading the light. This relationship is probably associated with the process which is responsible for the delays observed in the pulse measurements described in section 9.4. From figure 7.12, the bandwidth of modulation of the light, which is taken as the frequency separation between the points at which the light output is half the maximum, is 17 kc/s

and the maximum frequency of modulation is 500 kc/s, so that it must be concluded that the device has little probability of being employed in optical telecommunication systems. It is likely that themaximum frequency of modulation is limited by the phosphorescent nature of the luminescent process so that the lifetime associated with the luminescence is 2 microseconds.

9.4. Effects observed using pulsed D.C. voltages.

The current-voltage characteristic for device 39 when pulsed D.C. voltages were applied is shown in figure 7.13. The maximum voltage applied was less than V_B during the pulse so that the characteristic corresponds to the device in the off state. At low voltages ohm's law is obeyed, followed by a region where the current depends on the cube of the voltage. The cube law corresponds to the characteristic for a plasma injected into a trap free insulator (section 2.3). Measurements of the current-voltage characteristics of other devices have yielded a wide variety of power laws. All crystals had ohmic regions followed by power laws as high as 10. The wide variety of power laws indicates that in CdS there is a large variation of trap densities from crystal to crystal which makes it very difficult to produce a consistent explanation of the effects observed in this material.

The step in the current pulse already demonstrated in figure 7.14 owes its origin to similar hole trapping effects as those which are responsible for the switching effects described in section 9.1. The

explanation is as follows. Consider that a train of current pulses has been initiated (either by applying a voltage greater than V_B, or by irradiating the crystal with light). The waveform of the current pulse is as described in section 7.5. During the latter part of the pulse all the recombination centres are occupied with holes and the hole lifetime is high. At the end of the pulse the occupation of the recombination centres changes as the Fermi level shifts. This means that during the off time of the pulse a fractionof the centres becomes filled with electrons. When the next pulse arrives, the hole lifetime is low and enough holes must be injected to fill the centres occupied with electrons before two carrier current flow can be established. Thus the current remains in the low state until the requisite number of holes have been injected after which the current rises to a higher level. Once the current has risen to the higher level, the free holes can recombine via class I centres, and in particular radiative recombination can occur. This explains why in figure 7.14 there is no light emitted during the plateau, but only when the current starts to rise.

A simple model of the effect is as follows. Let the density of the recombination centres be N_R cm^{-3}. After time t measured from the end of the pulse, the number of centres containing holes will be

$$N = N_R . \exp(-pt)$$

where p is the probability that a hole can thermally escape from a centre. p is of the form

$$p = \nu . \exp(-E/kT)$$

where ν is the attempt to escape frequency. If t_1 is the time before the next pulse arrives, then the number of centres which must be filled by the next pulse is

$$N_R.(1-\exp(-pt_1))$$

If it is assumed that the rate of hole injection and hole trapping are linear with time, then the plateau length P will be given by

$$P = K.N_R.(1-\exp(-pt_1)),$$ where K is a constant.

Thus

$$\log(1-P/P_\infty) = -pt_1$$

where P_∞ is the value of the plateau length at large t_1. This only holds if the applied voltage is greater than V_B otherwise the device will switch off at low duty cycles. Figure 7.16 shows a plot of Log $(1-P/P_\infty)$ against t_1 for one crystal measured by Marlor[7] and one from which device 40 was constructed. In both cases a good straight line is obtained although the intercept in the plot for device 40 is some 15% away from the value unity as predicted by the theory.

This simple theory does not account for the behaviour under pulsed voltages observed in all devices. The results here are presented for the best two fits to the simple theory. Some crystals showed a marked departure from the predictions of this model, and some crystals had a second step which appeared at the back of the current pulse as the voltage was increased beyond a certain level. The second step could be due to to the filling of a second set of recombination

centres. Undoubtedly, the behaviour of all the crystals can only be satisfactorily explained using a very complicated model which is impossible to formulate on the evidence presented in this thesis.

The measurement of the change in the plateau length as the temperature was raised also indicates that the process is more complicated than the simple model would predict. The model already described was based on the assumption that the recombination centre released holes which were thermally liberated to the valence band. This process should have an activation energy of 0.98 eV which is the energy above the valence band at which the centre lies. The slope of the plot of log P against 1/T which is shown in figure 7.15 is 0.075 eV which is considerably less than 0.98 eV. It is possible that the recombination centre captures electrons not by direct excitation from the valence band to the centre, but by the thermal release of electrons from levels close (0.075 eV) to the conduction band followed by the electrons falling into the recombination centre. This explanation is only offered tentatively. A step in the current pulses through GaAs diodes has been observed by Ing et al [8], who attributed it to a redistribution of the trapped carrier population.

In addition to the delay between the application of a voltage pulse and the onset of light output due to the filling of the recombination centres with holes, there is a further delay effect which shows up at low pulse durations. At pulse durations of the order of a few microseconds, most of the light is emitted after the pulse has

finished. Initially the delay was thought to be caused by the transit of holes across the electrode spacing, but the delay is independent of the applied voltage and can be as large as 40 microseconds. No consistent pattern has emerged from observations of the delay except to contradict the hypothesis that it is associated with the transit of holes. Possibly the mechanism is associated with the release of carriers from traps as in the case of phosphorescence (section 3.2) and this would be similar in explanation to that offered in the previous paragraph to explain the variation of the plateau length with temperature.

The decrease in the plateau length when red, yellow and green light is incident on the crystal can be explained in terms of the occupancy of the recombination centres. The light provides a supply of holes, some of which are trapped at the recombination centres. Thus the number of holes which need to be injected during the plateau is less than in the dark, so the plateau is shorter. The behaviour with blue light is anomalous. The blue light passing through the filters has a component which is sufficiently energetic to eject electrons from the recombination centre, and this should lead to a reduction in the plateau length. Since the plateau length increases at low intensities, the rate of hole injection must be reduced by the light or some other process must affect the occupancy of the recombination centres in favour of electrons. Once the jump from long to short plateau length has taken place under more intense blue

illumination, the behaviour is as would be expected from the explanation of the effect with light of other wavelengths.

The efficiency of the radiative recombination process decreases as the temperature is raised. The variation of the light output with temperature is shown in figure 7.17. The classical theory of thermal quenching of luminescence is due to Schon and Klasens. The quenching is due to thermal activation of carriers of one sign from the recombination centre to the nearest energy band which prevents the recombination of carriers of the opposite sign through the centre. Thus if the recombination is through a level close to the conduction band then a free hole in the valence band cannot recombine through that level if the centre has already been filled with a hole by the thermal release of an electron from the centre to the conduction band. According to these ideas, the efficiency, η, falls off as

$$\eta = \frac{1}{1 + A.\exp(-W/kT)}$$

where A is a constant, and W is the activation energy.
Thus

$$\log(1/\eta - 1) = -W/kT + \text{constant}$$

The plot of $\log(1/\eta - 1)$ against $10^3/T$ for the points in the region where the light output is falling is shown in figure 7.18. The slope gives an activation energy of 0.16 eV, which is in reasonable agreement with the activation energies of 0.10 and 0.13 eV of the two centre model for the luminescence proposed in section 8.1.

9.5. Conclusions from the electrical measurements.

The double injection effects described in this chapter are governed by the dominant recombination centre in these crystals which has a capture cross section for holes much greater than that for electrons, and lies about 0.98 eV above the valence band. The theory of Ashley and Milnes describes the current-voltage characteristics more closely than that of Lampert. No theoretical model has so far been produced which explains the steep rise in the post-breakdown region. Both Ashley and Milnes, and Lampert's theories require the current to vary with the square of the voltage and this is not observed. Two explanations of post-breakdown characteristics with vertical rise in the current have been proposed by other workers performing measurements on other materials. Dumke (section 2.8) has explained the negative resistance and steep rise in the post-breakdown current in GaAs diodes as being due to the re-absorption of the recombination radiation, and Wagener and Milnes[9] have postulated that the vertical rise in the current in the post-breakdown region in silicon p-n diodes is due to the spread of filamentary breakdown through the device. Once the filament has spread throughout the whole cross section of the junction then the bulk properties govern the current flow and the square law dependence of current on voltage is observed. The current in the post-breakdown region rises by more than two orders of magnitude before the square law dependence

is observed. The filamentary model is unlikely to hold for CdS because if the breakdown were filamentary, then filaments of the crystal would emit light and spots at the ends of the filaments would be seen. This is not the case in CdS where the emission appears to emanate uniformly from the bulk of the material. The re-absorption of light postulated by Dumke could provide the explanation. Since the recombination is emitted via two separate paths the higher energy could be reabsorbed to activate the lower energy recombination. Further measurements in the post-breakdown region are necessary to elucidate the mechanism.

The plateau in the current pulse is explained by filling of the recombination centre 0.98 eV above the valence band with holes. The simple theory fits for two crystals but gives only poor fit for several other samples. Clearly the model is too simple to have general application. The activation energy for the thermal quenching of the luminescence is in good agreement with the energy level structure proposed in section 8.1.

Some of the measurements reported in this chapter were published in a recent paper by Rushby and Woods, a copy of which is attached in Appendix 5.

CHAPTER 10

CONCLUSIONS

10.1. Summary.

Double injection has been used as a tool for investigating the defects in CdS. Information about the dominant centre situated close to the middle of the forbidden energy gap, which cannot be obtained from thermally stimulated current measurements, has been found. The centre has a much larger capture cross section for holes than for electrons, and this gives rise to the switching effects and the steps observed in the current pulses. The study of the recombination radiation shows that the emission is due to the same processes whatever the mode of excitation, but that different mechanisms dominate in each case. The surface recombination is much stronger in the electro-luminescent spectra than in the photo-luminescent spectra. The surface recombination was found to depend on the treatment given to the crystal, and in particular it has been suggested that photo-assisted adsorption of gaseous impurities onto the surface is responsible for producing the levels via which the surface recombination proceeds. The wavelength of the edge emission in CdS is found to depend very little on the temperature in the range 77 to 107 ^{o}K, but shifts in the electro-luminescent spectra at currents above 10 mA indicate that the emission is probably temperature dependent above 110 ^{o}K. The major difficulty in the work

has been one that is common to all the work that has ever been performed on this material, namely that uniform samples with controlled properties cannot yet be produced. The recombination centre located about 0.98 eV above the valence band appears predominantly in crystals which were grown with excess sulphur added to the charge, and on this evidence it is tempting to assign the effect to cadmium vacancies. However, it is impossible to explain all the effects described in this thesis on a simple model.

10.2. Suggestions for further work.

The most difficult aspect of the work described in this thesis has been that although most of the crystals showed qualitatively the same behaviour, the quantitative results were widely different indicating a wide variation in the density of defects from crystal to crystal. Clearly if the work can be repeated on samples cut from a uniform large single crystal, many of the difficulties will be removed. Work is at present being successfully carried out in these laboratories to produce large uniform single crystals of CdS and in the very near future such crystals should be available.

The measurement of the spectral distribution of the photoluminescence in the temperature range 100 to 160 ^{o}K with the temperature accurately controlled should enable the shift in the first edge emission peak of the electro-luminescence to be elucidated. If the shift of this peak is due to the heating of the crystal as suggested in this thesis, then this would be evident from the

measurements at the different temperatures.

The theory that the high energy emission is due to photo-adsorption of gaseous impurities onto the surface of the crystal could be tested by exposing the crystal to a series of controlled atmospheres at different temperatures with and without illumination. This work could be carried out in conjunction with thermally stimulated current measurements.

The assignment of the delay in the light output under short duration pulses to phosphorescent effects could be verified by measuring the variation of the delay with temperature. If the delay is associated with the lifetime of a meta-stable state, then the relationship

$$1/\tau = S.\exp(-E/kT)$$

where τ is the lifetime, E is the activation energy, and S is a constant, should be obeyed. Alternatively chopped ultra-violet light or very short duration flash tube excitation could be employed to see if a similar delay exists in the photo-luminescence.

The variation of the stoichiometry of the CdS by heat treatment in atmospheres of cadmium and sulphur vapour changes the defect concentrations. The influence of such changes on the steps in the current pulses and on the switching of the D.C. current should enable further information to be obtained about the complex defect responsible for the effects observed.

APPENDIX 1

Details of crystal growing runs

Run	Starting charge	Dopant	Duration (min)	Result
1	Lights 1		80	Rods
2	Lights 1		110	Poor
3	Lights 1		90	Poor
4	Lights 2		120	Rods
5	Lights 1		120	12 Plates
6	Lights 1		75	15 Plates
7	Lights 1		35	Rods
8	Lights 1		90	Plates
9	Lights 1		90	Plates
10	Lights 1		45	Plates
11	Lights 1		60	Poor
12	Lights 1		45	Poor
13	Lights 1		45	Thin plates
14	Lights 1		45	Thin plates
15	Lights 2		45	Rods
16	Lights 2		40	Small plates
17	Lights 2		55	6 good plates
18	Lights 2		45	Small plates
19	Lights 2		40	Rods
20	Lights 3		50	Poor plates

Run	Starting charge	Dopant	Duration (min)	Result
21	Derby 1		25	Small plates
22	Elements		10	Poor
23	Run 22		35	3 Plates
24	Lights 3		45	Plates
25	Lights 3		55	Plates
26	Lights 3	In	60	Hollow rods
27	Lights 3	O_2	30	Good plates
28	Lights 3	Ga	100	Rods
29	Lights 3	Ga	75	Small rods
30	Lights 3	Cu	70	Plates
31	Lights 3		90	Plates
32	Lights 3	Al	60	Rods
33	Lights 3	B	120	Plates
34	Lights 3	Tl	180	Hollow rods
35	Lights 3	B	120	Rods
36	Lights 3	Tl	130	Rods
37	Lights 3	O_2	70	Plates
38	Lights 3		75	Thin plates
39	Lights 3	Cl	100	Plates
40	Lights 3	Cl	125	Large rods
41	Lights 3	Al	75	Plates
42	Lights 3	Cu:Cl	210	Poor
43	Derby 2	Xs S 1%	40	Good plates

Run	Starting charge	Dopant	Duration (min)	Result
44	Derby 2	Xs S 2%	35	Plates
45	Derby 2		45	Few plates
46	Derby 2	Xs S 1%	50	Poor plates
47	Derby 2	In:Cl .003%	120	Plates
48	Derby 2	In:Cl .006%	105	Plates
49	Derby 2	H_2:Cl	30	Poor
50	Derby 2	H_2:Cl	60	Poor
51	Derby 2	H_2:Cl	135	Rods
52	Derby 2	H_2:Cl	105	Rods

Pre-treatment of the starting charge

Lights 1: Powder baked at 900 ^{o}C under vacuum.

Lights 2: Powder baked at 500 ^{o}C under vacuum.

Lights 3: Powder baked at 500 ^{o}C under vacuum.

Derby 1: Luminescent grade powder baked at 500 ^{o}C under vacuum.

Derby 2: Electronic grade powder baked at 500 ^{o}C under vacuum.

APPENDIX 2

Programme for calculating the positions of the peaks

```
WAVELENGTH ENERGY AND WAVENUMBER'

BEGIN REAL        XO,YO'

      INTEGER      I,NP'

      ARRAY       X,Y,Z(1:1000)'

READ  NP,XO,YO'

FOR I:=1    STEP 1 UNTIL NP DO

READ      X(I), Y(I)'

FOR I:=1 STEP 1 UNTIL NP DO

BEGIN       Y(I):=5500-(X(I)-XO)/3.81'

            X(I):=12396.9/Y(I)'

            Z(I):=10^8/Y(I)'

PRINT ALIGNED       (4,0),Y(I),  SAMELINE,       ££S4??,

      ALIGNED        (1,3),X(I),        ££S4??

      ALIGNED       (5,0),Z(I)'

END'     END'
```

APPENDIX 3

Programme for scaling the emission spectra

```
GRAPH SCALE
BEGIN REAL      DX,   DY,   XSC,   YSC,   XO,   YO'
      INTEGER   NX,   NY,   I,   NP'
      ARRAY     X,Y(1:1000)'
BEGIN READ      NP,XSC, YSC,DX,DY,NX,NY,XO,YO'
ORIGIN(O,O)
XAXIS(O,O,DX,NX)'
YAXIS(O,O,DY,NY)'
FOR I:=1   STEP 1 UNTIL NP DO
BEGIN READ X(I),Y(I)'
           X(I):=XSC*(X(I)-XO)/254'
           Y(I):=YSC*(Y(I)-YO)/254'
END'
DRAW (X,Y,NP)'
END'     END'     END'
```

APPENDIX 4

Construction of the electro-luminescent devices

The electro-luminescent devices were made only from clear, unstriated CdS plates. The thickness of the plate was measured by focussing a metallurgical microscope on the top and bottom of the crystal. This gave the apparent thickness of the crystal. The real thickness was then obtained by multiplying by the refractive index of CdS (2.6). The average thickness was found by measuring the thickness at 10 places over the surface of the plate. The accuracy of the measurement was of the order of 10 microns.

In all cases the electron injecting contact was indium which was applied by evaporation from a molybdenum boat in a vacuum of the order of 10^{-5} to 10^{-6} torr as measured on a Mcleod gauge. This vacuum was maintained in a 6 inch diameter glass bell jar pumped by a mercury diffusion pump backed by a conventional rotary oil pump. A liquid nitrogen cold trap was employed to reduce contamination by volatile impurities. The evaporation was preceeded by bombardment of the crystal with hydrogen ions in a gas discharge.

Silver, graphite, gold, copper, and nickel were all found to be successful hole injecting materials. The final choice was evaporated gold as this adhered to the CdS well, and was free from electrical noise. Colloidal silver and graphite applied in the form of a paste were found to be poor both electrically and mechanically at

liquid nitrogen temperature.

The proceedure for constructing the devices was as follows:

1. The crystal was cleaved to provide a piece small enough to fit onto a TO-18 transistor header. The size was of the order of 2 X 2 mm.

2. The average thickness of the crystal was measured with a metallurgical microscope.

3. The indium cathode was evaporated following a one minute gas discharge in hydrogen.

4. The gold anode was evaporated onto the opposite face of the crystal without a preceding discharge. Both these evaporations were performed through a circular mask.

5. The crystal was placed indium face down on a TO-18 transistor header which had previously had a thin piece of indium melted onto it. The header and crystal were now heated to between 250 and 300 °C in an atmosphere of argon in a specially designed molybdenum strip heater. The temperature was monitored with a Pt:Pt 13%Rh thermocouple. The ensemble was maintained at the heater temperature for two minutes, then cooled down in argon. When cool, the crystal was bonded firmly to the header. Occasional failures due to poor wetting or poor flushing did occur, but only rarely.

6. A 0.25 mm diameter gold wire was now soldered to the header post with indium. This manipualtion was facilitated by observing the header through a X10 binocular microscope.

7. Connection between the gold film and the gold wire was achieved by bonding the two together with Johnson-Matthey thermosetting silver preparation FSP 43. The device was then stoved at 80 ^{o}C for 2 hours to cure the silver preparation.

The TO-18 headers were chosen because they were found to be a convenient size, and the thermal coefficient of expansion of the Nilo-K from which they are made, matched that of CdS fairly closely so that effects associated with piezo-electric voltages could be minimised. Occasionally, larger area devices were fabricated on TO-5 headers.

APPENDIX 5

Double injection effects and electro-luminescence in CdS

Reprinted from

British Journal of Applied Physics

The Institute of Physics and The Physical Society

Printed in Great Britain by Adlard & Son, Ltd., Dorking

BRIT. J. APPL. PHYS., 1966, VOL. 17

Double injection effects and electroluminescence in CdS

A. N. RUSHBY and J. WOODS

Department of Applied Physics, University of Durham

MS. received 21*st March* 1966, *in revised form* 20*th May* 1966

Abstract. Observations on the negative resistance of insulating crystals of CdS with indium cathodes and gold anodes are reported. With applied voltages below the critical voltage for the onset of negative resistance a crystal can be switched from a low current to a high current state by light of wavelengths shorter than 8100 Å. This effect is attributed to the presence of hole traps about 1 ev above the valence band. With pulsed applied voltages the current shows a steep rise to a highly conducting state after an induction time during which holes are being accumulated at the hole traps.

At low temperatures visible light is emitted when a crystal is in the highly conducting state. The spectral distribution of this radiation is compared with the photoluminescence.

1. Introduction

When electrons and holes are injected electrically into thin platelets of insulating CdS from suitable cathode and anode contacts, green recombination radiation can be observed provided the temperature is low enough. The main purpose of the present paper is to describe the spectral distribution of the recombination radiation and to report a variety of measurements made using pulsed voltages. A negative resistance region of the current–voltage characteristic is found and the crystals are bi-stable, that is to say crystals can be switched from a low current to a high current state by irradiation with suitable illumination. The results suggest that the effect is due to the presence of hole traps about 1 ev above the valence band. Similar negative resistance characteristics and switching effects have previously been reported in cadmium sulphide by Litton and Reynolds (1964); in Ge and Si by Ashley and Milnes (1964), Marsh, Baron and Mayer (1965) and Wagener and Milnes (1964); and in GaAs by Holonyak *et al.* (1962).

Two-carrier space-charge-limited currents in semiconductors and insulators have been studied extensively in recent years. The theoretical work has been summarized by Lampert (1962a) and Rose (1964). The double carrier models most appropriate to insulating CdS are those suggested by Lampert (1962b) and Ashley and Milnes (1964). The model proposed by the latter workers would appear to fit our results more closely.

2. Experimental technique

The crystals used in this work were thin (150–200 μm) plates of CdS grown by sublimation from a charge of high purity CdS powder in a stream of argon. The resistivity of all samples lay in the range 10^{10}–10^{12} Ω cm. Electrical contacts were applied to the large area faces of the platelets. Indium was used as the electron injecting cathode and gold as the hole injecting anode.

The sample was mounted on the copper block of an all-metal vacuum cryostat. The temperature which ranged between 77 and 300°K was monitored with a copper–constantan thermocouple.

To prevent the destruction of the sample under negative resistance conditions, d.c. current–voltage characteristics were made with the sample in a simple current-limiting circuit. For the pulse work, pulse lengths between 1 μsec and 100 msec were employed, at various repetition rates down to 1 per 10 sec. The resulting current and light output

pulses were displayed on a Tektronix oscilloscope type 545A. The light output was monitored with an EMI 9451 photomultiplier, and its spectral distribution was measured with an Optica DRNI recording spectrophotometer.

3. Negative resistance effects

The static current–voltage characteristic of a typical platelet of CdS is shown in figure 1. The measurements were performed at 77°K. The contacts were 1 mm² in area and the thickness of the crystal was 200 μm. At low applied voltages Ohm's law is obeyed. At some transition potential V_t, which in this sample is at 5v, the current begins to increase as V^2. As the voltage is still further increased a region of negative resistance is encountered (figure 1) which begins when the critical voltage V_c is exceeded. In the sample illustrated

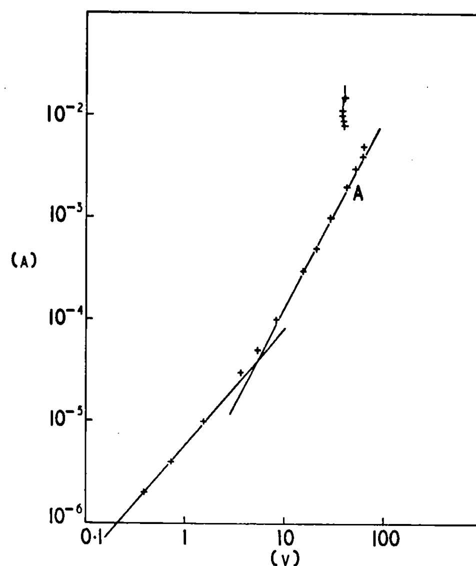

Figure 1. Current–voltage characteristic of a CdS platelet measured at 77°K.

$V_c = 68$ v. Because the current was limited the shape of the characteristic after the onset of negative resistance is not therefore significant. Similar negative resistance effects have previously been observed on CdS crystals examined in this laboratory by Marlor and Woods (1963). They applied Lampert's (1962b) theory of double injection to their results and concluded that at V_c the lifetime of an injected hole increased a thousand-fold from 10^{-8} to 10^{-5} sec. However their results were not completely consistent with Lampert's theory, in particular the negative resistance region should cover a voltage range of 1000 : 1, i.e. the ratio of hole lifetimes after and before the onset of double injection. In figure 1 this would require the voltage to fall to 0·068 v after the critical voltage was reached. Clearly this does not happen.

A characteristic similar to that illustrated in figure 1 would seem to be more closely described by the theory due to Ashley and Milnes (1964). Their theory differs from Lampert's in that Lampert considers a model with a single set of recombination centres which are fully occupied by electrons in thermal equilibrium, whereas Ashley and Milnes introduce a set of acceptor levels so that the recombination centres are partially compensated and therefore not fully occupied by electrons in equilibrium. According to Ashley and Milnes the square law region is still due to the space-charge-limited flow of one of the carriers as in Lampert's scheme (electrons in the case of CdS). The essential difference however is that both the electron and hole flows are limited by space-charge barriers in front of the respective metal contacts. When the applied voltage exceeds V_c, hole injection becomes large. Ashley and Milnes' model predicts a steep vertical increase in the current with a negative resistance region only if the recombination centres capture holes more

efficiently than they capture electrons. This model would appear to be more in accord with our observations than that of Lampert.

Little attempt has been made to test these conclusions since the main interest has been in the bi-stable behaviour described in §4.

4. Switching effects

A crystal biased in the state represented by A (figure 1) where it is passing a current of 1·8 mA can be switched to a higher current state passing 10–100 mA simply by illuminating the sample with visible light. Once the sample is switched into the high current state the high current persists until the applied voltage is removed. The switching can be performed at all temperatures in the range investigated, i.e. 77–300°K. Below 140°K the high current state is associated with the emission of recombination radiation.

Using the beam of light from the exit slit of a monochromator as the excitation for the switching, we have found that there is a wavelength threshold beyond which optical switching is no longer possible. This threshold lies at 8100 Å.

In our opinion Ashley and Milnes' model with a single incompletely filled recombination centre can be used to describe the observed behaviour. Thus light with $\lambda = 8100$ Å, $h\nu = 1{\cdot}52$ ev is required to eject electrons from the recombination centres so that in effect these centres become preponderantly occupied by holes. When this happens large hole injection occurs and the high two-carrier space-charge-limited currents can flow. With the crystal in the dark the high current state is achieved by increasing the applied voltage to V_c. At this stage injected holes are trapped at the recombination centres and the electronic configuration is identical to that described above when light is used to eject the electrons from the same centres. This experiment shows that the recombination centres lie about 1·5 ev below the conduction band and therefore 1·0 ev above the valence band.

Ashley and Milnes argue that to observe a negative resistance the capture cross section of these centres for holes, σ_p, must be much larger than their capture cross section for electrons, σ_n. If $\sigma_p \gg \sigma_n$ holes once trapped at such centres would remain there and the high current would continue to flow. A somewhat similar effect has been reported by Litton and Reynolds (1964).

Switching can be effected with greater efficiency when light is used which is absorbed at the optical absorption edge ($\lambda \sim 5100$ Å). Such light creates both free holes and electrons, hole trapping ensues followed by the switching effect.

When infra-red radiation which quenches the photoconductivity is used, no switching occurs. We have examined crystals which display a large infra-red quenching band centred at 0·85 μm at 100°K. This radiation is quite ineffective in switching the crystals from the low to the high current state or vice versa. Switching from the high to the low states might have been expected since infra-red quenching involves an electron transition from the valence band to a state approximately 1 ev above the top edge of the band.

The switching speed is usually slow, most crystals require a few tenths of a second following the onset of irradiation to switch to the high current state.

5. Switching with pulsed voltages

When the applied voltages are square pulses of about 1 msec duration a new range of phenomena is observed. At low voltages the current pulse is small and of the same shape as the voltage pulse. When the voltage is increased to the vicinity of V_c the current pulse develops a step as illustrated in the oscillograms of figure 2(*b*). At the beginning of the pulse, A, the current is small, corresponding to the low current state, but eventually there is a sharp rise at B, to a new high current state. This is the switching effect under pulsed conditions. The length of time t_0 during which the crystal remains in the low current state after the start of the pulse is a measure of the time it takes for the holes to be trapped at the recombination centres. Once the holes are trapped the current rises steeply to the high current level. When the voltage pulse finishes, the hole traps gradually fill with electrons before the next pulse begins. The period between consecutive pulses should therefore be

related to the length of time t_0 that the crystal remains in the low current state after the start of the next pulse. This is borne out in practice as the two sets of oscillograms in figures 2 and 3 demonstrate. In each sequence curve (*a*) is the light output pulse and (*b*) the current pulse. The important features are (i) that the induction time t_0 decreases with increase in pulse repetition frequency, and (ii) light is only emitted when the crystal is passing the higher current.

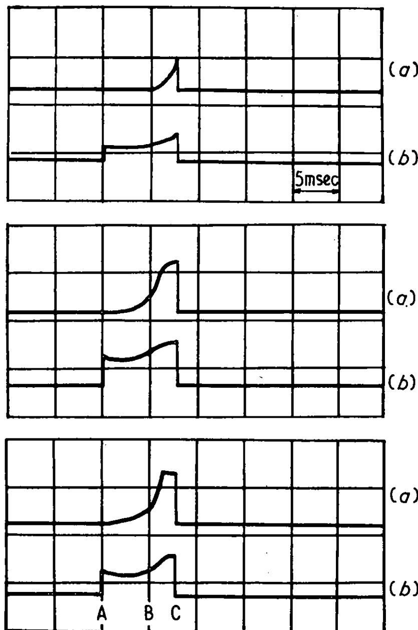

Figure 2. Oscillograms of (*a*) light output pulse, (*b*) current pulse with a pulsed voltage of 8 msec duration. Repetition frequency 5, 10 and 20 c/s.

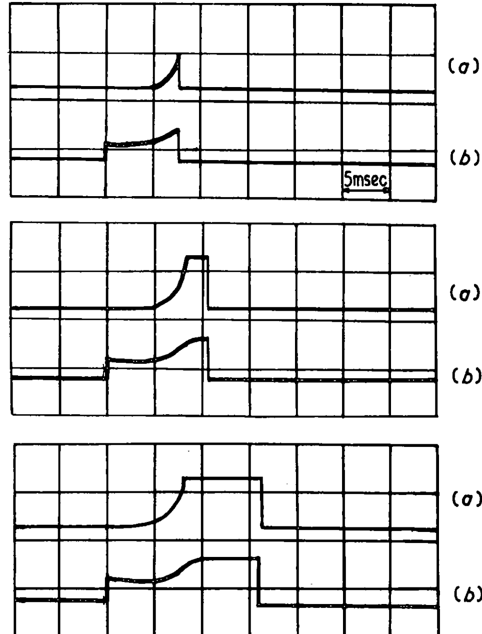

Figure 3. Oscillograms of (*a*) light output pulse, (*b*) current pulse with voltage pulses of 3 different durations and repetition frequency 5 c/s.

Consider two consecutive pulses. Suppose that time is measured from the end of the first pulse at C. At this point since the high current state prevails, the recombination centres, of which there are N_{R} per cm³, are completely empty of electrons. Suppose that the dominant process of emptying the centres of their trapped holes is by thermal excitation of electrons from the valence band, then at time t after the end of the first pulse, the concentration of recombination centres containing holes will be

$$N = N_{\mathrm{R}} \exp(-pt) \tag{1}$$

where p is the probability that a hole can be thermally excited from a recombination centre to the valence band. p is therefore of the form

$$p = \nu \exp(-E/kT)$$

where ν is the attempt to escape frequency and E is the energetic distance of a recombination level above the valence band. If the second pulse begins at time t_1, the number of recombination centres which will have lost their holes while no voltage is applied will be $N_{\mathrm{R}}\{1 - \exp(-pt_1)\}$. This therefore will be the number which have to be trapped following the start of the second pulse before the current can switch to the high level state. If it is assumed that the rate of hole trapping following injection is linear with time, then the induction time t_0 during which the holes are being trapped is given by

$$t_0 = KN_{\mathrm{R}}\{1 - \exp(-pt_1)\} \tag{2}$$

where K is a constant.

If the duty cycle is decreased so that t_1 tends to infinity, the induction time should saturate at a value t_∞. This is observed in practice. It follows from equation (2) that $KN_R = t_\infty$ and therefore

$$\ln(1 - t_0/t_\infty) = -pt_1. \quad (3)$$

A number of measurements of pulse shape were made as a function of repetition frequency and the results plotted in the form $\ln(1 - t_0/t_\infty)$ against t_1 are shown in curve A, figure 4, for a typical sample. Good straight lines were obtained with all crystals examined. The curve marked B, figure 4, was obtained from some previous unpublished results of

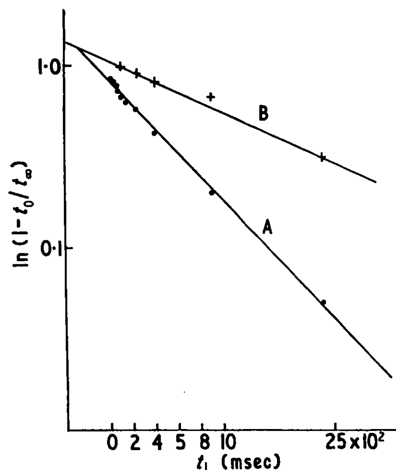

Figure 4. Plots of $\ln(1 - t_0/t_\infty)$ against t_1, the interval of time between consecutive pulses. The curve marked B was plotted from earlier data obtained by G. A. Marlor.

Marlor's. His measurements were made on different crystals at a different temperature. The difference in temperature explains the variation in the slopes of the lines. In principle if the slopes p of a number of lines such as those in figure 4 were measured as a function of temperature, a plot of $\log p$ against $1/T$ would yield the value of the activation energy E of the trap. We have so far failed to obtain such a line since the experiment requires a variety of low temperatures to be maintained for a considerable length of time. This experiment would require a redesigned cryostat. Rough preliminary experiments indicate that the trap activation energy is much smaller than 1 ev, i.e. the process of hole de-trapping is not one of thermal excitation of holes to the valence band, but is probably associated with the release of trapped electrons from relatively shallow electron traps which then recombine with the holes at the recombination centres.

6. Recombination radiation

With a crystal at low temperatures ($< 140°$K) and in the high current state a visible green recombination radiation can be readily observed. The intensity of this luminescence increases linearly with current density up to the highest currents used (10 A cm^{-2}, pulsed). At low temperatures from 77 to 130°K the intensity is practically independent of temperature, but as the temperature is increased further the luminescence is rapidly quenched. If it is assumed that the quenching can be described by the well-known formula

$$L = \{1 + B\exp(-W/kT)\}^{-1} \quad (4)$$

then the activation energy for quenching W is about 0·15 ev.

The spectral distribution of the recombination radiation at 100°K has also been measured and is compared with photoluminescence excited by ultra-violet light ($\lambda = 3650$ Å) from a high pressure mercury arc. Curve A, figure 5, illustrates the ultra-violet excited luminescence. The curve exhibits the well-known phonon-assisted 'edge' emission with peaks at

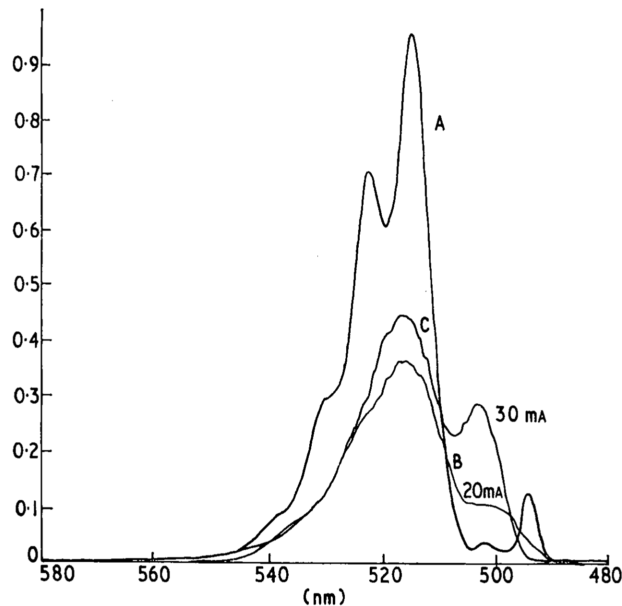

Figure 5. Spectral emission distribution of the photoluminescence (curve A) and the recombination radiation (curves B and C) of a sample at 100°K. The results on curve B were measured for a current density of 1 A cm^{-2} and curve C for 1·5 A cm^{-2}.

5150, 5233 Å etc. The photoluminescence when examined initially did not exhibit either of the two short wave peaks at 5050 and 4950 Å. These emission bands appeared after prolonged excitation with the ultra-violet light and are presumably associated with surface changes. Curves B and C show the spectral distribution of the recombination radiation at current densities of 1·0 and 1·5 A cm^{-2} respectively. The emission appears to be concentrated into one broad band centred at 5150 Å and second band at 5050 Å. It would seem reasonable to suppose that the longer wavelength emission is due to recombination in the bulk and is of the same nature as edge emission, whereas the shorter wavelength emission is associated with surface recombination effects. It is worth recording that no appreciable narrowing of the emission bands was observed at the highest current densities obtainable (10A cm^{-2}).

7. Discussion

The emission of recombination radiation at low temperatures when the crystal is passing current beyond the threshold V_c indicates that electrons and holes are injected into the insulating cadmium sulphide. Within the limits of experimental error the various CdS samples examined by us indicate that V_c varies as the square of the separation of the electrodes. This supports the idea that negative resistance occurs when the hole transit time equals the hole lifetime, as required by the theories of Lampert and Ashley and Milnes. The spectral distribution of the radiation and the activation energy for temperature quenching shows that the electron hole recombination takes place via the same defect which is responsible for edge emission (Marlor and Woods 1965). This defect is situated some 0·15 ev from a band edge. Microscopic examination of a crystal emitting light fails to reveal whether the emission is localized at the anode or cathode. This failure is attributable to the high refractive index of cadmium sulphide which causes too much total internal reflection for direct observations to be of any value. However, it does seem clear that the light is emitted uniformly and not from spots or streaks. That is to say the hole injection process takes place uniformly over the anode and not at localized spots or filaments.

The d.c. and pulsed voltage investigations of the switching effect indicate that the high current region is associated with hole trapping at recombination centres which are situated

1·0 ev above the valence band. These centres must have a much larger capture cross section for electrons than for holes, but quantitative values for these can only be obtained via Ashley and Milnes' ideas provided the concentration of free holes in thermal equilibrium is known, together with an estimate of the density of the recombination centres. The results, however, clearly show that a single recombination centre model with one set of donors is too simple to explain the behaviour of cadmium sulphide. The radiative transition takes place via an energy level situated 0·15 ev from a band edge and in addition the centres responsible for infra-red quenching of the photoconductivity are also present. The quenching centres are unlikely to be identical with those which allow the switching effect to occur. If they were, irradiation in the quenching band would switch the crystal from the higher current to the low current state. Further, infra-red quenching is observed in practically all CdS crystals, whereas the switching effect is prominant in crystals grown in an excess of sulphur vapour. This would suggest on a simple charge compensation argument that the recombination centres associated with the switching effect are cadmium vacancies.

The measurement of the switching threshold permits the measurement of parameters of centres with levels near the middle of the forbidden gap in CdS. Means of investigating such centres are unfortunately all too few. We propose to continue this work to investigate infra-red luminescence in switching crystals to try and correlate the luminescent emission with infra-red quenching and switching thresholds. We shall also conduct the experiment with varying repetition rates, discussed in §5, at various temperatures in an attempt to determine the thermal activation involved in the hole de-trapping process.

References

Ashley, K. L., and Milnes, A. G., 1964, *J. Appl. Phys.*, **35**, 369–74.

Holonyak, N. Jr., Ing, S. W. Jr., Thomas, R. C., and Bevacqua, S. F., 1962, *Phys. Rev. Letters*, **8**, 426–8.

Litton, C. W., and Reynolds, D. C., 1964, *Phys. Rev.*, **133A**, 536–41.

Lampert, M. A., 1962a, *Proc. Inst. Radio. Engrs*, **50**, 1781–96.

—— 1962b, *Phys. Rev.*, **125**, 126–41.

Marlor, G. A., and Woods, J., 1963, *Proc. Phys. Soc.*, **81**, 1013–21.

—— 1965, *Brit. J. Appl. Phys.*, **16**, 797–803.

Marsh, O. J., Baron, R., and Mayer, J. W., 1965, *Appl. Phys. Letters*, **7**, 120–2.

Rose, A., 1964, *J. Appl. Phys.*, **35**, 2664–78.

Wagener, J. L., and Milnes, A. G., 1964, *Appl. Phys. Letters*, **5**, 186–8.

REFERENCES

Introduction.

1. G.A.Marlor, M.Sc thesis, Durham University, 1962
2. J.Lambe and C.C.Klick, J. Phys. Rad., 17, 663, 1956

Chapter 1.

1. R. de L.Kronig and W.G.Penney, Proc. Roy. Soc.(London), A130, 1931
2. L.Brillouin, Wave propagation in periodic structures, McGraw-Hill, 1946
3. F.Bloch, Z.Physik, 52, 555, 1928
4. C.Hilsum and A.C.Rose-Innes, Semiconducting III-V compounds, Pergamon, 1961.
5. Conwell and Weisskopf, Phys. Rev., 77, 388, 1950
6. A.R.Hutson, J.A.P., 32, 2287, 1961
7. J.B.Gunn, I.B.M. Res. Dev., 6, 141, 1964
8. R.H.Bube, Photoconductivity of solids, Wiley, 1960
9. N.F.Mott and R.W.Gurney, Electronic processes in ionic crystals, O.U.P., 1948
10. M.A.Lampert, Phys. Rev., 103, 1648, 1956
11. G.A.Marlor and J.Woods, Proc. Phys. Soc., 81, 1013, 1963
12. N.Cusack, Electrical and amgnetic properties of solids, Longmans, 1958
13. I.E.Tamm, Z.Phys., 76, 849, 1932
14. W.Shockley, Phys. Rev., 56, 317, 1939

Chapter 2.

1.R.H.Parmenter and W.Ruppel, J.A.P., 30, 1548, 1959

2.M.A.Lampert and A.Rose, Phys. Rev., 121, 26, 1961

3. R.D.Larabee, Phys. Rev., 121, 37, 1961

4. M.A.Lampert, Phys. Rev., 125, 126, 1962

5. K.L.Ashley and A.G.Milnes, J.A.P., 35, 369, 1964

6.R.Hirota, S.Tosima, and M.A.Lampert, J.Phys. Soc. Japan, 18, 535, 1963

7. M.C.Steele, K.Ando, and M.A.Lampert, J. Phys. Soc. Japan, 17, 1729, 1962

8. W.P.Dumke, 7 th Int. semiconductor conference, Paris, 1964

9. V.I.Stafeev, Sov. Phys. solid state, 1, 763, 1959

10. A.Rose, J.A.P., 35, 2664, 1964

Chapter 3.

1. D.Curie, Luminescence in crystals, Methuen, 1963

2. A.K.Jonscher, Principles of semiconductor device operation, Bell, 1960

3. W.Shockley and W.T.Read, Phys. Rev., 87, 853, 1952

4. O.W.Lossew, Telegr. e. Telef., 26, 403, 1923

5. P.N.Keating, Phys. Chem. Solids, 24, 1101, 1963

6. A.G.Fischer and H.I.Moss, J.A.P., 34, 2112, 1963

7. M.G.A.Bernard and G.Duraffourg, Phys. Stat. Sol., 699, 1962

Chapter 4.

1. C.A.Escoffery, J.A.P., 35, 2273, 1964

2. J.L.Birman , J. Electrochem. Soc., 107, 409, 1960

3. M.Balkanski and J.Des Cloiseaux, J. Phys. Rad., 21, 825, 1960

4. M.Balkanski and R.Waldron, Phys. Rev., 112, 123, 1958

5. H.S.Sommers jr., R.E.Berry, and I.Sochard, Phys. Rev., 101, 987, 1956

6. D.Curie, Luminescence in crystals, Methuen, 1960

7. R.H.Bube, Photoconductivity of solids, p237, Wiley, 1960

8. J.Woods and K.H.Nicholas, B.J.A.P., 15, 1361, 1964

9. R.H.Bube, J. Chem. Phys., 23, 18, 1955

10. F.A.Kroger, H.J.Vink, and J.Volger, Philips Res. Rep., 10, 39, 1955

11. R.H.Bube, Phys. Rev., 99, 1105, 1955

12. W.E.Spear and G.W.Bradberry, Phys. Stat. Sol., 8, 649, 1965

13. J.Woods and J.A.Champion, J. Elect. Control, 7, 243, 1959

14. J.D.Zook and R.N.Dexter, Phys. Rev., 129, 1980, 1963

15. R.N.Dexter, J.Phys. Chem. Sol., 8, 39,216, 1959

16. J.J.Hopfield and D.G.Thomas, Phys. Rev., 122, 35, 1961

17. W.E.Spear and J.Mort, Proc. Phys. Soc., 81, 130, 1963

18. A.Rose, Prog. in semiconductors, Heywood, 2, 1957

19. F.A.Kroger, Physica, 7, 1, 1940

20. R.Marshall nad S.Mitra, Phys. Rev., 134, A1019, 1964

Chapter 4 contd.

21. J.J.Hopfield, J. Phys. Chem. Solids, 10, 110, 1959

22. G.A.Marlor and J.Woods, B.J.A.P., 16, 797, 1965

23. C.C.Klick, J. Opt. Soc. Am., 41, 816, 1951

24. D.C.Reynolds, C.W.Litton, and T.C.Collins, Phys. Stat. Sol., 9, 645, 1965

25. F.J.Bryant and A.F.J.Cox, B.J.A.P., 16, 1065, 1965

26. M.Balkanski and F.Gans, Phys. Stat. Sol.,

27. N.G.Basov, O.V.Bogdankevich, and A.G.Devyatkov, Sov. Phys. JETP., 20, 1067, 1965

28. C.E.Hurwitz, A. Phys. Letters, 8, 121, 1966

29. R.W.Smith, Phys. Rev., 93, 347, 1954

30. C.W.Litton and D.C.Reynolds, Phys. Rev., 125, 516, 1962

31. C.W.Litton and D.C.Reynolds, Phys. Rev., 133, A536, 1964

32. R.C.Janklevic, D.K.Donald, and W.C.Vassel, A.Phys. Letters, 2, 7, 1963

33. D.D.O'Sullivan and E.C.Malarkey, A.Phys. Letters, 6, 5, 1965

Chapter 5.

1. A.Vecht and A.Apling, Phys. Stat. Sol., 3, 7, 1963

2. W.E.Medcalf and R.H.Fahrig, J. Electrochem. Soc., Dec, 1958

3. P.W.Bridgman, Proc. Am. Acad. Arts and Sciences, 60, 303, 1925

4. R.H.Fahrig, Electrochem. Tech., Nov-Dec., 1963

5. W.W.Piper and S.J.Polich, J.A.P., 32, 1278, 1961

Chapter 5 contd.

6. L.Clark and J.Woods, B.J.A.P., 17, 319, 1966

7. G.A. Somorjai and D.W.Jepsen, J.Chem.Phys., 41, 1389, 1964

8. R.Nitsche, J.Phys. Chem. Sol., 17, 163, 1960

9. R.Frerichs, Phys. Rev., 72, 594, 1947

10. J.M.Stanley, J. Chem. Phys., 24, 1279, 1956

11. P.D.Fochs, J.A.P., 31, 1733, 1960

12. A.Vecht, B.W.Ely, and A.Apling, J.Electrochem. Soc, 111, 6, 1964

13. J.Woods, B.J.A.P., 10, 529, 1959

14. S.Ibuki, J. Phys. Soc. Japan, 14, 9, 1959

15. P.A.Jackson, Unpublished paper presented at the Hull conference on luminescence, Sept. 1964

Chapter 8.

1. G.A.Marlor and J.Woods, B.J.A.P., 16, 797, 1965

2. D.C.Reynolds, Phys. Rev., 118, 478, 1960

3. D.Curie, Luminescence in crystals, Methuen, 1963

4. R.H.Bube, J. Chem. Phys., 23, 18, 1955

5. L.R.Furlong and C.F.Ravilious, Phys. Rev., 98, 954, 1955

6. J.Woods and K.H.Nicholas, B.J.A.P., 15, 1361, 1961

7. T.A.T.Cowell and J.Woods, to be published

Chapter 9.

1. K.L.Ashley and A.G.Milnes, J.A.P., 35, 369, 1964

2. W.E.Spear and J.Mort, Proc. Phys. Soc., 81, 130, 1963

3. P.N.Keating, J. Phys. Chem. Sol., 24, 1101, 1963

Chapter 9 contd.

4. K.Friedrich, Dissertation, Halle, 1963

5. O.J.Marsh, R.Baron, and J.W.Mayer, A.P.Letters, 7, 120, 1965

6. N.Holonyak, S.W.Ing, R.C.Thomas, and S.F.Bevaqua, Phys. Rev. Letters, 8, 426, 1962

7. G.A.Marlor, M.Sc. thesis, Durham University, 1962

8. S.W.Ing, H.A.Jansen, and B.Stern, A.P.Letters, 4, 162, 1964

9. J.L.Wagener and A.G.Milnes, A.P.Letters, 5, 186, 1964